CATHOLIC UNIVERSITY OF PERNAMBUCO
PRO-RECTORY OF RESEARCH AND POST-GRADUATION
GRADUATE PROGRAM IN CIVIL ENGINEERING
MASTER'S COURSE

CAMILA MOTA DE ARAÚJO

NUMERICAL SIMULATION OF MOISTURE TRANSPORT ALONG CERAMIC BRICK INTERFACES

Recife
2022

CATHOLIC UNIVERSITY OF PERNAMBUCO
PRO-RECTORY OF RESEARCH AND POST-GRADUATION
GRADUATE PROGRAM IN CIVIL ENGINEERING
MASTER'S COURSE

Camila Mota de Araújo

NUMERICAL SIMULATION OF MOISTURE TRANSPORT ALONG CERAMIC BRICK INTERFACES

Dissertation submitted to the Graduate Program of the Catholic University of Pernambuco, as partial requirement for obtaining the Master's Degree in Civil Engineering.

Advisor: Prof. Dr. Fernando Artur Nogueira Silva

Recife
2022

CATHOLIC UNIVERSITY OF PERNAMBUCO
PRO-RECTORY OF RESEARCH AND POST-GRADUATION
GRADUATE PROGRAM IN CIVIL ENGINEERING
MASTER'S COURSE

Camila Mota de Araújo

NUMERICAL SIMULATION OF MOISTURE TRANSPORT ALONG CERAMIC BRICK INTERFACES

Examining Committee:

Prof. Dr. Fernando Artur Nogueira Silva

Advisor - Catholic University of Pernambuco, Brazil - UNICAP

Prof. Dr. Antônio Augusto Costa de Azevedo

Co-Advisor – Instituto Federal de Pernambuco

Prof. Dr. Joaquim Teodoro Romão de Oliveira

Internal Examiner - Catholic University of Pernambuco, Brazil - UNICAP

Prof. Dr. Angelo Just da Costa e Silva

Internal Examiner - Catholic University of Pernambuco, Brazil - UNICAP

Prof. Dr. João M. P. Q. Delgado

External Examiner – Faculdade de Engenharia da Universidade do Porto – FEUP

Recife
2022

FOLHA DE APROVAÇÃO

Aluno (a): CAMILA MOTA DE ARAÚJO

Título da Dissertação NUMERICAL SIMULATION OF MOISTURE TRANSPORT ALONG CERAMIC MATERIAL INTERFACES

Dissertação apresentada ao Programa de Pós-Graduação em ENGENHARIA CIVIL da Universidade Católica de Pernambuco (UNICAP) para obtenção do título de Mestre (a) em ENGENHARIA CIVIL. A presente dissertação foi defendida e aprovada em 26 de maio de 2022 pela banca examinadora e constituída pelos professores:

Orientador
Prof. Dr. Fernando Artur Nogueira Silva

Co - Orientador
Prof. Dr. Antônio Augusto Costa de Azevedo

Examinador Interno
Prof. Dr. Joaquim Teodoro Romão de Oliveira

Examinador Interno
Prof. Dr. Angelo Just da Costa e Silva

Examinador Externo
Prof. Dr. João M. P. Q. Delgado

Recife
2022

A663n Araújo, Camila Mota de.
Numerical simulation of moisture trnasport along Ceramic brick interfaces / Camila Mota de Araújo, 2022.
146 f. : il.

Orientador: Fernando Artur Nogueira Silva.
Dissertação (Mestrado) - Universidade Católica de Pernambuco. Programa de Pós-graduação em Engenharia Civil. Mestrado em Engenharia Civil, 2022.

1. Alvenaria. 2. Tijolos. 3. Engenharia civil. 3. Cerâmica. 4. WUFI (Programa de computador). 5. Métodos de simulação. I. Título.

CDU 693.27

Pollyanna Alves - CRB-4/1002

DEDICATORY

To God, my parents, family, teachers, and friends.

ACKNOWLEDGEMENTS

After years of hard study, effort, and dedication, I would like to thank everyone who made this dream come true. Therefore, I express here my sincere thanks and gratitude to everyone. First, I thank the Catholic University of Pernambuco and the Antonio dos Santos Abranches Foundation - FASA for providing me with free education, without which I could not have done this course. I also thank my family, friends, and teachers for all the support during these years of study, understanding my absence on many occasions, encouragement to never give up on any academic challenge, and understanding at all times. I thank in special Professor Dr. Fernando Artur Nogueira for having accepted me in his research, for having believed and placed his trust in me throughout all these years of work that started in the undergraduate and now in the postgraduate studies. For all the teachings, for all the opportunities offered during my academic journey that contributed to my academic and professional development. Such is the gratitude and admiration I have for my teachers throughout my academic journey, who have always opened doors of opportunities and thoughts, making me believe in an extraordinary present and future through education. I will be accomplished when as a teacher I can contribute to the development and with new opportunities for the students just as my teachers did for me.

Such is the trust we have in God, through Christ. Not that we can claim anything on our own merits, but our ability comes from God.

(2 Corinthians 3:4-5)

RESUMO

O transporte de humidade em alvenaria de tijolo é um fenômeno importante em vários mecanismos de deterioração. No entanto, é um processo muito complexo e é influenciado por muitos fenômenos físicos. A investigação da transferência de humidade através de uma parede de edifício, que em geral, consiste em múltiplas camadas, pressupõe o conhecimento sobre a continuidade entre as camadas. Neste estudo, foram analisados dois tipos de configurações de contato, como se segue: Contacto hidráulico perfeito e Interface de espaço de ar. Portanto, para compreender o transporte de humidade em alvenaria de tijolo, analisou-se o transporte de humidade através da interface dos materiais. Isto foi feito para amostras de argamassa de cimento-tijolo, argamassa de cal-tijolo e espaço de ar entre camadas de tijolo, bem como para amostras com diferentes alturas de localização da interface e diferentes espessuras de argamassa e espaço de ar. Principalmente, o presente trabalho tem a finalidade de simular o comportamento higrotérmico através de interfaces tijolo-argamassa e tijolo-tijolo em amostras com contato hidráulico perfeito e com espapaço de ar entre camadas de tijolo para comparar os resultados com as análises laboratoriais. As simulações numéricas de amostras de tijolo-argamassa e tijolo-tijolo foram realizadas com o software de simulação higrotérmica WUFI-2D. WUFI-2D é um programa de computador, baseado no modelo de cálculo higrotermal, que tem na sua base um sistema de equação de transporte acoplado e técnica de solução numérica, desenvolvido pelo modelo de Künzel (1995). Os dados utilizados para executar as simulações foram extraídos dos ensaios de absorção de água em amostras laboratoriais; os perfis de teor de humidade correspondentes foram medidos utilizando espectrómetros de raios gama. Embora os mecanismos de transporte de humidade num único material de construção tenham sido e continuam a ser amplamente estudados, as características hidráulicas da interface em diferentes tipos de contatos entre materiais são ainda pouco compreendidas e, por esta razão, a hipótese simplificada de contato hidráulico perfeito, é amplamente utilizada em modelos higrotérmicos. Em termos gerais, a presunção de contato hidráulico perfeito implica que a interface não terá qualquer efeito sobre o transporte de humidade. Em comparação, a presunção de contato hidráulico imperfeito implica que a interface entre os materiais de construção resistirá ao transporte de humidade. Contudo, as comparações entre os resultados experimentais e numéricos mostraram grande diferença no comportamento do transporte da umidade nas amostras com contato hidraulico perfeito e contato hidráulico imperfeito devido a influência causada pela interface.

Palavras-chave: Tijolo cerâmico, simulações numerica, WUFI, transporte de humidade, interface.

ABSTRACT

Moisture transport in brick masonry is an important phenomenon in various deterioration mechanisms. However, it is a very complex process and is influenced by many physical phenomena. The investigation of moisture transfer through a building wall, which in general consists of multiple layers, presupposes knowledge about the continuity between the layers. In this study, two types of contact configurations were analyzed, as follows: Perfect Hydraulic Contact and Air Space Interface. Therefore, to understand moisture transport in brick masonry, moisture transport through the materials' interface was analyzed. This was done for cement mortar and brick samples, lime mortar and brick samples, and samples with air space between brick layers, as well as for samples with different interface location heights and different air space thicknesses. Mainly, the present work aims to simulate the hygrothermal behavior through brick-mortar and brick-brick interfaces in samples with perfect hydraulic contact and with air space between brick layers to compare the results with laboratory analyses. The numerical simulations of brick-mortar and brick-brick samples were performed with WUFI-2D hygrothermal simulation software. WUFI-2D is a computer program, based on the hygrothermal calculation model, which has at its base a coupled transport equation system and numerical solution technique, developed by Künzel (1995). The data used to run the simulations were extracted from water absorption tests on laboratory samples; the corresponding moisture content profiles were measured using gamma ray spectrometers. Although the mechanisms of moisture transport in a single building material have been and continue to be extensively studied, the hydraulic characteristics of the interface at different types of contacts between materials are still poorly understood and, for this reason, the simplified assumption of perfect hydraulic contact, is widely used in hygrothermal models. In general terms, the assumption of perfect hydraulic contact implies that the interface will have no effect on moisture transport. In comparison, the assumption of imperfect hydraulic contact implies that the interface between building materials will resist moisture transport. However, comparisons between the experimental and numerical results showed a large difference in the moisture transport behavior for samples with perfect hydraulic contact and imperfect hydraulic contact due to the influence caused by the interface.

Keywords: Ceramic brick, numerical simulations, WUFI, moisture transport, interface.

FIGURE INDEX

TABLE INDEX

LIST OF SYMBOLS, ABBREVIATIONS AND NOMENCLATURES

Symbol	Symbol name	Unit
ρ_0	Density	Kg/m³
w	Moisture Content	kg/m³
μ	Moisture Content	kg/kg
Ψ	Moisture Content	m³/m³
Wmax	Maximum moisture content	kg/m³
μmax	Maximum moisture content	kg/kg
Ψmax	Maximum moisture content	m³/m³
Wcap	Capillary moisture content	kg/m³
μcap	Capillary moisture content	kg/kg
Ψcap	Capillary moisture content	m³/m³
Wcr	Critical moisture content	kg/m³
μcr	Critical moisture content	kg/kg
Ψcr	Critical moisture content	m³/m³
c_0	Specific heat capacity	J/(kg·K)
λ	Thermal conductivity	W/(m·K)
T	Temperature	ºC, K
μ	Vapor resistance factor	dimensionless
δ_a	Vapor permeability of stagnant air	kg/(m·s·pa)
P	Ambient pressure	Pa
P_0	Standard atmospheric pressure	Pa
R_v	ideal gas constant for water	J/(K·kg)
Ψ_0	Open porosity	m³/m³
ε	Porosity	m³/m³ or %
ρ_w	Density of water	kg/m³
A_w	Water absorption coefficient	kg/(m2·√s)
q_v	mass flux rate of vapor flow	(kg/m2·s)
D_v	diffusion coefficient of vapor in air	m2/s
P_v	partial vapor pressure	Pa
a	open pores	m³/m³
α	tortuosity factor	m³/m³
q_w	mass flux of liquid	(kg/m2·s)
D_ϕ	liquid coefficient	(kg/m·s)
g	gravitational acceleration	(m/s2)
σ	surface tension of water	(N/m)
r	capillary radius	m
ϕ	relative humidity	(-)
P_h	capillary pressure	Pa
k	thermal conductivity	(W/m·K)

ρ_a	Density of air	kg/m^3
v	Velocity	m/s
C_a	volumetric heat capacity	$(J/m^3 \cdot K)$
ε	emissivity of gray surface	(-)
σ	Stefan Boltzmann constant	W/m^2 K4
F	view factor	(-)
T_b	surface temperature	(K)
T_a	surrounding temperature	(K)
m_a	air mass flux	(kg/m2s)
k_a	air permeability	(kg/m·s Pa)
P_a	air pressure	(Pa)
P_g	gas mixtures pressure	Pa
P_w	liquid-water pressure	Pa
J_w	vapor flux	$kg/m^2 \cdot s$
D_v	diffusion coefficient	m2/s
c	water vapor concentration	kg/m3
c_w	diffusion flux	$kg/m^2 \cdot s$
p_w	water vapor pressure	Pa
c_w	vapor concentration	kg/m3
M_w	imolar mass of water	kg/mol
π	Water vapor permeability	kg/(m·s·Pa)
R	ideal gas constant	J/mol.K
P_c	macroscopic capillary pressure of a pore	(Pa)
ρl	mass density of liquid water	(kg/m3)
D_θ	moisture diffusivity	m2/s
K_{if}	interface permeability	kg/(m·s·Pa)
q_{if}	moisture flux across the interface	(kg/m2·s)
h	relative humidity	(-)
pv	vapor pressure	Pa
pvs	saturation vapor pressure	Pa

SUMMARY

CHAPTER 1. INTRODUCTION

1.1 IMPORTANCE

The hygrothermal behavior of the building envelope plays a very important role on the overall energy performance of buildings, the quality of indoor environments and the durability of structures with concerning the deteriorating effect of moisture migration.

Building envelopes are mostly made up of multi-layered walls and therefore, the transport of moisture through a building envelope usually involves interface phenomena, which is the transport of moisture across interfaces between building materials (DE FREITAS; ABRANTES; CRAUSSE, 1996). Thus, knowledge of interface phenomena is essential for predicting moisture transport across interfaces between building materials.

Most hygrothermal models treat materials as individual layers in perfect contact, i.e. the interface has no effect on moisture transport. However, in practice, this may not always be true. Therefore, to properly evaluate the moisture transport performance of a building envelope that may lead to design guidelines for a building envelope, it is mandatory to obtain a good understanding of interface phenomena.

Although, moisture transfer in buildings is a very complex process and it is influenced by many physical phenomena. The prediction of the hygrothermal performance of the building enclosure requires some knowledge of: geometry of the enclosure (building shape and height), boundary conditions (interior–exterior environment, boundary conditions between elements), material properties, physics, chemistry, thermodynamics and mathematics of combined moisture, heat and air transport and performance thresholds (TRECHSEL, 2001).

In the literature, there are many computational tools aimed at predicting the long-term hygrothermal performance of buildings. These models vary significantly in terms of their mathematical sophistication. The sophistication of the model depends on the degree that it takes into account parameters such as moisture transfer dimension (one, two or three), type of flow (time-stationary, quasi-static or dynamic), quality and

availability of information, and the stochastic nature of the data (KAROGLOU et al., 2007).

The understanding of moisture behavior through the interface between materials is essential to predict the effective moisture transport that exists in building walls and to predict the performance of multilayer components. Therefore, after reviewing the currently available literature on the influence of the interface in moisture transport in building materials, it was concluded that it would be pertinent, in this work, to perform numerical simulations that allow, through the results obtained, to analyze the effects caused in moisture transport at the interface of materials of multilayer components. The scarce studies performed with multilayer components simulation available in the literature, as well as the limited understanding of this phenomenon, justify the relevance of this work, which aims to compare the results obtained through the experimental tests of the wetting profiles performed in Azevedo AC (2019)'s work, in order to study the influence of the interface between the tested materials.

1.2 RESEARCH OBJECTIVES

This work aims to study the influence of the interface at different types of contact – perfect hydraulic contact and air space interface - on moisture transport, by analyzing profiles of moisture content obtained through simulations performed with the hygrothermal simulation software WUFI-2D v. 4.3. The numerical simulations were performed by introducing the experimental results of one-dimensional water transport in combined samples of brick and mortar and brick and air space, in order to simulate the different types of object contacts of this work. With the results obtained by WUFI it is intended to compare the experimental results with the numerical model results.

The simulations performed are intended to contribute to develop an appropriate level of understanding the influence of the interface on the moisture behavior. More specifically, aims of this work are:

1. To contribute to the exploration and analysis of the WUFI program, considering that there are few multilayer component analyses in the literature using this tool.

2. Compare the results of the moisture content profiles obtained in the experimental study of (AZEVEDO AC.,2019) and the numerical simulations performed in WUFI, in order to contribute to the experimental validation.
3. Investigate the influence of the interface between materials layers, on moisture transport, by interpreting the consequences of the variability of contact types and sample characteristics on the wetting and drying profiles;

Realizing the following complementary objectives made it possible to achieve the main objectives:

- Study of the fundamental moisture transport mechanisms;
- Brief review of the different contact conditions between porous media for moisture transfer through the interface;
- Study of the program manual WUFI-2D and other relevant articles;
- Analysis of the parameters requested by the program to perform the numerical simulations;
- To understand and describe the WUFI program and the numerical equations that underlie the software;
- Understand how to create climatic conditions that simulate an absorption test through a wet front, according to the laboratory conditions from the experimental tests object of this study;
- Understand how to characterize air layers with the properties required in the program.
- Calculate the moisture content profiles, for a given simulation time, for the two types of contact and interfaces at different heights under study in this work, using the WUFI program;

1.3 DISSERTATION STRUCTURE

- Chapter 1 - presents a brief introduction of the problem and the research objectives and methodology used to analyze the moisture transport behavior along brick interfaces;
- Chapter 2 - presents an essentially theoretical content, where the mechanisms of hygrothermal transport in porous materials, the forms of water transport and the main interface configurations of interest to this study are analyzed. A list of some 2D hygrothermal programs were mentioned with the main limitations and the physics governing these programs;
- Chapter 3 - systematizes the methodology applied for the tests simulation, the use of the WUFI-2D program and the description of all the necessary steps to perform a simulation with the software, as well as the material properties, the configurations and boundary conditions of each element to be analyzed;
- Chapter 4 – the simulations results carried out are presented, where a theoretical analysis of the interface influence on the transport of moisture in the samples is developed and compared with the results obtained in the experimental study by Azevêdo (2019).
- Chapter 5 – summarizes the achievements of this study and gives some recommendations for future works in this specific research area.

CHAPTER 2. LITERATURE REVIEW

2.1 MOISTURE TRANSFER CONCEPTS

2.1.1 Overview and introduction

In this chapter a literature review is provided for a proper understanding of moisture transport phenomena, including hygrothermal properties overall in building materials, knowledge about moisture movement and transfer and its effects in porous media, which are necessary knowledge to understand future moisture analyses related to the methodology of this study.

As indicated in the introduction, this work is mainly concerned with the numerical simulation of moisture transport through different types of contact between porous construction materials.

Building materials can be affected both by moisture and can affect the moisture performance of a building and its elements. The properties relevant to moisture analysis are discussed in more detail in this chapter.

The properties mainly relevant for the analysis of moisture with focus of the study are moisture transmission, moisture absorption and moisture storage, as well as the types of materials that cause concern in this area and focus of the study are bricks and mortar, considering that it is of major importance the actual knowledge of moisture transport through these materials to have an effective analysis of the effects caused by moisture in multilayered walls.

This chapter also intends to present the most relevant information concerning the moisture transport through the interface between the layers of porous materials, whereas each type of interface will contribute differently to a change in moisture transport, varying from when it passes in relation to a monolithic element.

2.1.2 Main material properties for the moisture transfer study

The envelope of any building is continuously exposed to changes in internal and external temperature, pressure, and humidity conditions. This results in an exchange of energy and mass (air and moisture) between the interior and outdoor environments through the envelope. Experts in the literature refer to this phenomenon as "heat, air, and moisture transport" through building materials and components.

For an advancement in building construction, considering a reduction in generated energy consumption and increased durability of components, designers and builders are always interested in knowing the long-term performance of the building envelope as subjected to transport processes.

But because the global differences in building practices, construction materials, climatic conditions, and indoor climate are so large, it is impractical to develop this knowledge only through experimental investigations.

Therefore, nowadays the knowledge of the performance of building components, as well as the whole building, is already possible due to the advancement of technology and is being improved over time through the development of calculation methods for this purpose.

However, the diverse set of procedures and computational models require information regarding the materials that are constantly evolving. The main consequence is a remarkable change in the properties of these materials. Therefore, the properties reported in the literature may become "unrepresentative" of actual products. This requires a continuous update of the hygrothermal properties. Otherwise, however, the sophisticated numerical calculation method employed may produce results that do not represent the real hygrothermal behavior of the building component under analysis.

The main hygrothermal properties of materials, considered in most of the existing numerical models for the analysis and knowledge of the building components performance undergoing moisture transport, will be presented below according to Kumaran’s (1996) review.

- *Density* (ρ_0 – kg/m³)

Density of a building material is defined as the mass of 1 m³ of the dry material. For practical reasons, the phrase “dry material" does not necessarily mean absolutely dry material. For each class of material, it may be necessary to adopt prescribed standard conditions.

- *Moisture Content* (w)

Moisture content of a building material is defined as: (i) mass of moisture per unit volume of the dry material (w - kg/m³), or (ii) mass of moisture per unit mass of the dry material (μ - kg/kg), or (iii) volume of condensed moisture per unit volume of the dry material (Ψ - m³/m³).

The definition (i) is generally used with reference to all building materials, while it is a common practice to use (ii) with reference to denser building materials such as concrete, brick, and wood products and to use (iii) with reference to lighter materials such as insulation.

Many building materials are porous bodies. In these porous bodies the moisture content may vary between the dry state referred to above and a fully saturated state when the open pores are completely filled with water. The moisture content that corresponds to the saturation state is called the *maximum moisture content* (W_{max} or μ_{max} or Ψ_{max}). Experimentally, a building material absorbs moisture to the maximum moisture content level if the process is carried out in vacuum. Otherwise, the saturation is complete at a lower moisture content level. This moisture content is referred to as *capillary saturation moisture content* (W_{cap} or μcap or Ψ_{cap}). Between the dry and saturated states, the moisture content varies with the water vapor pressure of the surroundings in a non-linear way. An example is shown in (Figure 1). The relation between vapor pressure (or more often relative humidity, RH) of the surroundings and the moisture content in the material is called the *sorption curve*. In the lower humidity range, the moisture is in an adsorbed state. This range varies from material to material, and for certain materials could be up to 98% RH. The range of RH until 98% is called the hygroscopic range of a material. At the higher end of the adsorption range, moisture from the surroundings begins to condense in the pores, but initially without any

continuity of the liquid at a macroscopic level. This continues until a *critical moisture content* (symbols: W_{cr} or μcr or Ψ_{cr}) is established. Thus, critical moisture content can be defined as the lowest moisture content necessary to initiate moisture transport in the liquid phase. Below this level, due to macroscopic discontinuity of the liquid, moisture is transported only in the vapor phase (and partly by surface movement in the adsorbed layer).

Figure 1 - Sorption Isotherm of porous building material.

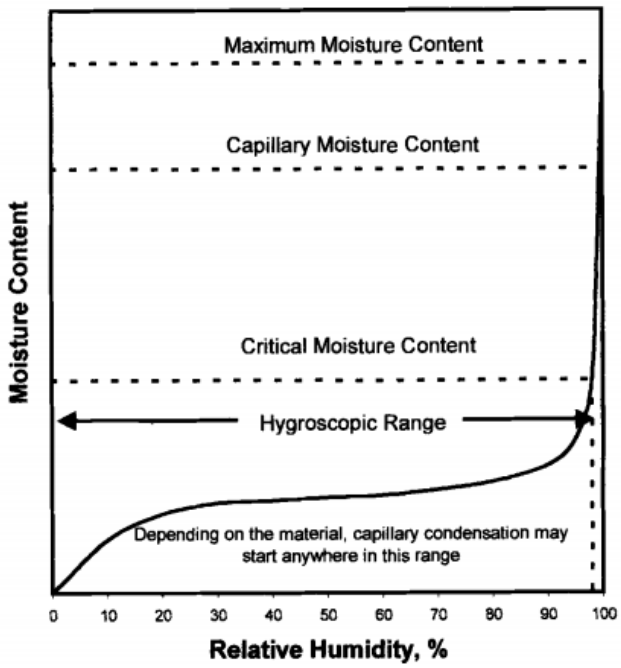

Source: KUMARAN (1996)

- *Specific heat capacity* (c_0 – J/(kg·K))

Specific heat capacity of a material is defined as the heat (energy) required to increase the temperature of unit mass of the material by 1 K.

The mass in the above definition refers to dry mass. If the material is wet, the specific heat capacity c is to be calculated as (Equation 1):

$$c = c_0 + 4187 \cdot \frac{W}{\rho_0} \qquad (1)$$

The above relation assumes that the specific heat capacity of water is a constant equal to 4187 J/kg·K.

- *Thermal conductivity* (λ – W/(m·K))

The thermal conductivity of a material at a point is defined as the ratio between the density of heat flow rate and the magnitude of the thermal gradient at that point in the direction of the flow.

The definition for thermal conductivity stems from Fourier (Equation 2) for heat conduction:

$$q = - \lambda \cdot \text{grad } T \qquad (2)$$

But in a dry building material the heat transfer is a result of conduction, radiation from the surfaces of the pores, and convection within the pores, and in a practical definition of thermal conductivity all three modes of heat transfer are included. If the material is wet, heat transferred by moisture in the capillaries and the enthalpy changes that accompany phase transitions also add to the density of heat flow rate.

- *Vapor resistance factor* (μ - dimensionless)

The vapor resistance factor of a material is defined as the ratio between the vapor permeability of stagnant air, δ_a, and that of the material under identical thermodynamic conditions (same temperature and pressure). The vapor permeability of stagnant air can be calculated according to the (Equation 3) given by (Schirmer, 1938) below:

$$\delta_a = \frac{2.306 \times 10^{-5} P_0}{RvTP} \left(\frac{T}{273.15} \right)^{1.81} \qquad (3)$$

Where, *T* is the temperature (K), P is the ambient pressure (Pa), P_0 is the standard atmospheric pressure (i.e., 101 325 Pa) and R_v is the ideal gas constant for water (i.e, 461.5 J/(K·kg)).

The concept of vapor resistance factor introduces two physical quantities that describe the pore structure of the building material. By definition, μ for stagnant air is 1. If in a slab of dry material, the pores connect two parallel bounding surfaces of the material

straight across and each pore is uniform with respect to the cross-sectional area, then (Equation 4):

$$\mu = \frac{1}{\Psi_0} \qquad (4)$$

Where Ψ_0 is called the open porosity (Ψ_0- m^3/m^3), and refers to the volume of pores per unit volume of the material, accessible for water vapor.

- *Porosity* (ε – m^3/m^3 or %)

Porosity is the ratio of the volume of the material's pore to its total volume. It can determine the maximum water content wmax (by multiplication by ρw = 1000kg/m^3).

- *Water absorption coefficient* (A_w - kg/(m^2·√s))

The property called water absorption coefficient quantifies the water entry into a building material due to absorption when its surface is just in contact with liquid water. It is defined as the ratio between the change of the amount of water entry across the unit area of the surface and the corresponding change in time expressed as the square root; in the early part of an absorption process, this ratio remains constant and that constant value is designated as the water absorption coefficient.

2.1.3 Transport Mechanisms

The transport of heat, air, and moisture has a complex physics involved. Heat and mass transport occurs simultaneously in each porous construction material. The interaction of one or more moisture phases: vapor, liquid, and solid ice, if present, can interact with the porous media's solid matrix phase. Besides the phase change physical phenomena such as evaporation, condensation, absorption heat, freezing and thawing, which can also occur during moisture transport.

This section aims to provide a theoretical review of the transport mechanisms present in hydrothermal processes in porous media. Authors such as Kuenzel (1995), Krus (1996), Kohonen (1984), Janssens (1998), and Luikov (1966) provide in their work more details on the theoretical development of various transport potentials. The choice

of moisture transport potential was made based on what was familiar to the author of the review.

Many older models of moisture transport were developed based on discontinuous potentials, such as moisture content [Luikov (1966), (Pel, 1995)]. Also, Trechsel (2001) reached the conclusion that the moisture content at an interface between two materials is discontinuous. Therefore, a more extensive analysis at the inhomogeneous material intersection is required.

2.1.3.1 Mass Transfer

(Keresteciogl u et al., 1989) and (Kaviany, 1993) provide a great description of the transport mechanism in porous media. However, it must be considered that the transport coefficients may not only be strong functions of the independent variable, but may change as a function of time and exposure. Some of the most important ways in which moisture can be transported are:

Molecular vapor diffusion, by partial vapor pressure gradients.

Molecular liquid diffusion, movement of the liquid phase due to liquid filled pores.

Capillary liquid flow, movement of the liquid phase due to capillary suction pressures.

Knudsen vapor diffusion, movement of the vapor phase in small pores and at low pressures; the mean free path is greater than the pore diameter and collisions of molecules with the pore walls occur more frequently than collisions with other diffusing molecules.

Evaporation-condensation vapor flow, movement occurs in conjunction with heat transfer, moisture evaporates and recondenses in a similar fashion to a heat pipe.

Gravity-assisted diffusion liquid flow, movement occurs due to gravity and occurs mostly in macroporous materials.

2.1.3.2 Vapor Transport

The diffusion of water vapor under isothermal conditions may be described by Fick's first law for unimpeded flow in still air (Equation 5) ((BELARBI; QIN; AÏT-MOKHTAR, 2006):

$$q_v = -D_v \nabla X \qquad (5)$$

where q_v is the mass flux rate of vapor flow (kg/m^2·s), D_v the diffusion coefficient of vapor in air m^2/s, and X the vapor concentration (kg/m^3).

$$q_v = -D_v \frac{M}{RT} \nabla P_v \qquad (6)$$

(Equation 6) where *R* is the universal gas constant (8.314 J/(mol·K)), P_v is the partial vapor pressure, *T* is temperature (K), and M is the molar weight of water (0.018 kg/mol).

In a porous material, diffusion is reduced in comparison to that in still air by a resistance that corresponds to the volume fraction of air-filled open pores a and a tortuosity factor α. This is expressed as (Equation 7):

$$q_v = -\alpha\, a\, D_v \frac{M}{RT} \nabla P_v \qquad (7)$$

European countries mostly introduce a resistance factor as μ= (1/a · α) leading to the following flux (equation 8) for vapor flow:

$$q_v = -\frac{D_v}{\mu} \frac{M}{RT} \nabla P_v \qquad (8)$$

2.1.3.3 Liquid Transport

The liquid flow is transported differently within the two regions of interest in building materials and can be defined in two ways: Capillary water region, which follows the hygroscopic sorption region and extends to free water saturation. This region can be characterized by equilibrium states. Liquid transport occurs under the influence of a pressure or suction force in the capillary regime, and the transport of wet liquids occurs

mainly in this region; Supersaturated capillary region, follows the capillary water region. Normal suction processes are not physically plausible in it. Liquid flow in this region occurs by diffusion under a temperature gradient or by external pressure under suction. In this region, there are no equilibrium states (TRECHSEL, 2001).

The laminar transport theory in capillary tubes developed by Darcy (1856) more than 150 years ago is still the most widely considered in formulations to explain liquid transport. Achilles N. Karagiozis in (TRECHSEL, 2001) extended the original formulation, to take into account the forces of gravity, thus the liquid transport in the capillary regime is given by (Equation 9):

$$q_w = -\left(D_\phi \nabla \phi + \frac{\left(D_\phi \frac{\partial \phi}{\partial u} \right)}{\frac{\partial P_h}{\partial u}} \rho_w \vec{g} \right) \qquad (9)$$

where q_w is the mass flux of liquid (kg/m^2. s), D_ϕ is the liquid coefficient (kg/m·s), g is the gravitational acceleration (m/s^2), and ρw is the density of water (kg/m^3). The suction pressure is usually described by employing a cylinder capillary model and can be presented as (Equation 10):

$$P_h = 2\,\sigma \frac{cos\theta}{r} \qquad (10)$$

where σ is the surface tension of water (72.75· 103 N/m at 20°C), *r* the capillary radius (m), and θ the contact angle or wetting angle (°).

Using thermodynamic equilibrium conditions for a cylinder capillary model, the relationship between relative humidity ϕ over a concavely curved water surface and the capillary pressure P_h is defined by Kelvin's equation as (Equation 11):

$$\phi = \exp\left(\frac{-P_h}{\rho_w R_v T} \right) \qquad (11)$$

where ρw is the density of water (kg/m^3), P_h is the capillary pressure (Pa), R_v is the gas constant for water vapor (J/kg·K), temperature T is in Kelvin (K) and ϕ is relative humidity (-).

2.1.3.4 Heat Transfer

Heat transfer can occur by conduction, convection, and radiation transfer within building envelopes. (Table) 1 lists the equations of state that govern these modes of heat transfer. The thermal conductivity k is a function of the ice and liquid content present in the porous material and can be strongly influenced by temperature, as can be direction dependent.

Table 1 - Energy Transport.

Conduction	Convection	Radiation
$q_c = -k \nabla T$	$q_a = \nabla \rho_a v C_a T$	$q_r = \varepsilon \sigma F (T_s^4 - T_\infty^4)$
where k = thermal conductivity (W/m·K) T = Temperature (°C)	Where ρ_a = Density of air (kg/m³) *v* = velocity (m/s) C_a = volumetric heat capacity (J/m³·K)	Where ε = emissivity of gray surface (-) σ = Stefan Boltzmann constant = (5.67×10^{-8} W/m² K⁴) *F* = view factor (-) T_b = surface temperature (K) T_a = surrounding temperature (K)

Source: adapted from TRECHSEL (2001)

2.1.3.5 Phase Change

The phase change conversion enthalpies contribute a local source of heat that is stored or released in a porous material when moisture accumulation or drying is present. If one considers that the amount of moisture I_{ij} of phase i is converted to j the control volume receives the following amount of heat (Equation 12):

$$q_r = \Delta h_{ij} \cdot I_{ij} \qquad (12)$$

where Δh_{ij} is the change in enthalpy, 3.34·105 J/kg for conversion of ice to water and 2.45·106 J/kg at 20°C for water to vapor.

This quantity of heat may be significant when drying or accumulation is present in porous media. A modeling challenge exists to properly accommodate this latent heat term in the governing equation of energy (TRECHSEL, 2001).

2.1.3.6 Air Transport

Airflow is driven by a difference of air pressure. The mass flux of air through a porous material may he expressed as (Equation 13):

$$m_a = -k_a \nabla P_a \qquad (13)$$

where m_a is the air mass flux (kg/m2s), k_a is the air permeability (kg/m·s Pa), and P_a is the air pressure (Pa).

2.1.4 Moisture transport in porous media

A porous building material can contain a multiphase combination of solids, liquids, and gas. Where heat and mass transfer occurs essentially at the microscopic level for each phase. Therefore, to solve the transport mechanisms at the microscopic level, a detailed description of the geometry and topology of the porous medium is required. This description of the porous medium and the associated transport processes at the microscopic level is difficult and complex, which results in most analyses of a porous material through laboratory characterizations being performed at the macroscopic level.

Employing this basic phase assumption allows the development of differential equilibrium equations for mass, momentum, and energy transfer in numerical models. The porous medium can then be described by three distinct phases, the solid, the liquid water, and the gas phase.

This work has previously described all the transport mechanisms in a porous material. This knowledge is important for understanding moisture transport using tools that simultaneously simulate Heat and Moisture transport in a material. However, since the object of study in this paper is focused on moisture transport, the two main forms of transfer will be further specified below.

2.1.4.1 Introduction of porous media

In general, porous media consist of a structure continuum and a fluid continuum, as shown in Figure 2. The structure continuum is formed from the solid particle and the connected empty pore. The fluid continuum is formed from the fluid saturating the connected and occluded pore (J. BEAR and Y. BACHMAT, 2012).

This is why hygrothermal studies become complex, as transport phenomena where the advancement of liquid water and the diffusion of gaseous mixtures occur in the void space, requires a configuration where the void space must satisfy the connectivity requirements.

Figure 2 - The infinitesimal volume of porous medium.

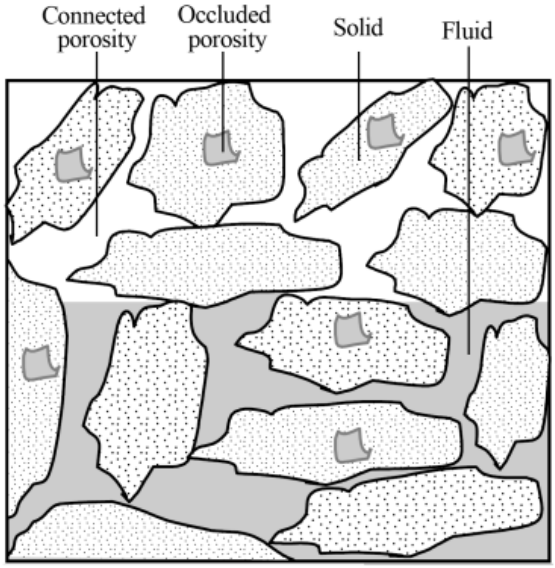

Source: J. BEAR and Y. BACHMAT (2012)

2.1.4.2 Moisture sorption isotherms

Building materials are mostly hygroscopic as they absorb water vapor from the environment until equilibrium conditions are reached. This behavior can be described by sorption curves over a humidity range between 0 and 95% RH. Materials that have water content that is not very sensitive to temperature changes have sorption curves called sorption isotherms. Sorption curves and sorption isotherms for these materials from 95% RH to capillary saturation at 100% RH are difficult to measure. In this range, the equilibrium water content of a material is still a function of relative humidity. It is therefore difficult to determine the function by sorption tests in climatic chambers and

makes it necessary to use a pressure plate apparatus in order to complete the sorption curve in the high humidity range.

The resulting water retention curve has great importance in the study of moisture transport through numerical modeling and is a prerequisite for simulations including liquid transport.

The sorption isotherms are the equilibrium moisture content states in a porous material as a function of relative humidity at a particular temperature. Families of sorption isotherms that encompass both the hygroscopic and capillary regimes are:

Absorption isotherm

Desorption isotherm

Hysteresis isotherms (the equilibrium moisture content curves that span the complete spectrum of moisture equilibrium during both absorption or desorption)

Temperature-dependent sorption curves (the equilibrium moisture content curves dependent on temperature)

The units for moisture content employed in the sorption isotherms are:

water content (kg/m^3)

moisture content by mass (kg/kg)

moisture content by volume (m^3/m^3)

A schematic representation of a typical sorption isotherm with a hysteresis between the adsorption and desorption isotherms is plotted in Figure 3.

These two relationships can be transformed from one to the other on the basis of Kelvin's equation. That means there is an intrinsic relationship between capillary pressure, water saturation and relative humidity.

The sorption consists of adsorption and desorption. The adsorption is induced by interaction forces between water molecules and solid surface. These forces include physical and chemical parts. The physical sorption is due to van der Waals attraction

between adsorbate and adsorbent. The chemical sorption is due to the attractive chemical bonding between adsorbate and adsorbent (YULIANG ZOU, 2020).

Figure 3 - A schematic representation of a sorption isotherm with a hysteresis between the adsorption and desorption isotherms.

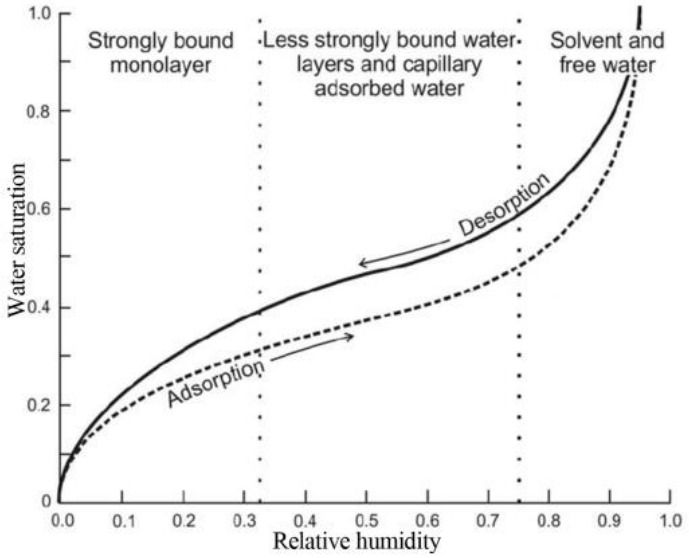

Source: S. AIRAKSINEN (2005)

The capillarity is formed due to menisci between liquid water and gas mixtures. The existence of surface tension γ is the main cause of capillarity. The Young-Laplace (Equation 14) gives the value of force balance at this interface:

$$P_c = P_g - P_w = \frac{2\gamma}{r^*} \qquad (14)$$

where P_g and P_w are gas mixtures pressure and liquid-water pressure, respectively. $r*$ indicates the mean radius of curvature.

The hysteresis between absorption and desorption isotherms is usually not very pronounced. (Rode, 1990) approximated the effect of hysteresis and found that the effect on the calculated water content results was not large. Currently still a large part of the heat and moisture models doesn't incorporate hysteresis and use the absorption isotherm or, where necessary, an average function of absorption and desorption.

Neglecting the hysteresis might not have a great influence on the water content but it dampens the fluctuations in relative humidity within the building assembly. In order to

avoid this effect separate absorption and desorption isotherms and a validated method to interpolate between both curves must be employed (TRECHSEL, 2001).

2.1.4.3 Mechanisms of moisture transport

Briefly, Trechsel (1994) described that moisture in the form of water vapor moves from one place to another either through mass transport, that is, by the movement of moist air, or through diffusion. The driving force of mass transport is air pressure; the driving force of diffusion is vapor pressure. The movement of liquid water can also result from wind pressure moving raindrops through cracks and joints, but as a general rule follows gravity forces.

Therefore, moisture transport in porous materials is very complex, which is a comprehensive expression of various mechanisms. As for weakly permeable porous media, it includes a series of phenomena, i.e. adsorption, desorption, condensation, evaporation, water flow, vapor diffusion, etc. A schematic representation of mechanism of moisture transport is presented in (Figure 4). Generally, the description of moisture transport can be divided into three stages according to the degree of relative humidity condition (YULIANG ZOU, 2020).

Figure 4 - A Schematic representation of mechanisms of moisture transport.

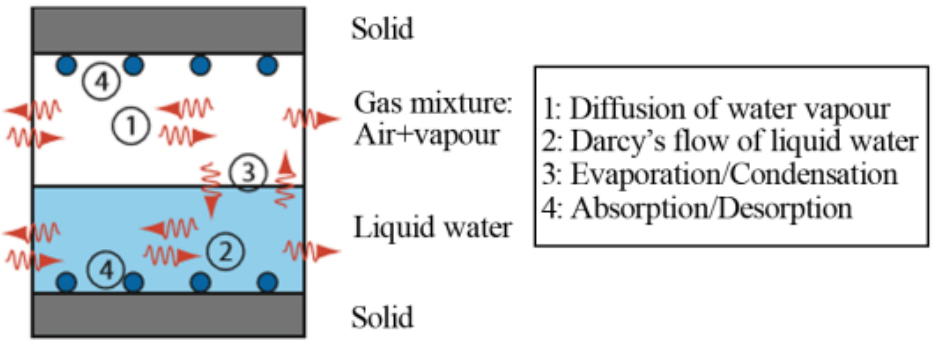

Source: F. BENBOUDJEMA (2002)

According to the aforementioned transport mechanisms, it is possible to arrive at a definition of moisture transport as follows:

1) At high relative humidity stage, the water saturation is high which indicates most of the free liquid water is continuous. The transport of moisture is principally in the form

of liquid water. The gradient of capillary pressure is the driving force for this movement, thus the extended Darcy's law can be applied.

2) At intermediate relative humidity stage, the region of continuous liquid-water continues to reduce which weakens the capillary transport. On the other hand, the vapor diffusion continues to strengthen. It means that the liquid water flow and vapor diffusion occur simultaneously. As the drying develops further, the vapor diffusion has preponderance compared with liquid water flow.

3) At low relative humidity stage, there is no continuous liquid water in the pore, while the gas mixtures are continuous. The vapor diffusion plays more important role in moisture transport. While, the contribution of liquid water flow is almost negligible. Indeed, the water molecules are adsorbed on the surface of pore walls due to van der Waals forces [(M. Iwamatsu and K. Horii, 1996), (M. Tuller and D. Or, 2001)]. Evaporation occurs at the interface between liquid water and gas mixtures. This procedure is caused by the non-equilibrium between capillary pressure and vapor pressure. Then the evaporated vapor can be transported by diffusion through the pore. The diffusion includes ordinary diffusion, Knudsen diffusion (E. A. Mason, 1983), and surface diffusion (K. Higashi, H. Ito, and J. Oishi, 1963). The specific diffusion procedure is demonstrated in (Figure 5).

Figure 5 - A schematic representation of diffusion.

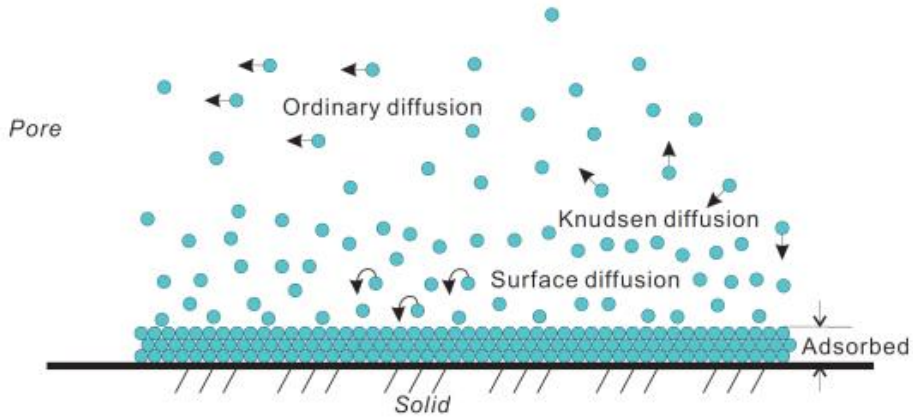

Source: Y. XI et. Al. (1994)

2.1.4.3.1 Water transport in the liquid phase

The water transport in the liquid phase can be processed through the phenomena of capillarity, thermal diffusion, electrokinetic, hydraulic flow and by the gravity effect. However, some of these phenomena can be neglected, such as thermal diffusion a very low rate of the total value of moisture transfer in buildings. Knowledge about the influence of electrokinetics is still very limited.

The influence of gravity on water transport is limited to large pore sizes (>10-6 m) and since building materials mostly have smaller pores, this phenomenon can be neglected. However, in the liquid phase the phenomenon responsible for most of the moisture transport in porous materials is capillarity (QIU, X, 2003).

The capillarity phenomenon can be described by the capability of the liquid to pass through the porous medium without the help of external forces such as gravity, due to the attractive forces that are generated between the liquid and the solid material, overlapping the cohesive forces of the liquid and the gravitational action (GONÇALVES, 2007).

Due to the complexity of the capillary network in a porous material to make it possible to perform an individual capillary analysis, the characterization of these materials regarding the transfer of water by capillarity, is performed at the macroscopic level through the global coefficients determination that are obtained in the capillarity test.

From (Equation 15) and (Equation 16) it is possible to describe the amount of water absorbed and the water rise height at the scale of porous building materials. The total amount absorbed (W) and the height of capillary rise (H) are directly proportional to the square root of time. A (kg·/(m²·√s)) is the capillary water absorption coefficient and B (m/√s) is the capillary penetration coefficient. The initial values of w0 and h0 should also be observed, even if the specimens were oven dried.

$$W(t) = A \cdot \sqrt{t} + w_0 \qquad (15)$$

$$H(t) = B \cdot \sqrt{t} + h_0 \qquad (16)$$

The capillarity test is performed using a specimen made of a porous material, waterproofed on the lateral faces, in partial immersion, allowing capillary absorption to

occur at its base (Figure 6) and from periodic weighings, the amount of water absorbed is determined, which in general is expressed through a graph similar to the one in (Figure 7).

Figure 6 - Capillarity absorption test.

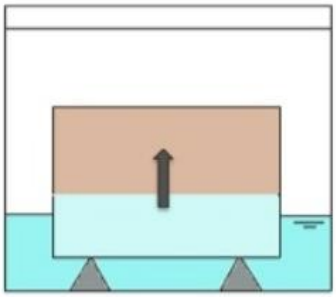

Source: GONÇALVES (2007)

Figure 7 - Typical capillary absorption curve for a porous material.

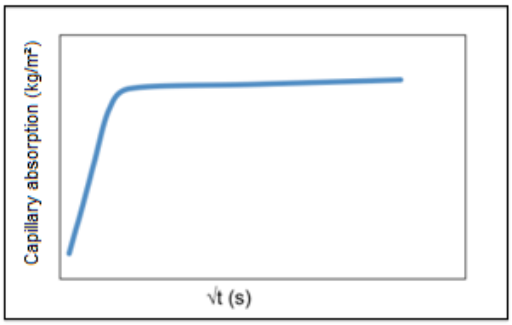

Source: AZEVEDO (2013)

Therefore, water vapor diffusion implies the existence of a water vapor concentration gradient that promotes the flow of water molecules to places where the water vapor concentration is lower until a concentration homogenization is obtained.

2.1.4.3.2 Water transport in the vapor phase

The water vapor transport in building materials is conditioned by diffusive processes and by convective movements inside the pores. The diffusive processes are essentially due to the existence of temperature gradients (thermal diffusion or Soret effect) and water vapor pressure gradients (gaseous diffusion proper). The existence of temperature gradients and convective movements are also usually neglected due to the low influence and the difficulty of determining the air pressure around the building and its reduced influence under normal conditions. However, diffusion becomes the phenomenon to promote most of the moisture transport in porous materials at that stage.

Therefore, water vapor diffusion implies the existence of a water vapor concentration gradient that promotes the flow of water molecules to places where the water vapor

concentration is lower until a concentration homogenization is obtained. This phenomenon can be expressed by Fick's first law (Equation 17).

$$\overrightarrow{J_w} = -D_v \cdot \overrightarrow{\nabla c} \qquad (17)$$

Where, J_w is the vapor flux, in kg/m²·s, D_v is diffusion coefficient, in m^2/s, and c represents the water vapor concentration, in kg/m^3.

The flow direction from the higher vapor concentration zone to the lower concentration zones is represented by the negative sign.

Assuming that air behaves as an ideal gas, the diffusion flux (c_w) can be expressed as (Equation 18) a function of the water vapor pressure (p_w).

$$p_w = \frac{c_w \cdot R \cdot T}{M_w} \leftrightarrow c_w = \frac{p_w \cdot M_w}{R \cdot T} \qquad (18)$$

Where p_w is the water vapor pressure in Pa, c_w is the vapor concentration in kg/m3, R is the ideal gas constant, T is the temperature in Kelvin, M_w is the molar mass of water in kg/mol.

Water vapor permeability, π (kg/(m·s·Pa)), (Equation 19), is a characteristic quantity of each material, and expresses the amount of vapor (kg) that passes through a material's unit thickness (m), per unit time (s) and surface area (m^2), when the pressure difference between the two material faces is also unit (Pa).

$$\pi = \frac{D_v \cdot M_w}{R \cdot T} \qquad (19)$$

2.1.4.3.3 Drying Process

The drying process in a porous material can be defined as the removal of all water present in that material. The 1-D isothermal drying (one drying front) from the saturated state of the material, the specific interest of this study, is characterized by the following stages:

During the initial phase (Phase I), the material is saturated, with high moisture concentration at its surface, and the liquid water present in the porous matrix is moved to the upper surface through capillarity due to the high capillary pressure that exists at the surface. The moisture content in the material decreases through the surface by evaporation. The drying rate is controlled by environmental conditions such as wind speed, air temperature, air humidity, etc. (C. HALL, 2009). At this stage, there is a homogeneous moisture distribution and the drying rate is constant, with a linear decrease in moisture content over time and moisture transport within the material is faster than mass transfer to the atmosphere at the surface.

The second phase (Phase II) begins when the capillary flow is no longer sufficient to compensate for the amount of water evaporating. Thus, there is no longer an equilibrium between the liquid transported to the surface and the liquid that is being evaporated, causing a regression of the wet front into the interior of the material. The moisture transport mechanism to the surface of the material is by vapor diffusion above the wet front and by capillarity below the wet front. At this stage the drying rate declines, as the progressive decrease of the wet front increases the thickness of dry material that the vapor has to traverse to the surface. However, the drying process becomes dependent on the moisture transport properties of the material.

In the last phase (Phase III) the liquid discontinuity occurs below the moist zone. The beginning of this phase is unclear and is usually set as a virtual boundary (J. SELIH, 1996). The liquid water transport in this phase is limited to the finest pores, which although visually the material looks dry, there are still small pores saturated or partially saturated. The main mechanism of moisture transport is vapor diffusion (M. AZENHA, 2009).

The mechanism implies that the drying is complex, multiple and interdependent (M.MAINGUY et. al., 2001). Figure (8) shows the representation of the three phases.

The literature still presents few studies related to drying kinetics in porous materials. Freitas et al. (1996) studied the influence of the interface on the drying kinetics of cellular concrete and red brick samples. The effect caused by parameters such as thickness, porosity and the drying conditions were studied by Derdour et al. (200).

Figure 8 - One-directional drying of porous materials.

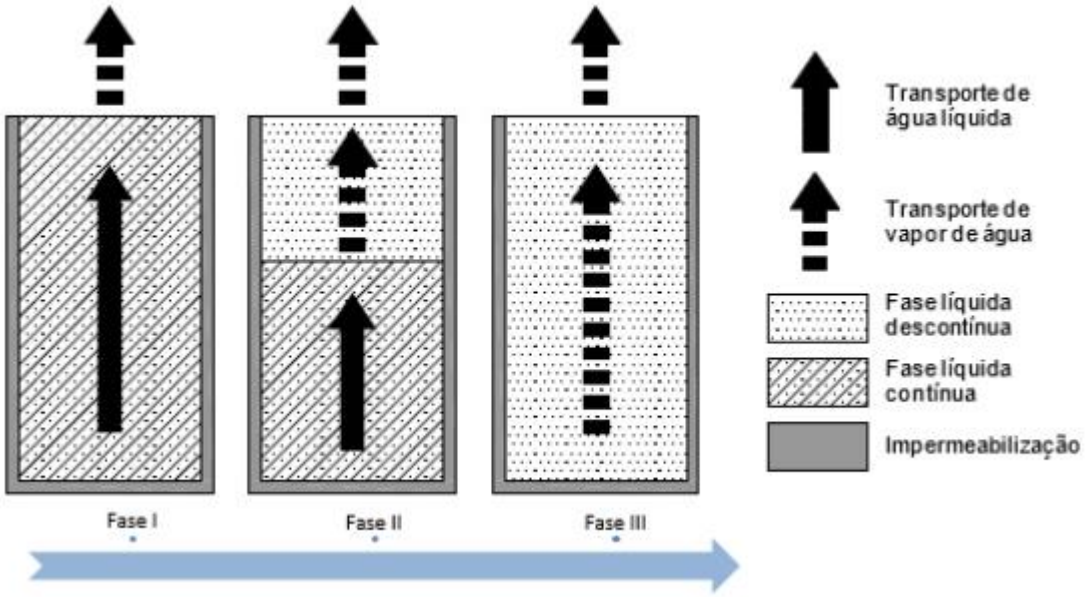

Source: REGO (2014)

2.1.5 Moisture transport across interfaces

The moisture transport across masonry is considered to be a governing parameter in several in several deterioration processes of masonry. Therefore, the study of moisture transport across the material interface is important to provide insight into the continuity between masonry wall layers.

Generically, three types of contact configurations can be considered in a multilayer wall, as illustrated in (Figure 9):

Figure 9 - Sketch of different contact configuration observed in building component.

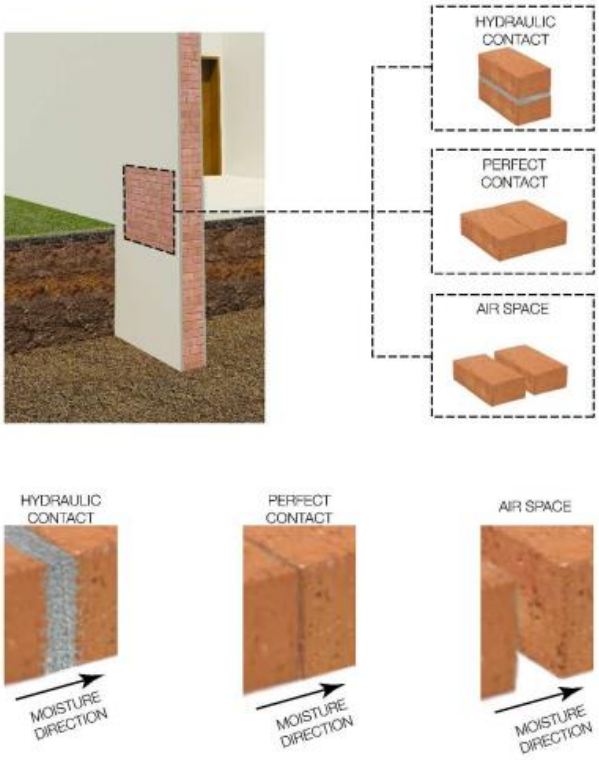

Source: AZEVEDO AC (2019)

The three configuration types observed were defined by (FREITAS, 1991) as follows:

‘Hydraulic continuity (Hydraulic Contact)’ when there is interpenetration both layers’ porous structure.

‘Perfect contact’ when there is contact without interpenetration of both layers’ porous structure.

‘Air space between layers’ when there is an air pocket a few millimeters wide.

Hydraulic continuity (Hydraulic Contact) occurs in situations where the second layer is applied over the first layer and there is penetration of this material into the first layer, during the curing process of the second layer material. A practical example of this setting is the contact between the brick and the fresh mortar.

Perfect contact corresponds to cases where two layers are superposed; even if the contact surface is perfect, there is no continuity of the porous structure and, consequently, there is a hydric resistance that disrupts the transmitted flows.

Air space between layers reflects the case where the two layers have no physical contact and there is a few millimeters thick space separating them. It is an existing configuration at the interface between layers in the walls of some buildings.

The idealization of the hydraulic contact is used by some programs, being known as perfect hydraulic contact. Where it is considered a perfect contact when there is even interpenetration between the layers. In these idealistic scenarios, the type of contact is known as a Perfect Hydraulic Contact.

However, Pel L. (1995) suggested that there is no perfect hydraulic contact between brick and mortar and that the moisture flux across the material interface is bound by maximum given by the hygric resistance of the interface (FREITAS, 1992). Hydric resistance is defined as the greater or lesser ease of water diffusion.

Afterwards, several hypotheses were given for the origin of such a resistance, like an imperfect contact between material layers or the presence of an interface zone in the mortar layer.

The absorption behavior of brick/cement masonry composites with different interfacial configurations, was studied by Derluyn et al.(2011) and Janssen et al. (2012) in order to explain the imperfect hydraulic contact at the brick-mortar interface. Their studies confirmed that interfacial effects were proportional to the water extraction from the mortar during curing.

Other causes for hydraulic resistance at the brick-mortar interface could be the presence of air cracks resulting from damage (cracking) or due to poor workmanship during application of the fresh mortar (C. Groot, 2010). Brocken (1998) concludes in his study that even if the application and curing conditions were optimal, a certain hydraulic resistance is expected due to the discontinuity of the pore structure between the materials.

However, few studies have been developed in this area, namely numerical simulation studies, which justifies the need for an extended study of moisture transport in multilayered walls, trying to understand the influence of the interface in this process.

2.1.5.1 Perfect hydraulic contact

A perfect hydraulic contact is characterized by the continuity of the macroscopic capillary pressure and the moisture flux across the interface (BEAR AND BACHMA, 1990):

$$P_{c,i}\left(\theta_{l,i}\right) = P_{c,ii}\left(\theta_{l,ii}\right) \quad (20)$$

Where the subscript i and ii refer to the material layers at both sides of the interface, P_c is the macroscopic capillary pressure of a pore, define as the pressure difference between the liquid phase and the gas phase ($P_c = P_l - P_g$) and θ_l is the volumetric liquid water content.

For different porous materials at both sides of the interface (Equation 20), these interface conditions result in a jump of the moisture content at the interface due to the difference in the moisture retention curve of the two materials (Equation 21).

$$\theta_{l,ii} = P_{c,ii}^{-1}\left(P_{c,i}\left(\theta_{l,i}\right)\right) = f\left(\theta_{l,i}\right) \quad (21)$$

Assuming that hysteresis can be neglected and, consequently, that the capillary pressure curve is a single-valued function, this relation between the moisture contents of the two materials is unique.

Illustration of perfect hydraulic contact (hydraulic continuity) across the interface of two porous material layers with different capillary pressure curves is show in (Figure 10); the capillary pressure is continuous across the interface (BROCKEN, 1998).

Figure 10 - Illustration of perfect hydraulic contact (hydraulic continuity) across the interface of two porous material layers with different capillary pressure curves.

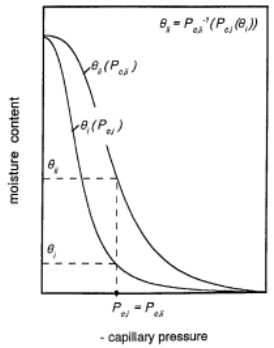

Source: BROCKEN (1998)

The moisture flux across such a material interface will be continuous (Equation 22):

$$q_i = q_{ii}$$

$$\rho_l D_{\theta,i}(\theta_{l,i})\frac{\partial \theta_{l,i}}{\partial x} = \rho_l D_{\theta,ii}(\theta_{l,ii})\frac{\partial \theta_{l,ii}}{\partial x} \qquad (22)$$

Where q is the macroscopic isothermal liquid water flux (kg/m^2·s) by Darcy`s law, as mentioned before, D_θ is the moisture diffusivity and ρ_l is the mass density of liquid water (kg/m^3).

If both materials are identical no influence of the interface will be observed when a water flow is crossing the interface and the governing moisture transport equation reduces to diffusion (Equation 23) for a monolithic material.

The total mass balance for moisture transport combining the water vapor content θv with liquid water content θ_l, written as (Equation 23):

$$\frac{\partial \theta}{\partial t} = \nabla(D_\theta \nabla \theta) \qquad (23)$$

Where, $D_\theta = D_{\theta,v} + D_{\theta,l}$ and $\theta = \theta_v + \theta_l$.

If $\theta_l > \theta_v$, the contribution of water vapor transport to the total moisture transport can be negligible. However, for the dry state of a material, this condition is generally not satisfied.

Since hysteresis effects are neglected, the moisture diffusivity, D_θ, is a single valued and continuous function of the moisture content. Usually the differential Equation (23) can simply be solved with numerical algorithms applied for modeling unidirectional moisture transport for either water absorption or drying.

2.1.5.2 Imperfect hydraulic contact

An imperfect hydraulic contact between two porous materials in (Brocken, 1998) studies, have the interface (having no hygroscopic capacity) characterized by a so-called ‘interface permeability’. This interface permeability is considered to be a

macroscopic parameter which may originate either from a discontinuity of the pore structure of the materials at their interface, called by 'natural contact', from an air space between the material layers, or from a combination of both phenomena. Interface permeability was defined as (Equation 24):

$$K_{if} = -\frac{q_{if}}{P_{c,ii}(\theta_{l,ii}) - P_{c,i}(\theta_{l,i})} \qquad (24)$$

Where K_{if} is the interface permeability and, q_{if} the moisture flux across the interface. Water transport is assumed to be from material i to material ii. Hence, during the moisture transport, a jump in the capillary pressure will occur across the material interface (Equation 25):

$$P_{c,ii}(\theta_{l,ii}) = P_{c,i}(\theta_{l,i}) - \frac{q_{if}}{K_{if}} \qquad (25)$$

As a result, the relation between the moisture contents of the two materials at their interface is not unique. Assuming that q_{if}/K_{if} is constant, two different relations exist depending on the direction of the moisture transport. From Figure 11 it is possible to see that the relations between the moisture contents of material i and ii also depend on the trend of the capillary pressure curves of both materials.

The resulting moisture across the material interface is written as Equation (26):

$$q_i = q_{ii} = q_{if}$$

$$\rho_l D_{\theta,i}(\theta_{l,i})\frac{\partial \theta_{l,i}}{\partial x} = \rho_l D_{\theta,ii}(\theta_{l,ii})\frac{\partial \theta_{l,ii}}{\partial x} = K_{if}\left(P_{c,ii}(\theta_{l,ii}) - P_{c,i}(\theta_{l,i})\right) \qquad (26)$$

Figure 11 - Illustration of imperfect hydraulic contact (hydraulic discontinuity) across the interface of two porous material layers with different capillary pressure curves.

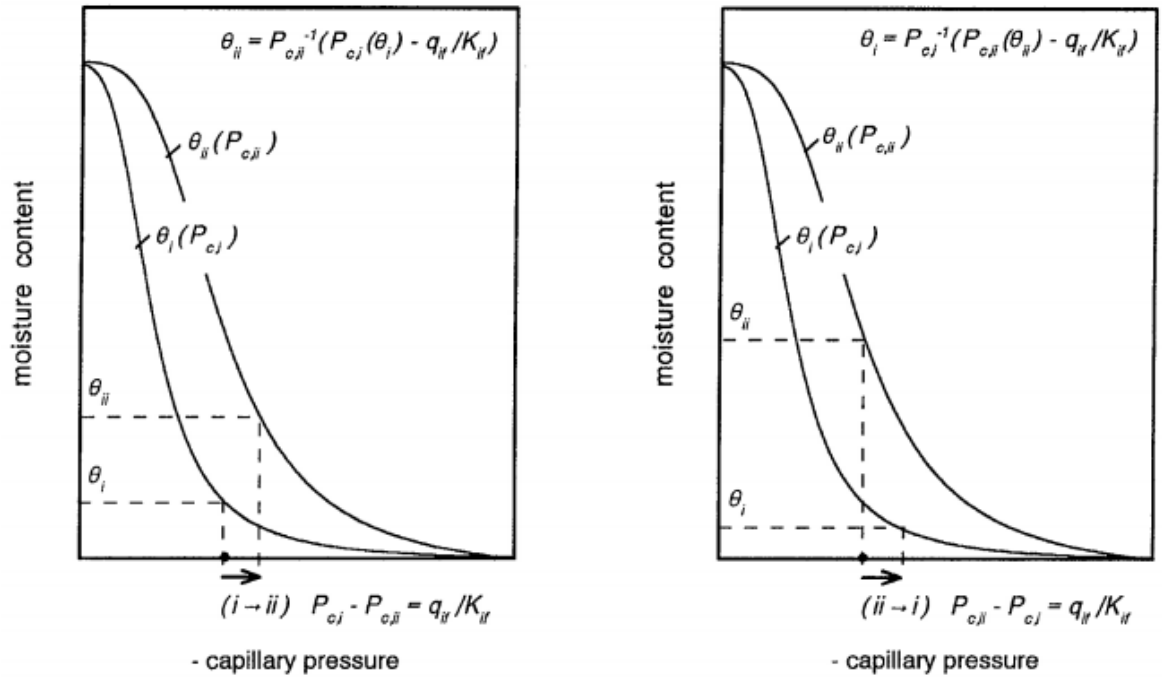

Source: BROCKEN (1998)

2.1.5.3 Air space between layers

An air space between two porous layers has the isothermal moisture flux over this space (with stagnant air) written as Equation (27) (BROCKEN, 1998):

$$q_{if} = -\delta_a \frac{\Delta p_v}{d} = -\delta_a p_{vs} \frac{\Delta h}{d} \qquad (27)$$

Where, δ_a is the water vapor permeability, d is the thickness of the air space, h is the relative humidity, p_v e p_{vs} represent the vapor pressure and the saturation vapor pressure respectively, and v_l and v_v are the molar volume of liquid water and water vapor respectively. The flux moisture flux (Equation 28) can be rewritten using Kelvin's Equation (11):

$$q_{if} = -\frac{\delta_a p_{vs}}{d} \left(\exp\left(\frac{v_l P_{c,ii}(\theta_{l,ii})}{RT} \right) - \exp\left(\frac{v_l P_{c,i}(\theta_{l,i})}{RT} \right) \right) \qquad (28)$$

The interface permeability resulting from the air space configuration will depends on the thickness of the air space between the material layers and the trend of the capillary pressure curves is variable. The Equation (29) show the interface permeability resulting from an air space between two material layers, where the thickness of the air space is a constant value.

$$K_{if} = -\frac{\frac{\delta_a p_{vs}}{d}\left(\exp\left(\frac{v_l P_{c,ii}(\theta_{l,ii})}{RT}\right) - \exp\left(\frac{v_l P_{c,i}(\theta_{l,i})}{RT}\right)\right)}{P_{c,ii}(\theta_{l,ii}) - P_{c,i}(\theta_{l,i})} \qquad (29)$$

Figure 12 - Schematic representation of imperfect hydraulic contact resulting from an air space of thickness d between materials layers.

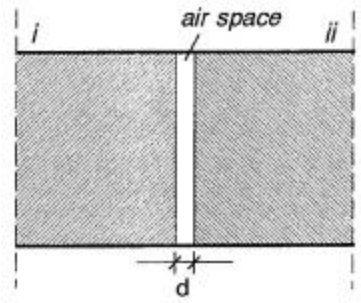

Source: BROCKEN (1998)

An air space between two porous layers leads to a discontinuity in the moisture profile by a one-dimensional free water imbibition test (de Freitas et al, 1996): The free water level in contact with the first layer and the moisture content will evolve to the capillary moisture content of the porous material while the moisture content of the other layer will evolve to a hygroscopic moisture equilibrium by water vapor transport over the air layer interface from the first to the second material layer.

2.2 MOISTURE TRANSFER COMPUTER SIMULATION PROGRAMS

Moisture problem is one of the most important factors related to the performance of the building (GUIMARÃES et al., 2018). Evaluating the moisture behavior in the building envelope is important to avoid the damage caused by moisture accumulation in the building envelope which can cause structural and physical problems for the building.

The first models developed to analyze moisture transport were focused on the analysis of porous soils. Lewis (1921), Richards (1931), Phillip and DeVries (1957) and Luikov (1966) elaborated the first phenomenological models to characterize transport in unsaturated porous media. The first coupled HAM model was instituted by Philip and De Vries in 1957. The model has as a function of temperature soil moisture transport and the main driving forces considered for its penetration are temperature and volumetric water content. Luikov's model presented a descriptive study for the estimation of MAP transport on the macroscopic scale in capillary porous media. Whitaker (1977) developed a detailed theory describing each phase of the transport equations in the year 1977. This assisted in the development of the first technique designed to assess moisture in building materials in the 1980s, known as the Glaser method. Pedersen (1992) and Kunzel (1995) developed more complete models that take into account the transport of liquids and diffusing vapors. The model is based on Kiebl's theorem, and was based on experimental work to simplify the models and the determination of the transfer coefficients. Mendes et al. (1999) developed a model based on the Philip and DeVries model. The developed model predicts heat and moisture transfer through porous building elements as well as complex configuration cases such as multilayer walls (MENDES et al., 2002).

Hygrothermal simulations in the field of building physics are widely used to predict the hygrothermal performance of building materials, components, and entire buildings. The available tools vary in their degrees of mathematical sophistication and runtime requirements, i.e., based on different mathematical models (physical descriptions), use different driving potentials, and use different numerical methods for space and time discretization. Thus, the tools have different potentials, strengths and weaknesses, for example, the ability to include air transfer (LANGMANS et al., 2012), 2D or 3D

phenomena (RUISINGER et al., 2020), or the ability to simulate a large number of zones in a reasonable runtime (ASPHAUG; TIME; KVANDE, 2021).

The main difference considered in studying moisture transport with hygrothermal models for porous building materials and envelopes is the moisture migration conduction potential. The moisture conduction potentials used in hygrothermal models in the existing literature include water vapor partial pressure, moisture content, capillary pressure, relative humidity, and air moisture content. (CHANG et al., 2020). This variety of models encompassing different methods and input and output parameters makes it challenging to seal the most suitable tool for studying a specific problem.

Computational fluid dynamics (CFD) is the main numerical simulation approaches used in the moisture transport analyses. The CFD approach, focuses on the numerical meshing of the entire building component volume into small elements or volumes, which results in a large computing load, particularly for unsteady states simulations.

The mathematical model of this system is consist in a set of partial differential equations (PDEs) for describing the laws of physics (the conservation of momentum, mass, and energy) for the space and time-dependent descriptions (HENS, 2020).

The mathematical model can consist of one or several PDEs (describing the relevant laws), together with boundary and initial conditions. Normally, the right-hand side of the PDE represents the transfer of heat and moisture, as quantified by different material properties and different potentials. The left-hand side represents the storage (HENS 2007). The solution to the PDEs is represented by dependent variables (e.g. temperature fields, RH fields, or velocity fields) described in space and time along the independent variables x, y, z, and t.

For building envelopes, the current challenge for hygrothermal models is to consider the discontinuity at the interface between material layers in multilayered walls.

2.2.1 Simulation programs with wider applicability

In a recent study by (VERMA et al., 2022) was highlighted the utilization of some major simulation tools in the literature studied for hygrothermal dynamics for developing energy-efficient buildings, considering building materials (Figure 13).

Figure 13 - Utilization of different tools in hygrothermal analyzing.

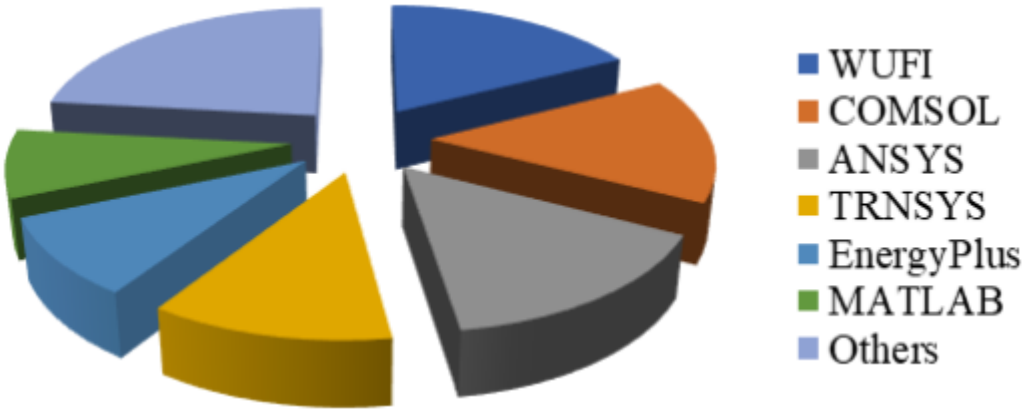

Source: VERMA et al. (2022)

An accurate hygrothermal model is essential to improve and evaluate the moisture transport. The types model interesting to know in this is study are based on physical knowledge of the system and energy balance equations. These are often obtained through energy simulation software such as TRNSYS, EnergyPlus, WUFI, COMSOL Multiphysics. However, as all model, for such models exists disadvantages. M. H. Benzaama et al. (2020) worked out a comparative study and presented drawbacks like: (i) such models often require a great large set-up and computation time. (ii) involve a lot of inputs to define the model, such as the composition of the building envelope. In some studies, it is difficult, if not impossible, to recover this input.

The commercially available tools WUFI® Pro and 2D (applying the PDEs described in Kunzel, (1997)) is widely used by researchers to investigate the heat and moisture performance of building components.

WUFI was the program used in this study and will be described extensively in section 3.2.1 as it being the specialized tool for studying hygrothermal performance is used

most, while Ansys and EnergyPlus due to their wider range of applicability are gaining the attention of users. However, there is a diverse range of tools and each of them is having typical utilization.

COMSOL Multiphysics® is a simulation platform that provides fully coupled multiphysics and single-physics modeling capabilities. Its originates from partial differential equation (PDE) Toolbox of MATLAB. Since it officially named COMSOL Multiphysics in 2003, it has been absorbing new calculation methods and techniques, and also extending new application modules.

The software based on finite element analysis, which has a large set of functions for analyses and solution. It includes heat transfer module, electromagnetic module, acoustics module, earth science module, chemical engineering module and structural mechanics module.

The platform provides two kinds of operation modes, graphical user interface style, and command style by creating scripts. Both modes provide convenience for users mostly (SUN et al., 1991). Script mode is mainly for optimum design and second development for COMSOL Multiphysics. The software includes three sections. Pre-process, solution, and post- process. Creating finite element model and setting load parameters are belonging to pre-processing. Mesh division and solving equations are all belong to solution section. Results visualization and analysis are belong to post- processing (WANG et al., 2011)

The Model Builder includes all of the steps in the modeling workflow — from defining geometries, material properties, and the physics that describe specific phenomena to solving and postprocessing models for producing accurate results. According to the comsol.com/comsol-multiphysics website (as of February, 2022).

ANSYS is a general-purpose finite-element modeling package for numerically solving a wide variety of mechanical problems. These problems include static/ dynamic, structural analysis (both linear and nonlinear), heat transfer, and fluid problems, as well as acoustic and electromagnetic problems. In general, a finite-element solution may be broken into the following three stages (NAKASONE; YOSHIMOTO; STOLARSKI, 2006).

(1) Preprocessing: defining the problem

The major steps in preprocessing are: (i) define keypoints/lines/areas/volumes, (ii) define element type and material/geometric properties, and (iii) mesh lines/areas/ volumes as required. The amount of detail required will depend on the dimensionality of the analysis, i.e., 1D, 2D, axisymmetric, and 3D.

(2) Solution: assigning loads, constraints, and solving

Here, it is necessary to specify the loads (point or pressure), constraints (translational and rotational), and finally solve the resulting set of equations.

(3) Postprocessing: further processing and viewing of the results

In this stage one may wish to see (i) lists of nodal displacements, (ii) element forces and moments, (iii) deflection plots, and (iv) stress contour diagrams or temperature maps.

TRNSYS [Klein et al., 2007] is a transient system simulation environment with a modular structure that allows independent components, consisting of validated mathematical models representing individual components in an energy system, to be joined together based on (real life) scenarios to produce an output based on the model requirements. TRNSYS also allows the user to link to external programs for further analysis of results (e.g. Microsoft Excel, MATLAB).

According to the trnsys.com website (as of February, 2022) TRNSYS is made up of two parts. The first is an engine (called the kernel) that reads and processes the input file, iteratively solves the system, determines convergence, and plots system variables. The kernel also provides utilities that (among other things) determine thermophysical properties, invert matrices, perform linear regressions, and interpolate external data files. The second part of TRNSYS is an extensive library of components, each of which models the performance of one part of the system. The standard library includes approximately 150 models ranging from pumps to multizone buildings, wind turbines to electrolyzers, weather data processors to economics routines, and basic HVAC equipment to cutting edge emerging technologies. Models are constructed in such a

way that users can modify existing components or write their own, extending the capabilities of the environment.

Steeman et al. [62] used the coupling heat, air and moisture transfer (HAM) in porous materials within the Building Energy Simulation tool TRNSYS with implicit time discretization scheme. The developed coupled model is flexible and is able to simulate multilayered walls with variable boundary conditions in real building application modeling.

Building energy simulation softwares like TRNSYS and EnergyPlus are mainly used to simulate temperature variations and energy demands in specific spaces at a large scale (DJEDJIG et al., 2015). As a result, moisture exchange models at the wall scale were used in these tools using a simplified model that neglects the coupling of heat and moisture transfer phenomena through the building envelope (PREUSS, 2015).

EnergyPlus is a whole building energy simulation program that engineers, architects, and researchers use to model both energy consumption—for heating, cooling, ventilation, lighting and plug and process loads—and water use in buildings. Some of the notable features and main capabilities of EnergyPlus include: Heat balance-based solution of radiant and convective effects that produce surface temperatures, thermal comfort, and condensation calculations; Combined heat and mass transfer model that accounts for air movement between zones; Functional Mockup Interface import and export for co-simulation with other engines; Transient heat conduction through building elements such as walls, roofs, floors, etc. using conduction transfer functions; Thermal comfort models based on activity, inside dry-bulb temperature, humidity, etc. (CRAWLEY et al., 2001).

MATLAB is a high-level technical computing language and interactive environment for algorithm development, data visualization, data analysis, and numerical computation. Using MATLAB, you can solve technical computing problems faster than with traditional programming languages, such as C, C++, and Fortran. Millions of engineers and scientists worldwide use MATLAB® to analyze and design the systems and products. The matrix-based MATLAB language is the world’s most natural way to express computational mathematics. Built-in graphics make it easy to visualize and gain insights from data. The desktop environment invites experimentation, exploration,

and discovery. These MATLAB tools and capabilities are all rigorously tested and designed to work together. MATLAB code can be integrated with other languages, enabling the users to deploy algorithms and applications within web, enterprise, and production systems, according to the mathworks.com website (as of February, 2022).

Among the other programs used, the following have been chosen as interest programs that are commonly used in moisture transfer studies.

Delphin 5 is a commercial two-dimensional numerical simulation program for the transport of heat, air, moisture, pollution and salt transport in porous building materials. This program can be used to simulate mass and energy transport processes for user-defined climatic conditions or real climates (temperature, relative humidity, incident rainfall, wind speed and direction, longwave and shortwave radiation) (NICOLAI, 2007).

MOISTURE-EXPERT is a one or two-dimensional numerical modeling software of heat, air and moisture transport in building construction systems. The program is basically software developed by Oak Ridge National Laboratory and the Fraunhofer Institute for Building Physics to adapt the original European version of the WUFI software for the US and Canada. The model handles vapor and liquid transport separately. The moisture transport potentials are vapor pressure and relative humidity, and the energy transport potential is temperature. The model includes the ability to handle absorption and adsorption isotherms, temperature dependent, and transport properties as a function of drying or humidification processes. It can be considered as a disadvantage for use, but as an advantage in the accuracy of the results, the fact that the program is highly complex, typically requiring more than 1000 inputs for the one-dimensional simulations. The inputs include outdoor weather conditions, indoor weather conditions, material properties, and system characteristics (KARAGIOZIS, 2001).

2.2.2 Common limitations in mathematical models

Engineers who use finite element analysis must understand the limitations of the finite element procedures. There are numerous circumstances that can degrade the quality of a calculation or even render it worthless.

There are various sources of error that can contribute to incorrect results (“Finite element analysis—theory and application with ANSYS”, 1999). They include:

1. Wrong input data, such as physical properties and dimensions. This mistake can be corrected by simply listing and verifying physical properties and coordinates of nodes or keypoints (points defining the vertices of an object) before proceeding any further with the analysis.
2. Selecting inappropriate types of elements. Understanding the underlying theory will benefit you the most in this respect. You need to fully grasp the limitations of a given type of element and understand to which type of problems it applies.
3. Poor element shape and size after meshing. This area is a very important part of any finite element analysis. Inappropriate element shape and size will influence the accuracy of your results. It is important that the user understands the difference between free meshing (using mixed-area element shapes) and mapped meshing (using all quadrilateral area elements or all hexahedral volume elements) and the limitations associated with them.
4. Applying wrong boundary conditions and loads. This step is usually the most difficult aspect of modeling. It involves taking an actual problem and estimating the loading and the appropriate boundary conditions for a finite element model. This step requires good judgment and some experience.

Many hygrothemal analysis tools require a building model to be created specifically for that tool, often graphically but sometimes via text input. (MURRAY et al., 2009)

The complex hygrothermal processes in a building component need to be simplified to make their simulation accessible to present-day computers.

With the vast number of hygrothemal analysis tools available and with their varying capabilities, it is often to find studies using different tool because of the limitations found

according to the models. Any software has its share of limitations, requires a certain skill level, and the user must be aware of what the model can and cannot do.

Common limitations in mathematical models include:

- Effects associated with phase change, liquid to ice, are neglected.
- Climatic load due to driving rain is simplified; Wind-driven rain is an approximation of surface wetting.
- No hysteresis is accounted for; Hysteresis of the moisture retention curve is not taken into account.
- No chemical reactions are considered.
- Ageing effects or changes in the geometrical dimensions are neglected.
- Deformation of the porous structure caused by the ice content changes is neglected.
- The interface between two capillary-active materials is treated as ideally.
- No user-friendly interface for inputting data.
- Limited material properties are currently available; A limited number of laboratory benchmarking tests have been performed, none with field data.

CHAPTER 3. COMPUTATIONAL MODELING PERFORMED

3.1 INTRODUCTION

In this chapter it is possible to understand the functionality of the WUFI-2D program that was used in this study to simulate moisture transport in samples with different contact configuration between the materials. Characteristic information of the simulations performed in this study was also provided.

The simulations performed in this work aim to analyze the influence of the interface in the different types of contact - perfect hydraulic contact between mortar and brick and the air gap between brick layers - on moisture transport, through the verification of moisture content profiles obtained with the simulations performed. Also, it is intended to briefly compare the results of moisture content profiles obtained in the experimental study of (AZEVEDO AC.,2019) and the numerical simulations performed in WUFI-2D, in order to contribute to the experimental validation and also analyze the influence of the interface in the hydraulic contact. For this purpose, the same material properties, initial conditions and boundary conditions of the experimental study were used in the execution of the simulations.

The mathematical model used in WUFI-2D has as a potential conductor for the capillary moisture transport the relative humidity, which is continuous in multi-layered building components, i.e. continuous across material independent material boundaries. This is why the hydraulic contact configuration is considered as perfect, with no consideration of the second layer material penetrating into the first layer and the porous network discontinuity at the interface, thus treated as ideal between two active capillary materials for the contact condition of the configurations in the simulations performed.

Although the mechanisms of moisture transport in a single building material have been and continue to be widely studied, the hydraulic characteristics of the interface at different types of contacts between materials are still poorly understood and, for this reason, the simplified assumption of perfect contact is widely used in hygrothermal models. However, compared to a monolithic element, the multilayer element exhibits

delayed liquid transport across the interface between the layer materials (Azevedo, 2019).

3.2 METHODOLOGY

3.2.1 WUFI-2D

For the purpose of this study, the moisture performance simulation model WUFI 2D v.4.2, which is a windows based program for the hygrothermal analysis of building envelope and components constructions, is selected. WUFI (Warme und Feuchte instationar - Transient Heat and Moisture) is a one-dimensional, two-dimensional or 3D model for heat and moisture transport developed by the Fraunhofer Institute in Building Physics (IBP) in Holzkirchen, Germany. Which can be used to assess the heat and moisture distributions for a wide range of building material classes and climatic conditions.

The program requires only the standard material properties and allows the determination of moisture storage and liquid transport functions. It was validated through in situ and laboratory data, allowing a realistic simulation of the hygrothermal behavior of building elements, monolithic or multilayer, exposed to real climatic conditions.

The two-dimensional analysis performed by the WUFI-2D program is based on the finite-volume method, allowing the modeling of building elements with complex geometries (FREITAS, 2008).

3.2.1.1 The Calculation Model of the simultaneous heat and moisture transport

The mathematical model used in WUFI was developed by Kunzel (1995) based on Kiebl's theorem. In this model the non-steady heat and moisture transport processes in building components are described by the following coupled differential equations for heat transport (Equation 30) and moisture transport (Equation 31):

$$\frac{\partial H}{\partial v}\frac{\partial v}{\partial t} = \frac{\partial}{\partial x}\left(\lambda\frac{\partial v}{\partial x}\right) + h_v\frac{\partial}{\partial x}\left(\frac{\delta}{\mu}\frac{\partial p}{\partial x}\right) \qquad (30)$$

$$\rho_w \frac{\partial u}{\partial \varphi}\frac{\partial \varphi}{\partial t} = \frac{\partial}{\partial x}\left(\rho_w D_w \frac{\partial u}{\partial \varphi}\frac{\partial \varphi}{\partial x}\right) + \frac{\partial}{\partial x}\left(\frac{\delta}{\mu}\frac{\partial p}{\partial x}\right) \qquad (31)$$

Where,

D_w [m²/s] -	Liquid transport coefficient
H[J/m³] -	Enthalpy of moist building material
h_v [J/kg] -	Evaporation enthalpy of water
p [Pa] -	Water vapor partial pressure
u [m³/m³] -	Water content
δ [kg/msPa] -	Water vapor diffusion coefficient in air
v [°C] -	Temperature
λ [W/mK] -	Heat conductivity of moist material
μ [-] -	Vapor diffusion resistance factor of dry material
ρ_w [kg/m³] -	Density of water
φ [-] -	Relative humidity

The left-hand sides of both equations consist of the storage terms. Heat storage comprises the heat capacity of the dry material and the heat capacity of the moisture present in the material. Moisture storage is described by the derivative of the moisture storage function mentioned above. On the righ-hand side of the equations we find the transport terms. Heat transport is the sum of moisture-dependent thermal conductivity and vapor enthalpy flow. This heat transport by vapor enthalpy flow is due to water evaporating in one place and thereby absorbing latent heat from this place, and then diffusing to a different place, condensing there and releasing latent heat. This kind of heat transport is often called latent heat effect. Liquid transport (through surface diffusion and capillary conduction, both due to a gradient of relative humidity) shows only a relatively minor temperature dependence. Vapor diffusion, on the other hand, is strongly affected by the temperature field, since the saturation vapor pressure increases exponentially with temperature. The differential equations are discretized by means of an implicit finite volume method and are iteratively solved according to the scheme described by the flow chart shown in Figure 14. The accuracy of the numerical solution depends on the mesh widths of the numerical grid, the size of the time steps and the choice of the convergence criteria. Usually the numerical solution is sufficiently accurate, so that the effect of numerical parameters can be ignored in comparison with the effects of the physical parameters like material and climate data. After the

calculation the result should be critically assessed in order to exclude user errors or severe convergence errors. Convergence errors are indicated by WUFI, and their effect is assessed by a comparison of the sum of the moisture flows with the water accumulated in the component. False input or unrealistic material data can only be controlled by plausibility checks. According to the wufi-wiki website (as of February, 2022).

Figure 14 - Flow chart for the WUFI model.

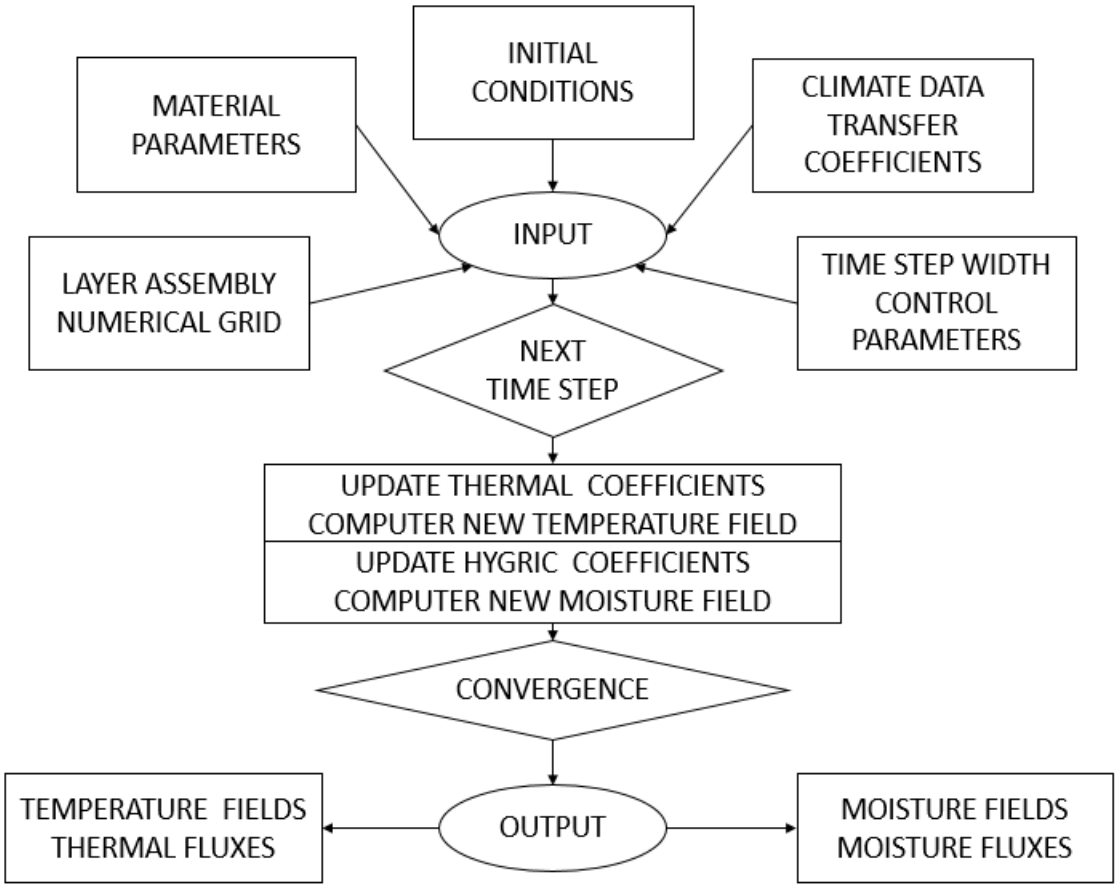

SOURCE: wufi-wiki website (2022) ADAPTED.

3.2.1.2 Program running

3.2.1.2.1 Program structure

- The Main Window of WUFI 2D

On starting the program, the main window opens as shown in Figure 15. This window summarizes all the menus and dialogs in a convenient way for the user to access the individual elements.

Figure 15 - The Main Window of WUFI 2D.

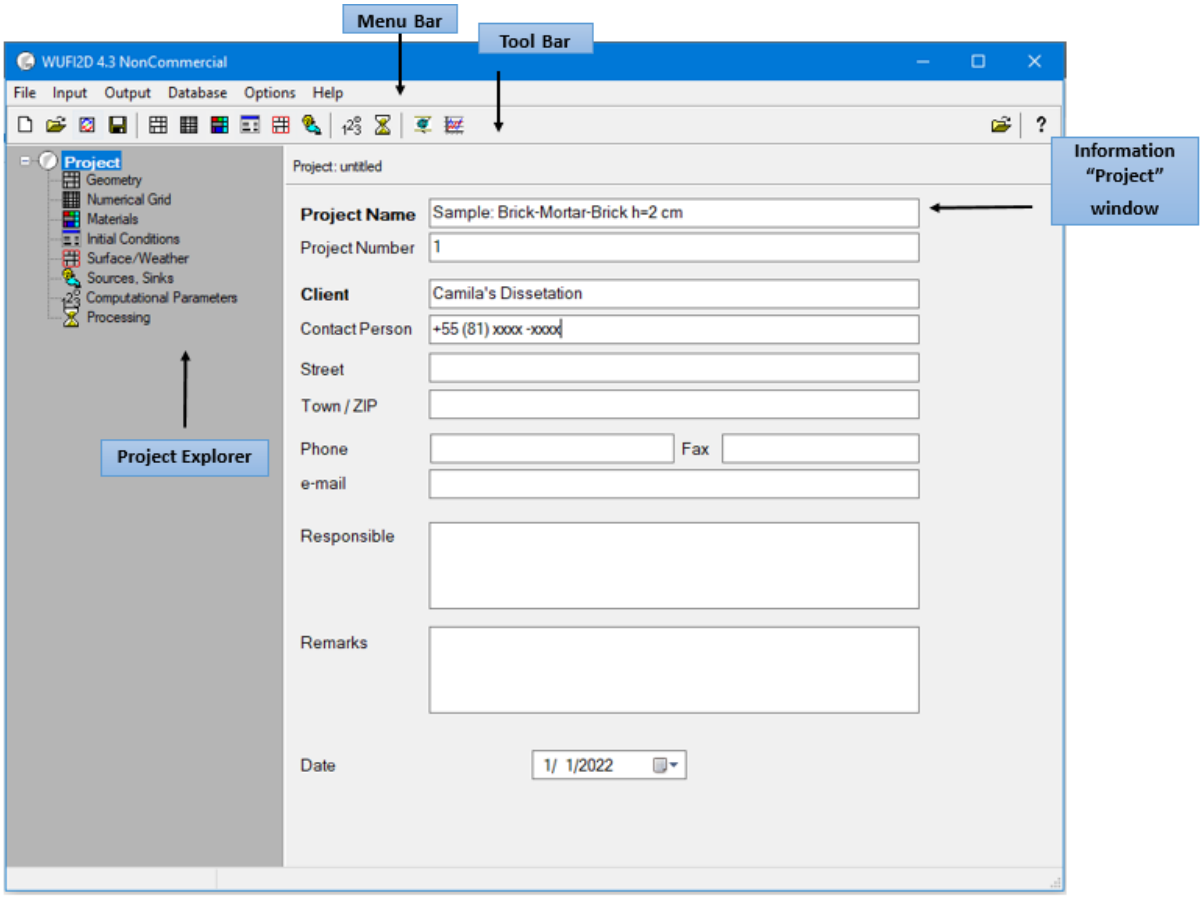

Source: Author.

Menu bar: Locates the program's menu collection containing submenus and commands.

Tool bar: locates frequently used commands, allowing for quicker access.

Project explorer: This is an alternative to the "Input" menu on the menu bar, allowing quick and ready access to the various input dialogs.

Information "Project": This is an optional dialog that serves as a notebook about the project.Barra de menu: loca a coleção de manu do programa aonde se encontram submenus e comandos.

- The Menu Bars of WUFI 2D

The menu bar contains the six menus, as shown in the Figure 16.

Figure 16 - The Menu Bars of WUFI 2D.

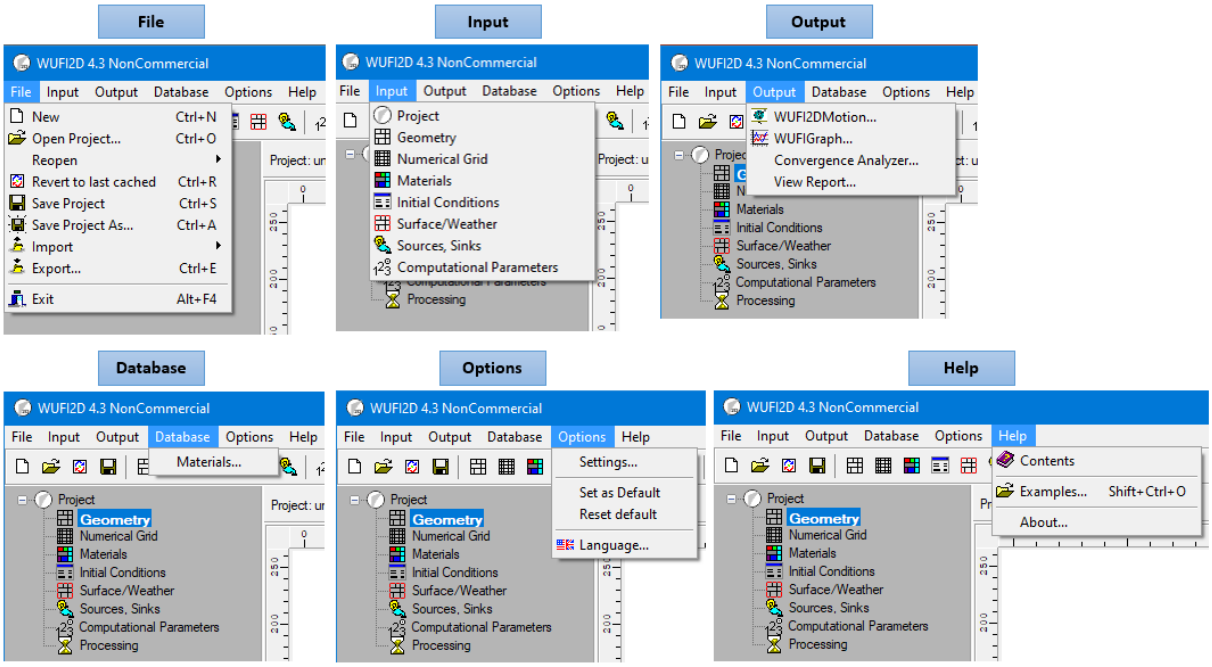

Source: Author.

File: The "Open" and "Save" commands always access the respective project (existing or new) directory, not individual files, as the project consists of several files which reside all in a common directory.

Input: Specify the construction geometry and the numerical grid of the building component. Assign material data to the different elements of the building component. Specify the temperatures and moisture contents existing in the different materials at the start of the calculation. Assign surface coefficients and climatic boundary conditions to the different surface segments of the component. Fine-tune the way the calculation is performed through computational Parameters. Start the calculation through processing command.

Output: Visualizes the results of the calculation/modeling.

Database: Opens the material database. it is also possible to add and edit the new materials database.

Options: Edit some basic settings of the program. Define the current project as the default project or Reset de default definition.

Help: Displays the contents list of the online help. Provides quick access to the different help topics and Info about WUFI 2D.

3.2.1.2.2 Simulation execution

- Input

- Define the geometry of the building component:

Figure 17 - Item "Geometry".

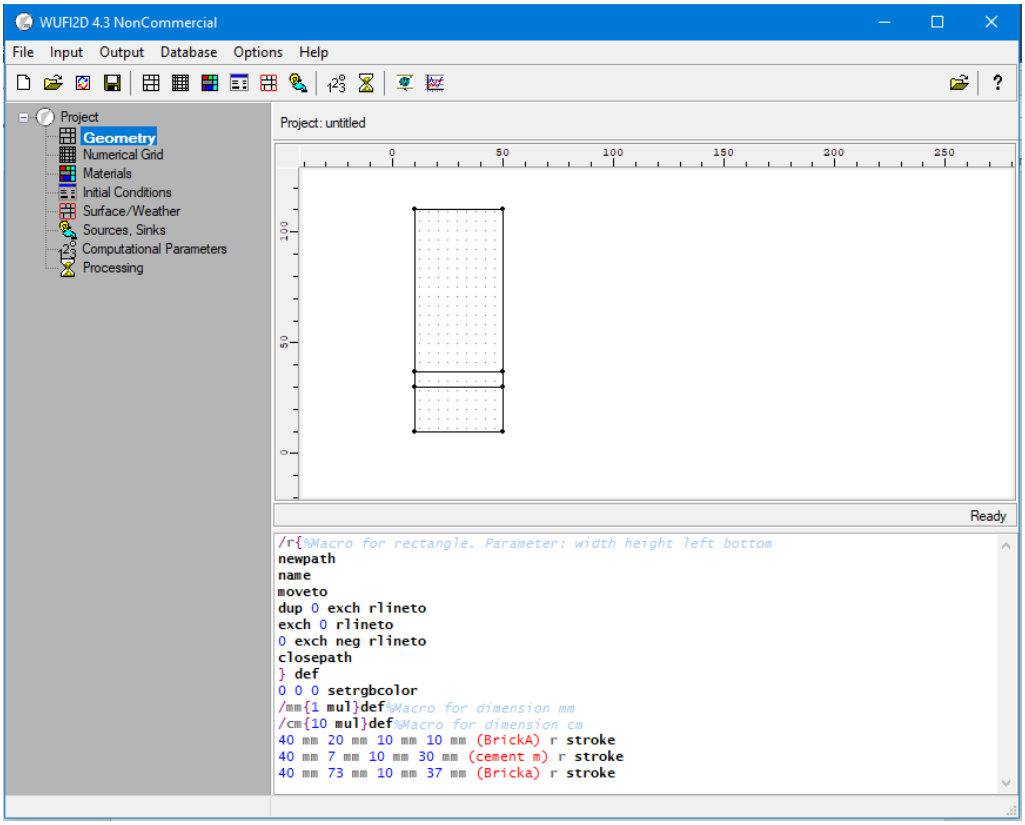

Source: Author.

The graphical interface (Figure 17) is used to build up the component from rectangular elements. Each material is drawn as an individual rectangle and located via coordinates.

- Automatic numerical grid for the component:

As soon as the dialog panel "Grid" is opened, WUFI 2D's automatic grid generator creates a numerical grid for the component. For all geometry created the program generate a sufficient automatic grid, but in this work, as the geometry are simple, it was increased to the maximum number of elements to 150 in x-direction and to 150 in

y direction, for working with a finer grid (see Figure 18). The numerical solver of WUFI 2D works most reliably if the grid is as fine as possible because here steeper temperature and moisture profiles are to be expected.

Figure 18 - Item "Grid".

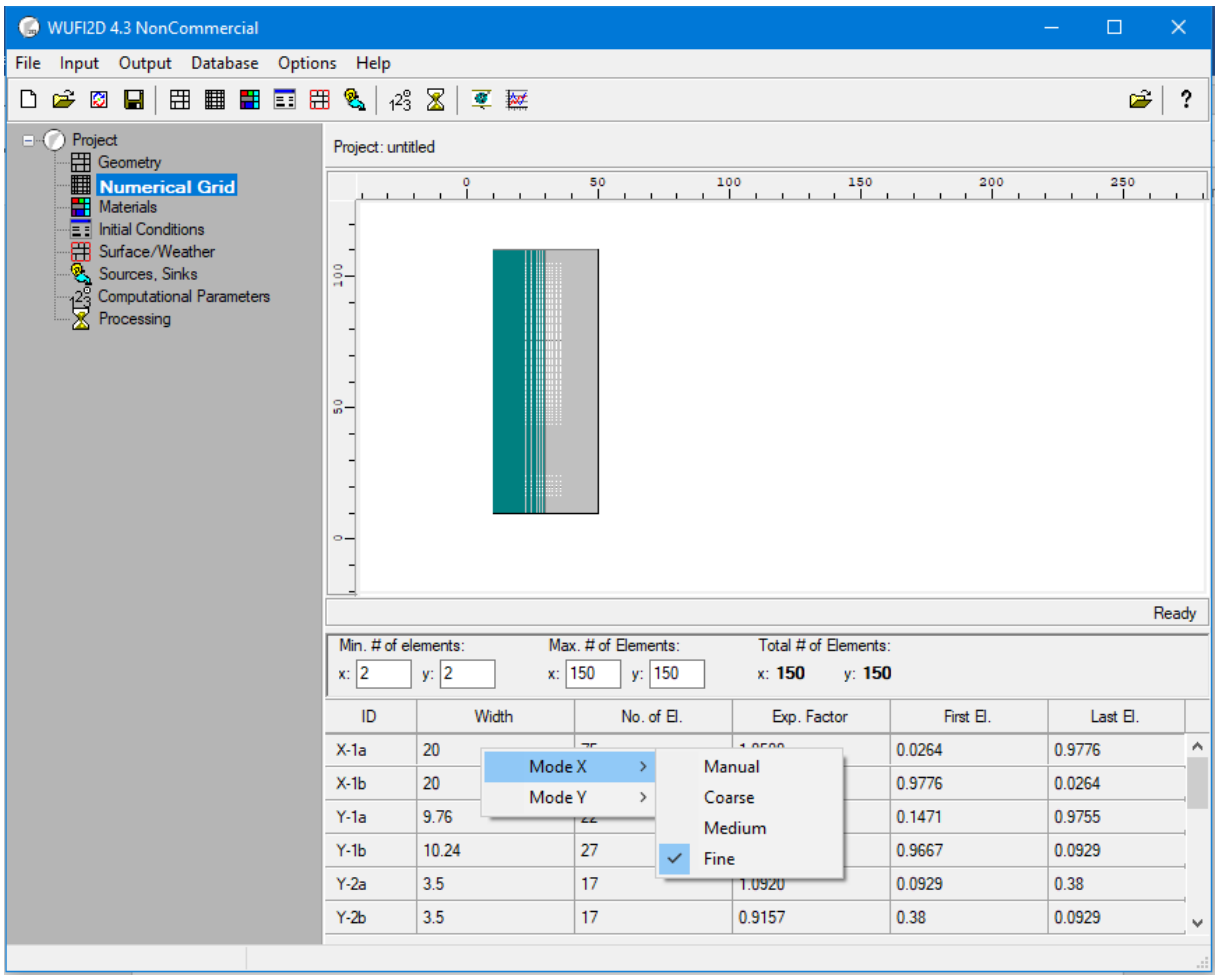

Source: Author.

- Material properties:

The Materials dialog box allocates the material properties to each element layer. The allocation of material properties to the component layer can be either by selecting a material from the program's database or by creating a new material entering the material properties into the program's database. Figure 19 shows the dialog box for the allocation of properties, which gives access to the database and the insertion of new properties and also shows the data box of the material allocated for a given layer.

The input of the hygroscopic curves for new materials can be done by entering the materials' adsorption curve or by entering the saturation moisture content (wsat) and the moisture content for 80% relative humidity (w80) of the material. Through these two values the program provides the hygroscopic behavior for most building materials.

The suction liquid transport coefficients (Dws), describes the absorption of water when the surface is completely wet (in the presence of rain), and the redistribution liquid transport coefficient (Dww), which describes the redistribution of absorbed water after the liquid water disappears from the surface (migration of moisture in the absence of rain) are estimated by the program from the basic material properties.

Figure 19 - Item "Material".

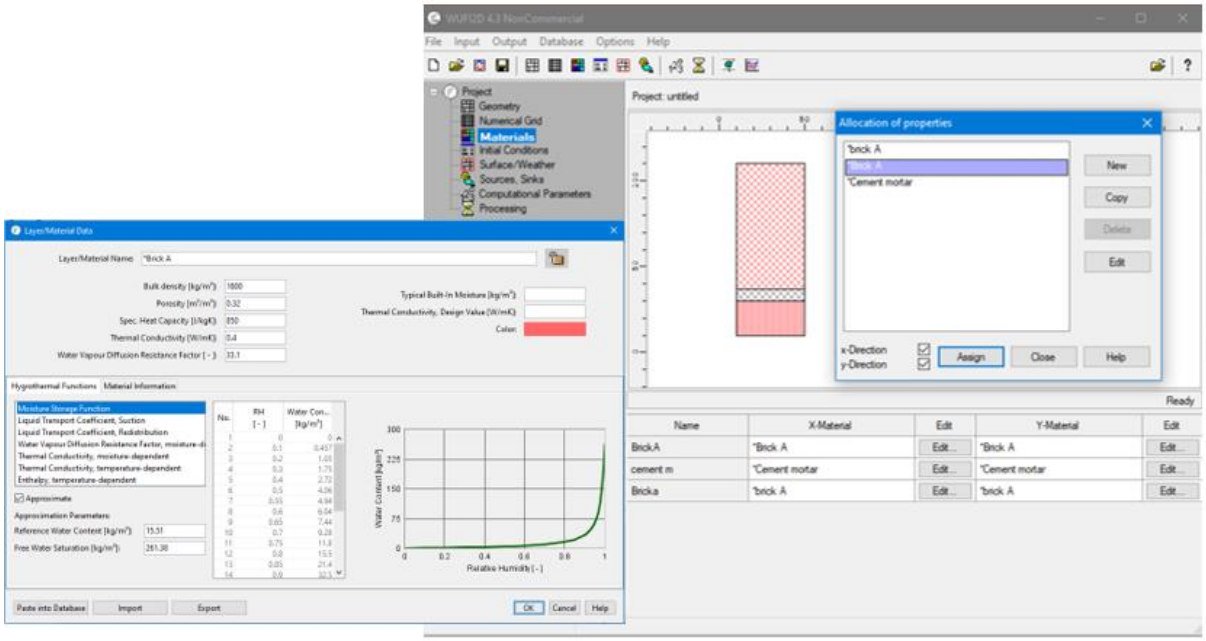

Source: Author.

The basic properties required to be defined for the simulation are as shown in Table 2.

Table 2 - Material properties required WUFI-2D.

Properties	Units
Bulk density, ρ	[kg/m³]
Porosity, ε	[m³/m³]
Specific heat capacity, C	[J/kgK]
Thermal conductivity (Dry), λ	[W/mK]
Water vapor diffusion resistance factor, μ	[-]
Moisture Content, w80% - for 80% relative humidity	[kg/m³]
Moisture Content, wsat - Free water saturation	[kg/m³]
Water absorption coefficient	[kg/m²√s]

Source: Author.

- Initial Conditions:

For each material assigned to the component, you can specify the initial temperature and the initial water content or relative humidity in the initial conditions dialog. The predefined initial temperature of 20 °C within the whole component will usually be good enough, considering that the thermal conditions of a building component usually adapt very quickly to the boundary conditions.

- Boundary Conditions (Surface/weather):

The data needed to define the boundary conditions are specified in the next dialog boxes descriptions.

The conditions for the segments of the component surfaces should be defined, and they can be treated as exposed to external weather, internal weather, or as adiabatic (i.e. no heat or moisture can flow through them). In this paper we aim to study one-dimensional transport (across a single surface) and therefore the surfaces are considered to be adiabatic. Only the base surface will be exposed to an indoor climate, in which we will use a rain climate file to provide the water that will be transported across the surface, simulating a soaking test (See Figure 20).

Figure 20 - Item "Surface/weather".

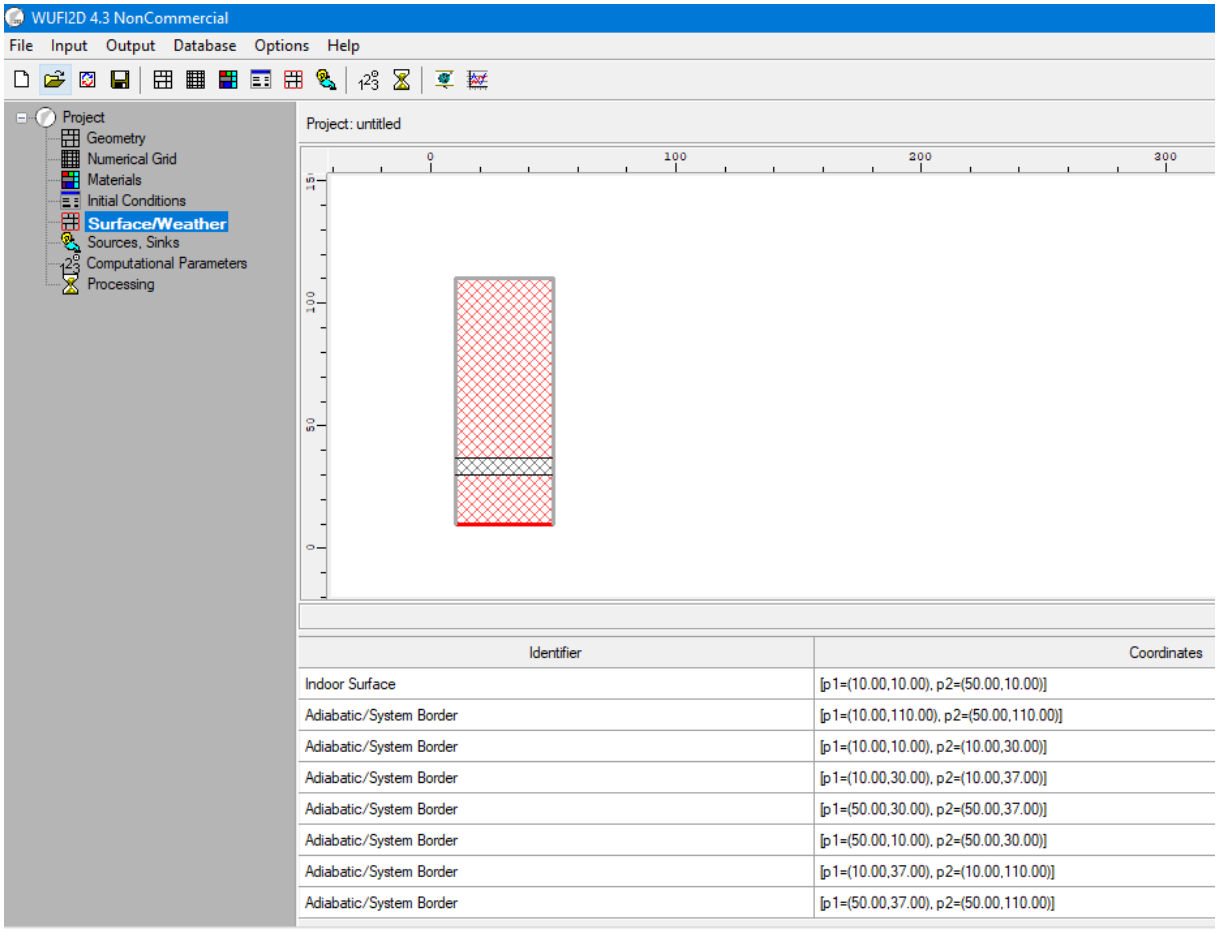

Identifier	Coordinates
Indoor Surface	[p1=(10.00,10.00), p2=(50.00,10.00)]
Adiabatic/System Border	[p1=(10.00,110.00), p2=(50.00,110.00)]
Adiabatic/System Border	[p1=(10.00,10.00), p2=(10.00,30.00)]
Adiabatic/System Border	[p1=(10.00,30.00), p2=(10.00,37.00)]
Adiabatic/System Border	[p1=(50.00,30.00), p2=(50.00,37.00)]
Adiabatic/System Border	[p1=(50.00,10.00), p2=(50.00,30.00)]
Adiabatic/System Border	[p1=(10.00,37.00), p2=(10.00,110.00)]
Adiabatic/System Border	[p1=(50.00,37.00), p2=(50.00,110.00)]

Source: Author.

Surface Coefficients

Indoor surface: This option specifies the surface as an interior (room-side) surface. WUFI 2D automatically computes the surface transfer coefficient for vapor flow from the surface transfer coefficient for heat flow (unless overridden, see below), and the details of this computation depend on whether the surface is an interior or an exterior surface (See Figure 21).

Sd-value: Allows to model a diffusion-impeding surface layer (if any, e.g. wallpaper, tiles, vapor barrier...) by specifying its sd-value, thus avoiding the need to include the layer explicitly in the component model. The natural diffusion resistance caused by the boundary air layer is automatically computed and added by WUFI 2D. In most cases (using standard values for the natural diffusion resistance and no surface layer), simply enter sd-value=0 or as no coating.

Figure 21 - Item "Surface Transfer Coefficients" for indoor surface file.

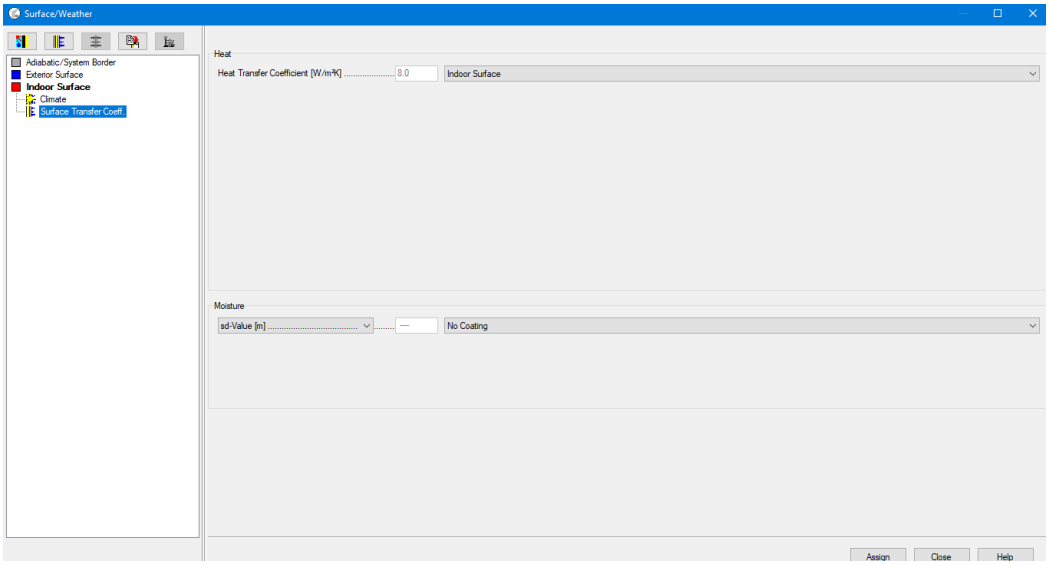

Source: Author.

Climate

Here can select the appropriate exterior or interior climate that shall act on the surface currently being edited. You may select cities from a map or specify a climate file provided by yourself. When a climate file has been selected, WUFI 2D automatically displays its temperatures and relative humidities on the tab “Temperature/Relative Humidity” (See Figure 22).

Figure 22 - Item "Climate”.

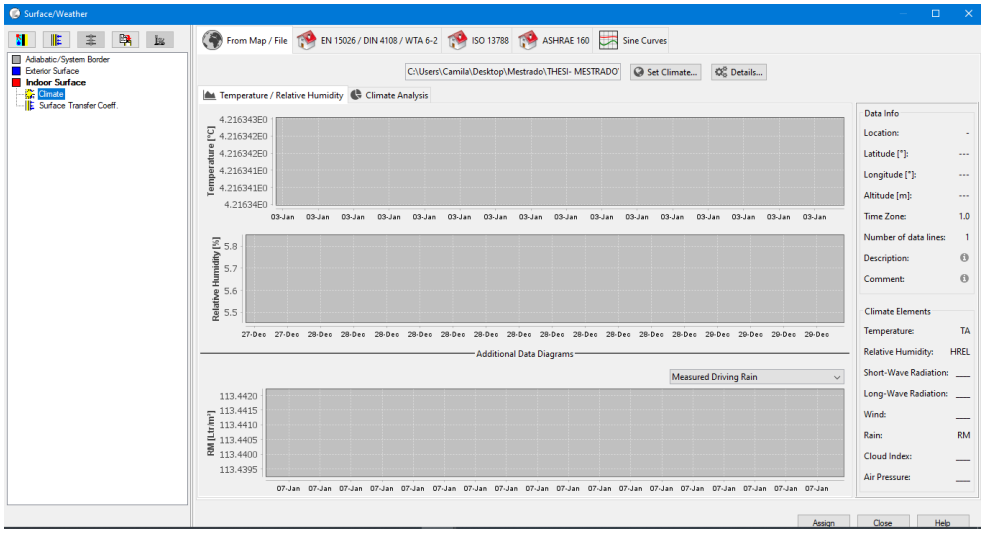

Source: Author.

- Sources, Sinks:

A new feature in the WUFI-2D is the option to add a source. It is possible to add a Heat source, Moisture source or air exchange source entering the coordinates of the source at the building component (See Figure 23). The associated boundary is needed, if prefer use a fraction of solar radiation for example. The value is taken from the given boundary condition. In this work it was not necessary to add any sources.

Figure 23 - Item "Sources, Sinks".

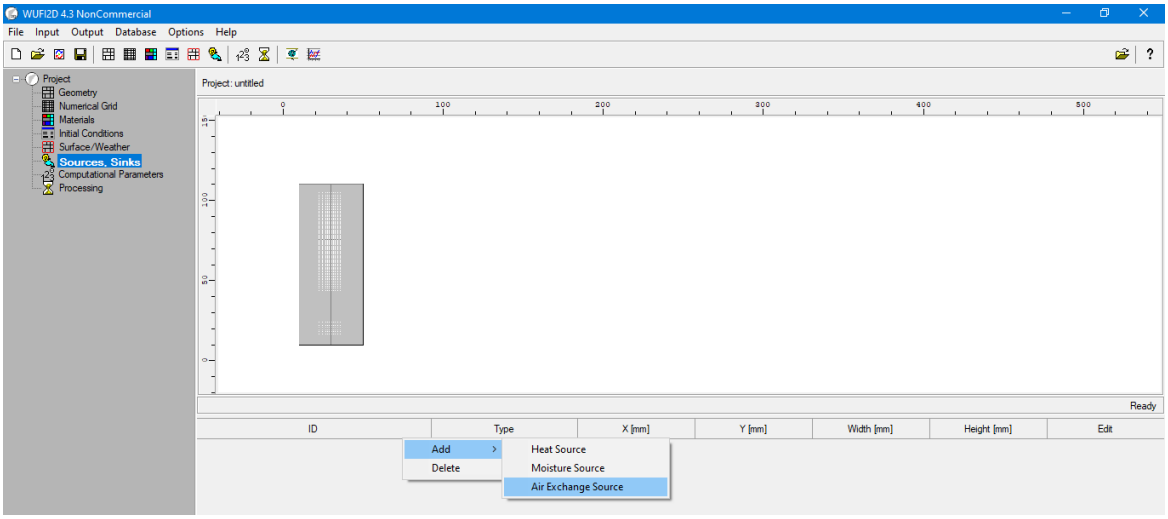

Source: Author.

- Computational parameters:

In the Computational Parameters dialog (Figure 24) is where the specification of the details of the computation is performed. Tab "Simple" there are basic settings for the computation. Tab "Enhanced" there are numerical parameters for the solver.

At period of calculation are define the starting date/time and the number of time steps (of one hour each) for the calculation. At Mode of Calculation it is possible to choose the calculation mode. The program provides two calculation options, which are heat transfer calculation and moisture transfer calculation.

Also, the dialog box offers a hygrothermal special options, where is possible to exclude latent heat evaporation effects when moisture evaporates or condenses, exclude latent

heat of fusion when moisture freezes or melts exclude and exclude capillary conduction but allow for vapor diffusion transport.

The specification on the numerical Parameters allows the user to use tighter convergence criteria and stronger convergence damping (increases the computation time).

The options "result file contains" gives result files for Water Content [kg/m3], Relative Humidity [0..1], Temperature [°C], Vapor Pressure [hPa], Capillary Flux [kg/m^{2}s], Diffusion Flux [kg/m^{2}s] and Heat Flux [J/m^{2}s]. In this work all result options were selected, except for heat flux, because the simulation results can be used in the future for more specific studies.

Figure 24 - Item “Computational parameters”.

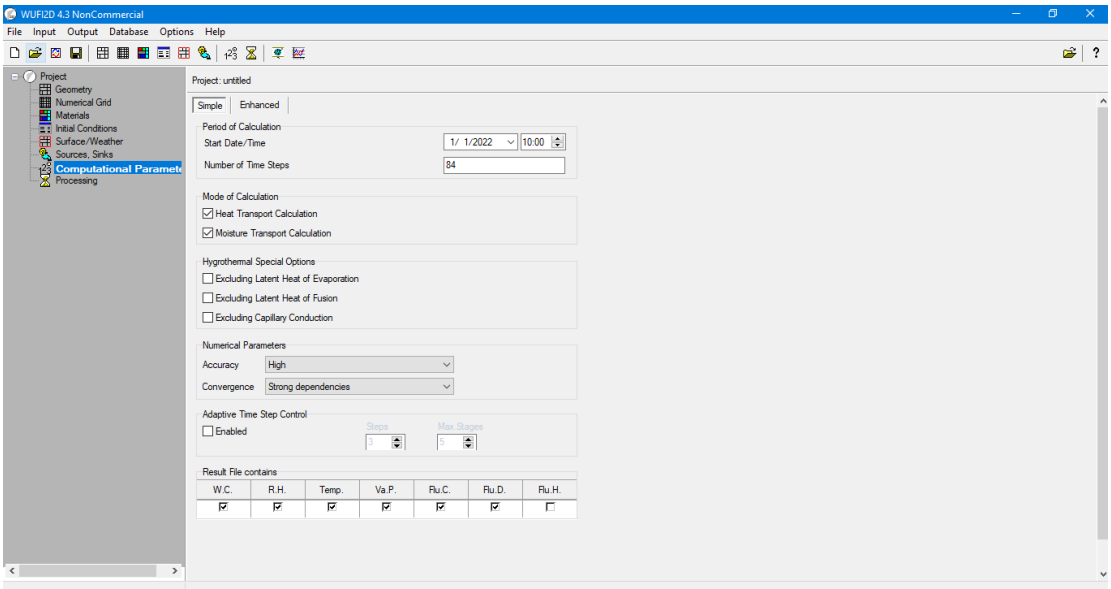

Source: Author.

- Processing:

In this step the computation of the transient thermal and hygric transport processes in the component is performed (see Figure 25).

Figure 25 - Item “Processing".

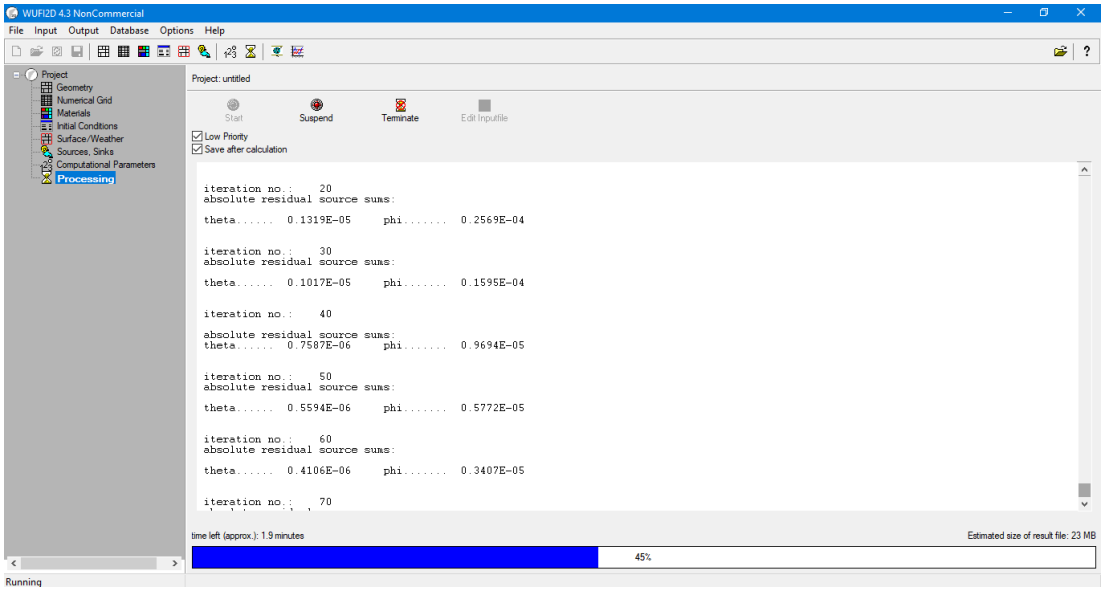

Source: Author.

- Output

In this step we analyze and assess the results. The results may be viewed with WUFI2DMotion as a 2D animation or with WUFIGraph as curves showing the temporal evolution of the various quantities.

- Viewing the Results with WUFI2DMotion:

WUFI2DMotion displays one window for each of the calculated quantities you selected for output. In the Figure 26 are showed the displays windows for relative humidity and water content, which are shown as one and two-dimensional color coded fields.

- Viewing the Results with WUFIGraph:

WUFIGraph displays the results as curves showing the temporal evolution of the various computed quantities (Figure 27). The display is organized in pages, diagrams and curves. Each page contains one or several diagrams, and each diagram contains one or several curves.

The behavior of the total water content allows a first assessment of the results. It shows whether the overall water content of the component increases or decreases during the period under investigation.

Figure 26 - Item "Viewing the Results with WUFI2DMotion" – two displays window for each of the calculated quantities (relative humidity and water content) results in 2D and 3D view.

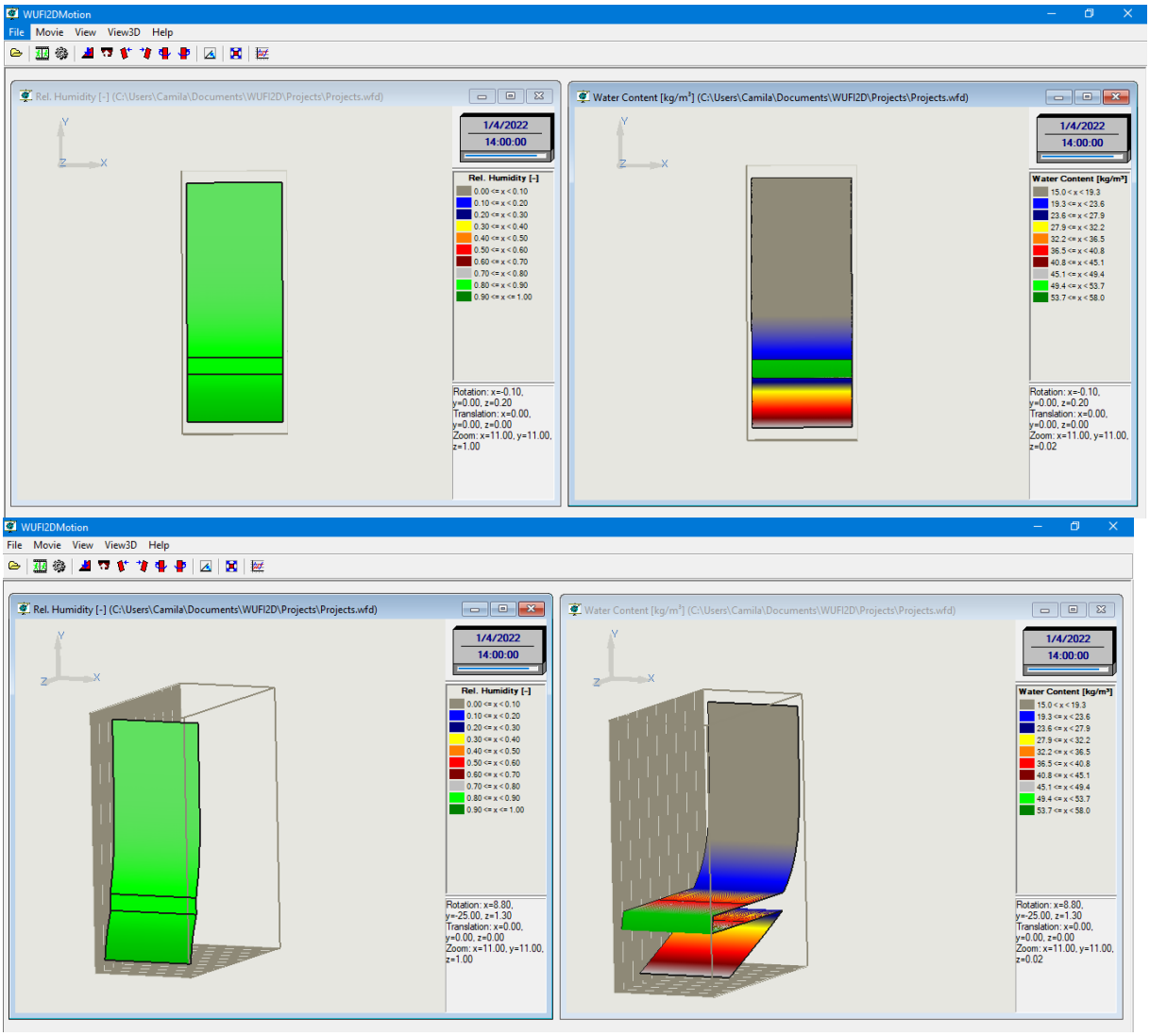

Source: Author.

Figure 27 - Item " Viewing the Results with WUFIGraph" – two displays window for each of the calculated quantities (relative humidity and water content) results as curves.

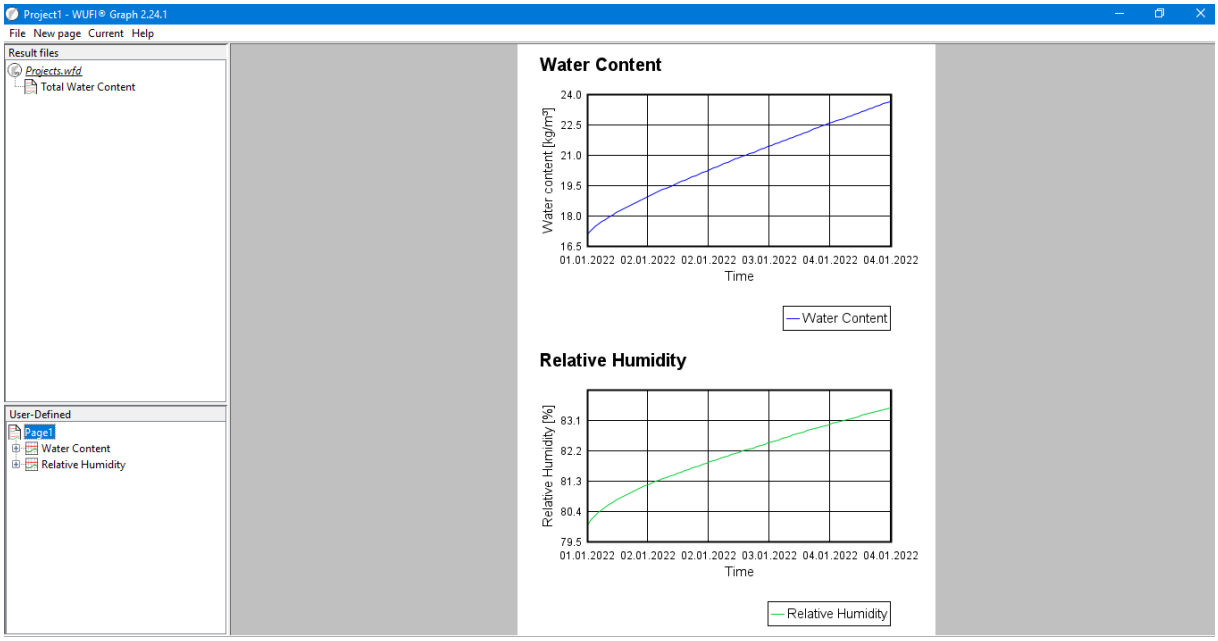

Source: Author

3.2.2 Elements necessary for the execution of the simulations

The following presents the required elements for running the simulations in a summarized form, as it was presented in detail in section 3.2.1.

- Definition of the specimens' geometry, through a configuration summary. The maximum number of elements will be used for the composition of the geometry grid;

- Hygrothermal properties of all materials involved in the study;

- Initial conditions of the materials (temperature and relative humidity/moisture content);

- Boundary conditions on all specimen's surfaces;

- Computational Parameters;

3.2.3 Settings of the simulations performed

The geometry and properties of the samples to be analyzed took into consideration two types of red ceramic bricks: Brick A and Brick B; two types of mortars: Cementitious and Lime; three configurations for the application of hydraulic joint for each type of

brick and each type of mortar; and six configurations for air gap application between brick layers for each type of brick. The same configuration for the moisture transport analysis in the simulation during the wetting process is used for the moisture transport analysis during the drying process. The simulations of monolithic bricks samples are used as a basis for comparing the effects caused by the interface on the samples.

The configurations of the simulated models are presented in Figure 28, Figure 29 and Table 3, the properties and initial conditions of the materials used in the simulation are presented in Tables 4 and 5 respectively.

Figure 28 - Simulation setup: i) monolithic block; ii) a block with cement and lime mortar interface at 2cm, 5cm and 7 cm; iii) an air space with 0.5 cm and 0.2 cm cavity at 2cm, 5cm and 7 cm;

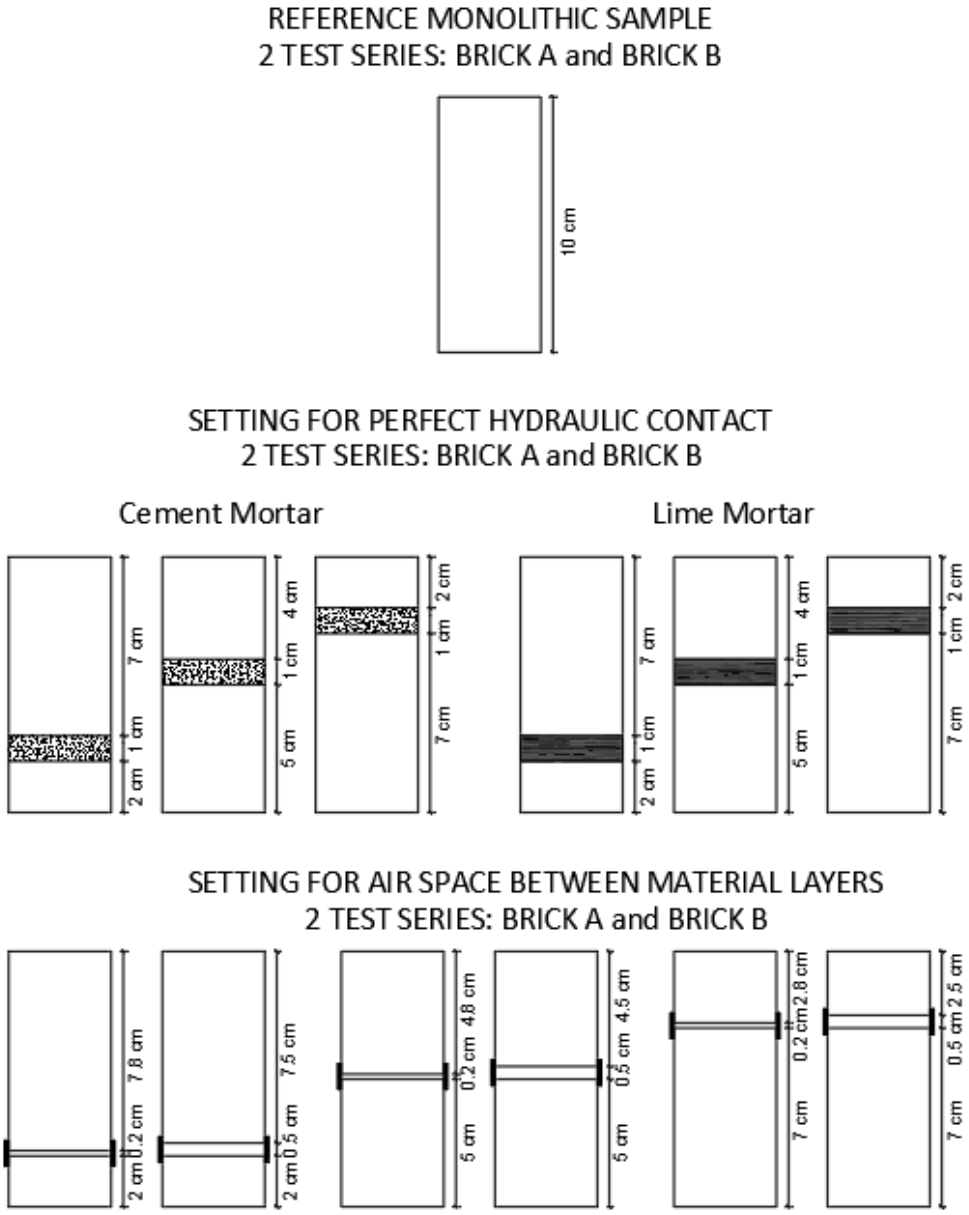

Source: Author.

Table 3 - Settings for the simulations.

Material	Wetting environment 1 (21 °C, RH 50%) , Dry environment 1 (20°C , RH 50%) Dry environment 2 (70 °C , RH 3%)		
	Monolithic	**Perfect hydraulic contact**	**Air space**
Red brick type A 40 mm x 100 mm		Cement Mortar at h= 20 mm Cement Mortar at h= 50 mm Cement Mortar at h= 70 mm Lime mortar at h= 20 mm Lime mortar at h= 50 mm Lime mortar at h= 70 mm	Cavity of 2 mm at h= 20 mm Cavity of 5 mm at h= 20 mm Cavity of 2 mm at h= 50 mm Cavity of 5 mm at h= 50 mm Cavity of 2 mm at h= 70 mm Cavity of 5 mm at h= 70 mm
	1 sample	6 samples	6 samples
Red brick type B 50 mm x 100 mm		Cement Mortar at h= 20 mm Cement Mortar at h= 50 mm Cement Mortar at h= 70 mm Lime mortar at h= 20 mm Lime mortar at h= 50 mm Lime mortar at h= 70 mm	Cavity of 2 mm at h= 20 mm Cavity of 5 mm at h= 20 mm Cavity of 2 mm at h= 50 mm Cavity of 5 mm at h= 50 mm Cavity of 2 mm at h= 70 mm Cavity of 5 mm at h= 70 mm
	1 sample	6 samples	6 samples
Wetting	2 samples	12 samples	12 samples
Dry	2 samples	24 samples	12 samples
	4 SIMULATIONS	36 SIMULATIONS	24 SIMULATIONS
TOTAL	64 SIMULATIONS		

Source: Author.

For the water absorption simulation on the samples with perfect hydraulic contact of mortar (cement and lime) with 2 cm, 5 cm and 7 cm distance from the base of the sample (Figure 28), a 1 centimeter thick layer of each material was inserted between the two blocks. All materials had a dry initial condition. The adiabatic system was applied to the lateral surfaces, as the goal is to analyze moisture transport on a single surface and avoid heat and moisture exchange at the borders. The water available for absorption is taken from an exterior climate file with rain of 1000Ltr/m²h, at a 20°C temperature and 100% relative humidity. The program calculates the water content absorbed from the surface by measuring the rainfall incident on the surface every one hour. For the top surface an indoor climate with 20ºC and RH 50% was applied according to the laboratory conditions for the experimental test (Figure 29).

For the drying process simulation, adiabatic systems were applied for all surfaces, except for the top face that was exposed to two different types of indoor climates: Environment 1- 20ºC and RH 50% and Environment 2- 70ºC and RH 3%. All materials had a saturated initial condition (Figure 29).

Figure 29 - Settings for the simulations processes.

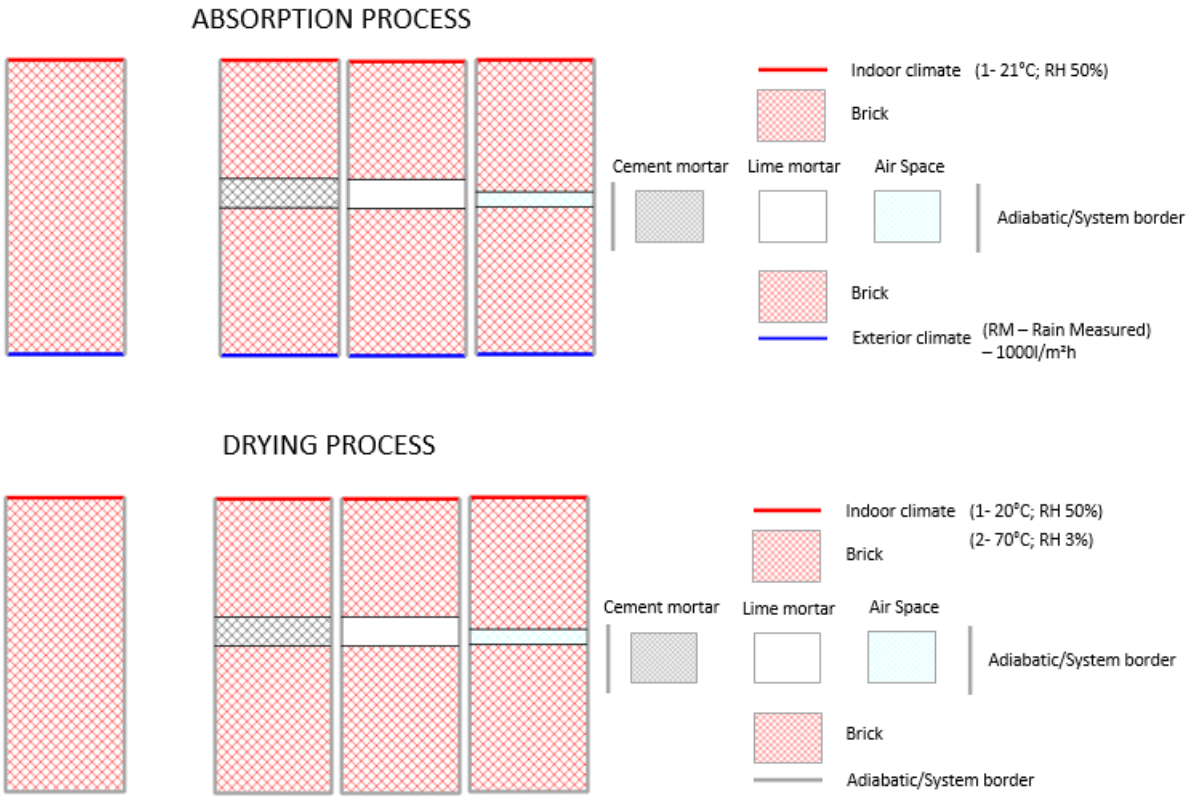

Source: Author.

The properties of air layers must be described by sets of material parameters which had been intended to describe porous materials. The effective material parameters of the air layers describe total heat transport and total vapor transport (due to diffusion and free convection) in an unventilated air layer between non-metallic surfaces. Since the percentage of convection in the total transport is affected by the thickness of the air layer, the effective material parameters also depend on the layer thickness. Air layer thicknesses not provided in the database can be created with the method discussed in the online help.

Currently the program has in the database new air layers "without additional moisture capacity". Their free saturation of 17 g/m3 corresponds to the saturation moisture of air at 20°C. However, the free saturation is always fixed at the value cited and does not vary with temperature, as it would in real air. The moisture contents and hygroscopic inertia of these air layers are at a realistic level, but can prove numerically challenging.

- Determining the effective transport parameters for air layers (WUFI 2D-help)

The relative contributions of heat conduction, convection and radiation are dependent on the thickness and orientation of the air layer, the nature of the two surfaces and the temperature. Fortunately, the dependence on the temperature may be neglected in building physics.

for WUFI the effective heat conductivity l* has to be chosen so that for an air layer with a given thickness the heat resistance Rnon-met as determined

The heat resistance of an air layer with the desired thickness, orientation (vertical, horizontal) and surfaces (metallic, non-metallic) may be looked up in a relevant table (for R_{met} and $R_{non\text{-}met}$).

Since water vapor diffusion and convective water vapor transport are based on analogous mechanisms as heat conductivity and convective heat transport, the coefficients describing vapor transport can be derived from the coefficients for heat transport, using similarity relations.

Finally, we have the freedom to choose an arbitrary thickness Δx^* (Equation 32) with which the layer is included in the component assembly for calculation, since the real thickness was already allowed for in the choice of the specific value for R_{met}.

$$\mu^* = 0.09 \cdot \frac{R_{met}}{(3.5 \cdot \Delta x^*)} = \mathbf{0.026} \cdot \frac{\mathbf{R_{met}}}{\mathbf{\Delta x^*}} \quad (32)$$

The other basic material parameters may be determined according to the following:

- if Δx^* was chosen not equal to the real thickness, multiplication of the 'bulk density' 1.29 kg/m³ by (real thickness)/Δx^* results in the correct heat capacity;
- the 'porosity' should be chosen very high (e.g. 0.999 m³/m³);
- the specific heat capacity by mass of the air layer is 1 kJ/kgK, even if Δx^* is chosen not equal to the real thickness.

The moisture storage function of non-hygroscopic materials (essentially insulating materials, but air layers as well) is theoretically more or less zero in the region φ = 0..1,

whereas for φ = 1 it takes on some indefinite value between zero and Wmax, so that no well-defined functional relationship exists. Since WUFI needs a well-defined moisture field at each time step, however, it assigns a (low) artificial moisture storage function to all materials which nominally don't have any appreciable moisture content or for which the user did not define such a function for whatever reason.

If no moisture storage function has been defined in the material data dialog, WUFI therefore uses the following default moisture storage function (33):

$$w(\varphi) = \frac{a}{b - \varphi} + c \quad (33)$$

Since W must be 0 for φ = 0, it follows immediately that c = -a/b. The constants a and b are determined as follows: b is set to 1.0105.

The moisture content at free saturation, Wf, corresponds to a relative humidity φ of 1 (=100%). Since WUFI also needs a unique relationship between moisture content and RH for moisture contents above free saturation, this oversaturation region is assigned RHs greater than 1, up to φmax = 1.01. This value φmax is reached when the moisture content reaches maximum saturation Wmax which is determined by the porosity:

Wmax = porosity * 1000 kg/m³. Therefore, we have Wmax = a / (b-φmax) - a/b.

The definition of the diffusion resistance factor (μ-value) for an air layer is considered as for very permeable materials, such as mineral wool, which the μ-value is thus close to 1, whereas it increases for materials with greater diffusion resistance. So, whereas the diffusion flow through an air layer, the diffusion resistance factor μ=1 with thickness Sd is Sd = μ·s.

Table 4 and Table 5 summarize the property and initial conditions of the materials and air layers used in the simulations.

Table 4 - Hygrothermal properties of materials.

Properties	Materials / Layers					
	Red brick type A	Red brick type B	Cement Mortar	Lime mortar	Air Space 2 mm	Air Space 5 mm
Bulk density, ρ [kg/m³]	1800	1600	1878	1810	12.9	12.9
Porosity, ε [m³/m³]	0.32	0.38	0.20	0.21	0.999	0.999
Specific heat capacity, C [J/kgK]	850	850	900	900	1000	1000
Thermal conductivity (Dry), λ [W/mK]	0.40	0.38	0.786	0.799	0.0125	0.02778
Water vap. diff. resist. factor, μ [-]	33.1 (dry cup)	21.4 (dry cup)	23.90	14.25	5.59	3.224
Moisture Content, w80% [kg/m³] for 80% relative humidity	w80% = 15.51	w80% = 9.75	w80% = 38.16	w80% = 8.16	0.0136	0.0136
Moisture Content, wsat [kg/m³] Free water saturation	wsat = 261.38	wsat = 233.07	wsat. = 228.59	Wsat. = 186.61	0.017	0.017
Water absorption coeff. [kg/m²√s]	0.10	0.19	0.15	0.12	-	-

Source: Author.

Table 5 - Initial conditions of materials/layers.

Initial Conditions			
	Temperature °C	Moisture Content, w (Kg/m³)	Relative Humidity, RH (%)
Red brick type A	**20°C**	w80% = 15.51 wsat = 261.38	0.8 1
Red brick type B	**20°C**	w80% = 9.75 wsat = 233.07	0.8 1
Cement Mortar	**20°C**	w80% = 38.16 wsat. = 228.59	0.8 1
Lime mortar	**20°C**	w80% = 8.16 wsat. = 186.61	0.8 1
Air Space	**20°C**	w80% = 0.0136 wsat. = 0.017	0.8 -

Source: Author.

The simulations were performed for the same time period, being 72h for the wetting process and (720h – Environment 1; 72h – Environment 2) for the drying process. These parameters were used in the Azevedo (2019) experimental trial.

3.2.4 Hydric Resistance – New calculation methodology proposed by Azevedo (2019)

Although the program considers a continuous transport across the interface between the materials, it is still possible to analyze a discontinuity caused by the difference in materials. This result will be important to validate the experimental results that identifies the discontinuity at the interface and which contributes to higher water resistance values.

The method used to measure the water resistance values for the simulations was the same method used for Azevedo (2019) to obtain the values through the experimental gravimetric method.

The water absorption curve increases over time exhibits instants (points of change) where the rate of absorption seems to decrease significantly. These instants correspond to the contact of the water with a different material (contact with the interface). Only one point of change is expected for the air space interface (see Figure 30a), different from what happens for the hydraulic interfaces (see Figure 30b) where it can be observed two discrete knees, one before the interface and another when the interface is saturated. Since the goal is to address the effect of the interface in water absorption, the water resistance is measured immediately after the first changing point, which is the time interval of interest. The final measurement is performed by calculating each Hydric Resistance (RH). Figure 31 depicts how the several values are measured. Considering this measuring procedure, it is important to detect the exact time instant of the “knee point” automatically and with some precision (AZEVEDO,2019).

Figure 30 - Water absorption profile and the changing instant.

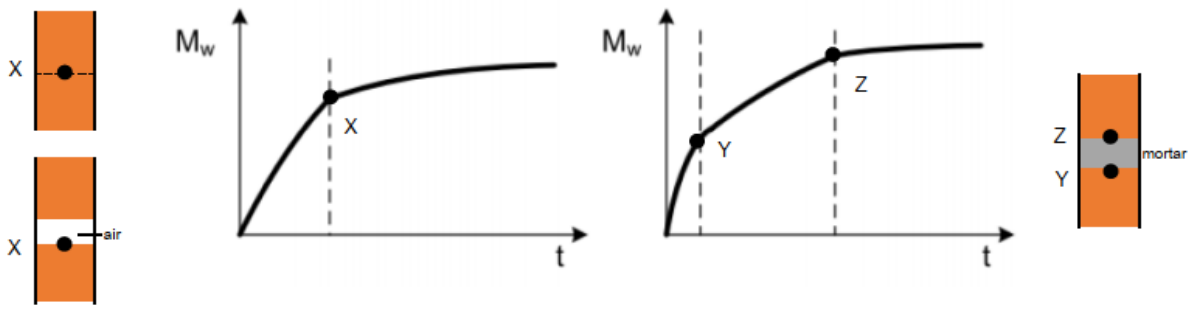

Source: (AZEVEDO, 2019)

Figure 31 - Method of RH measurements.

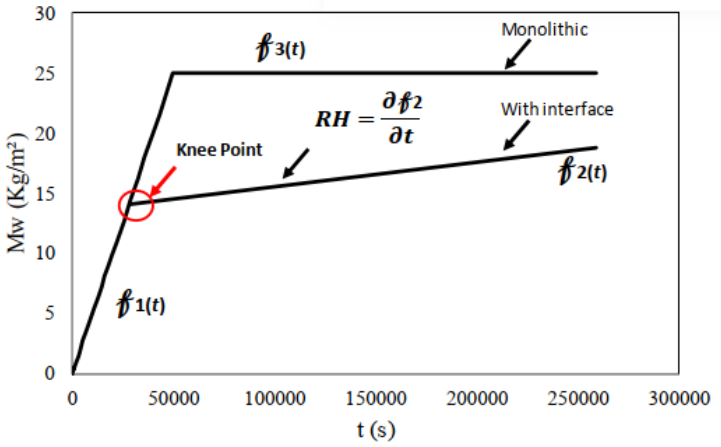

Source: (AZEVEDO, 2019)

- Empirical Equations for Imbibition – Perfect Hydraulic Contact

In accordance with the above description, a logarithmic function was selected to fit the points after the first knee point,

$$Mw\ (t) = a\ln(t) + b \quad (34)$$

For the calculation of the hydric resistance, the derivative of logarithmic function is presented,

$$g(t) = \frac{d\big(Mw(t)\big)}{dt} = \frac{a}{t}\left(\frac{kg}{m^2 s}\right) \quad (35)$$

$$RH = g\ (t_k) = \frac{a}{t_k} \quad (36)$$

where t_k is the time instant at which the second knee point occurs. When using the 3rd method to determine the 2nd knee point, the time tk = 86.400 second.

- Empirical Equations for Imbibition – Air Space Interface

For air space, a linear model was chosen to fit the points (ti, Mw) after the knee in imbibition regression curves, since the points present a line trend. The linear model is expressed as Equation 37:

$$Mw\ (t) = at + b \quad (37)$$

where *a* is the line slope which represents the hydric resistance (RH) and b is the ordinate value at the origin. This appears to be the amount of moisture absorbed by the part of the specimen prior to arriving at the interface.

The equation 38 presents the same concept as the hydric resistance (RH) in the equation (37),

$$RH = \frac{\Delta M_w}{\Delta t} \qquad (38)$$

where Δt (s) and ΔM_w (kg/m^2) are the variation of the time and water absorption immediately after the knee point, respectively. Nevertheless, the program generates graphs on moisture content (kg/m$^{3)}$ by time in hours (h).

The program interprets the material properties' influence on moisture transport, thus increasing or reducing the water absorption during the absorption test simulation. The hydric resistance (RH) is the measurement calculated experimentally (during a water absorption test) by the slope of the curve of mass change as a function of time, after the knee point (Figure 31). The measured values of the hydric resistance for the simulations followed the same methodology, using the variation curve of water content as a function of time after the slope point that intersects the moisture transport curve for the monolithic sample.

CHAPTER 4. RESULTS AND DISCUSSIONS

4.1 NUMERICAL SIMULATION - EVALUATED PARAMETERS

4.1.1 Moisture transport across perfect hydraulic contact – Absorption process

The simulation of moisture transport along ceramic brick specimens with perfect hydraulic contact and air space interface between material layers were performed. The objective is to analyze the moisture behavior in monolithic samples, multilayer samples of different materials and samples with air space between ceramic material layers. By comparing the monolithic samples with the multilayer samples, it is possible to evaluate the influence that different types of contact between different materials have on moisture transport in multilayer components.

As stated in the methodology, this work also performs comparisons with the experimental survey results of Azevedo (2019), in order to validate the experimental result and contribute to the evaluation of the tool in real applications.

However, since it is considered that the existence of the interface between the materials layers generates a hydric resistance in the water transport, the simulations performed analyze the transport of the moisture front in immediately after the first change point in comparison with the monolithic sample, according to new calculation methodology proposed by Azevedo (2019) in section 3.2.4.

Figure 32 and Figure 33 shows the plot of the simulations after 72h for the moisture transport (kg/m³) per hour along the samples with perfect hydraulic contact between brick and mortar layer, comparing with the moisture transport behavior in the monolithic brick sample. Also shown is the zoom in at the time when the multilayered sample curves intersect the monolithic sample curve and reduce the transported moisture content.

As reported previously, for the perfect hydraulic contact analysis, two configurations are shown: The first configuration has the cement mortar between two layers of brick and has three samples with different interface location height (2cm, 5cm, 7cm) and the second configuration has the lime mortar between two layers of brick and also has three samples with different interface location height (2cm, 5cm, 7cm).

Figure 32 - Water content graph along brick A after 72h of simulated transport for perfect hydraulic contact (cement x lime).

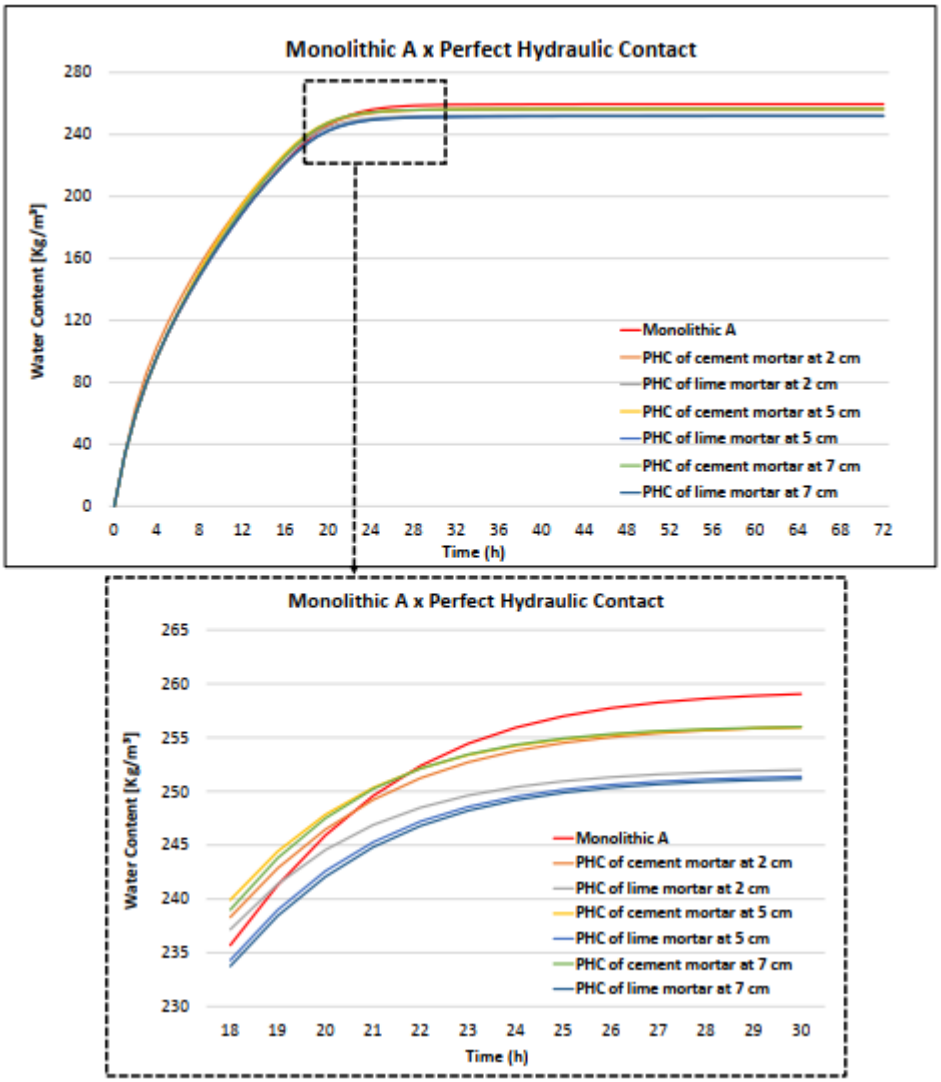

Source: Author.

Through the results obtained in the graphs (Figure 32 and Figure 33), it was observed that there is a reduction in the water content transported for the samples with perfect hydraulic contact in relation to the transport on the monolithic sample. For samples with lime mortar there was a greater reduction in the amount of water content absorbed compared to the samples with cement mortar.

Figure 33 - Water content graph along brick B after 72h of simulated transport for perfect hydraulic contact (cement x lime).

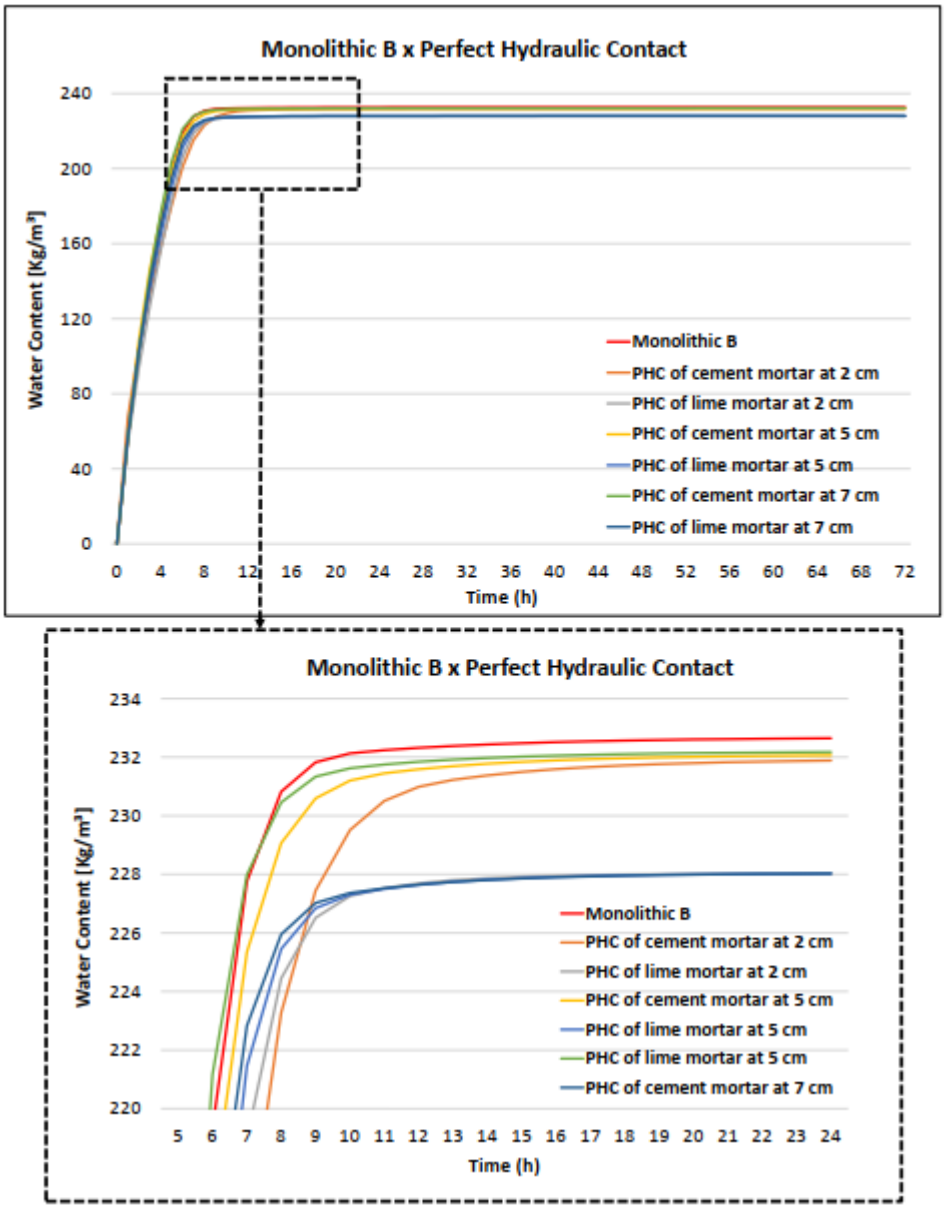

Source: Author.

Figure 32 and Figure 33 indicate a decrease in the water absorption rate after the intersection point in the water content curve for the monolithic sample. As explained earlier, this drop point is considered as the transition of moisture transport after the interface.

To understand the calculated result for the hydric resistance values, it is important to understand how the program uses material properties to interpret moisture transport. When the surface is completely wet (considering the presence of rain) the program calculates the liquid transport coefficient for suction using Equation 39:

$$D_{ws}(w) = 3.8 \left(\frac{A}{w_{sat}}\right)^2 1000^{\left(\frac{w}{w_{sat}}-1\right)} \quad (39)$$

Where, D_{ws} is the liquid transport coefficient for suction (m^2/s), A is the water absorption coefficient ($kg/(m^2.\sqrt{s})$), w_{sat} is the moisture content when the material is saturated (kg/m^3) and w is the moisture content (kg/m^3).

In equation 39 it is possible to identify the relationship between the moisture content and the water absorption coefficient for the liquid transport coefficient in the suction. Freitas (2008) concludes in his study that the material permeability increases with the increase of the water absorption coefficient and that this coefficient causes an increase in the height reached at the wet front on the surface of the material.

Table 6 - Values of hydric resistance for the perfect hydraulic contact samples.

Material	Sample / (interface type)	Hydric Resistance (AZEVEDO,2019) Kg/m²s	Hydric Resistance kg/m³h
Red brick Type "A"	Perfect hydraulic contact (cement mortar at 2cm)	9.7x10-5	0.1421
	Perfect hydraulic contact (cement mortar at 5cm)	7.1x10-5	0.0869
	Perfect hydraulic contact (cement mortar at 7cm)	4.2x10-5	0.0871
	Perfect hydraulic contact (lime mortar at 2cm)	7.9x10-5	0.1505
	Perfect hydraulic contact (lime mortar at 5cm)	5.8x10-5	2.1055
	Perfect hydraulic contact (lime mortar at 7cm)	5.4x10-5	1.0382
Red brick Type "B"	Perfect hydraulic contact (cement mortar at 2cm)	7.9x10-5	1.4384
	Perfect hydraulic contact (cement mortar at 5cm)	4.8x10-5	0.4932
	Perfect hydraulic contact (cement mortar at 7cm)	3.2x10-5	0.0274
	Perfect hydraulic contact (lime mortar at 2cm)	7.9x10-5	2.4471
	Perfect hydraulic contact (lime mortar at 5cm)	4.2x10-5	1.7953
	Perfect hydraulic contact (lime mortar at 7cm)	4.2x10-5	1.2865

Source: Author.

Table 6 shows the values obtained for the hydric resistance of the simulated samples, using the same methodology as Azevedo (2019). The resistances values for brick A differ from the results obtained in the experimental test. This divergence may be related

to the perfect hydraulic contact type interpreted by the calculation program that does not consider the hydric resistance caused by the discontinuity at the interface.

For brick A with cement mortar, a higher hydric resistance value was identified for the sample with interface at 2cm. Although the resistance values were very similar for the samples with interface at 5cm and 7cm, the lowest hydric resistance was presented for the sample with interface at 5cm. For brick A with lime mortar, a higher hydric resistance was identified for the sample with 5cm interface and the lowest hydric resistance was presented for the sample with interface at 2cm.

The results for brick A samples with cement mortar proved to be consistent, considering that cement has a higher water absorption coefficient and liquid transport coefficient for suction than brick A. Therefore, the resistance is higher for interface located at 2cm, because the liquid has to be transported through a thicker brick A layer to the top face.

The results for the brick A samples with lime mortar proved to be more challenging. Although lime has a lower water absorption coefficient and liquid transport in suction than cement mortar, but still higher than brick A's coefficients, it has a lower resistance for the sample with interface at 2cm and higher for the sample with interface at 5cm. The explanation may be related to the low water storage capacity (water content) for lime. Therefore, for the layer close to a higher water content, the resistance will be lower due to a higher water absorption by the second layer of brick A due to the lime layer saturation. For the interfaces at 5cm and 7cm, the saturated wet front does not approach the interface. The resistance is higher for the interface at 5cm because it has a thicker brick A layer after the interface for moisture transport to the top.

For brick B samples with cement mortar and samples with lime mortar, higher water resistance was identified for samples with interface at 2cm and lower resistance for samples with interface at 7cm. The resistance results for brick B were consistent compared to the results obtained in the experimental test.

The higher resistance results in the interfaces located at lower heights are explained by the lower water absorption coefficient and liquid transport coefficient values of the mortars compared to the coefficient values for brick B, since mortars are more

impermeable than brick B. Thus, the mortar layer after the interface acts as a water barrier in transporting water through the second brick B layer. However, the moisture transport does not behave uniformly throughout the sample surface during the entire simulation period on account of the material layer influence and this influence will be shown in Figure 34 to Figure 39.

For an open scale (Figure 34) it can be seen that the water content transport on the surface of the samples with brick A is similar for all samples when a low water content is transported on the wet front. Compared to the monolithic sample, there is a delay in moisture transport when transported across the interface due to the interface material's porosity being smaller than the porosity of brick A. For this condition the influence of the material interface on vapor water transport is verified. This condition is not verified when analyzing the transport of high water contents (Figure 35).

Figure 35 indicates faster water transport across the interface for the samples with cement and lime compared to the monolithic sample A. The sample with cement interface at 2cm shows slower water transport compared to the samples with interface at 5cm and 7cm. Although the interface at 2cm is closer to a higher water content, this water is transported with greater resistance through brick A which is less permeable than concrete and has a lower liquid transport coefficient in suction. The water transport for the samples with interface at 5cm becomes faster in relation to the samples with interface at 7cm because it is closer to a higher water content.

The sample with lime interface at 2cm shows faster water transport compared to the samples with interface at 5cm and 7cm. This result is directly related to the interface position height with access to the higher water content. The lime layer when it contains a high water content allows a faster transport through the second layer of brick A.

For the influence of the interface in brick A, one can conclude that the resistance to water transport has more influence on brick A due to its higher impermeability compared to mortars and will depend on the interface location with access to higher water content.

Figure 34 - Effect of perfect hydraulic contact on moisture surface progression after cement mortar and lime mortar interface at different simulation times for ceramic block A.

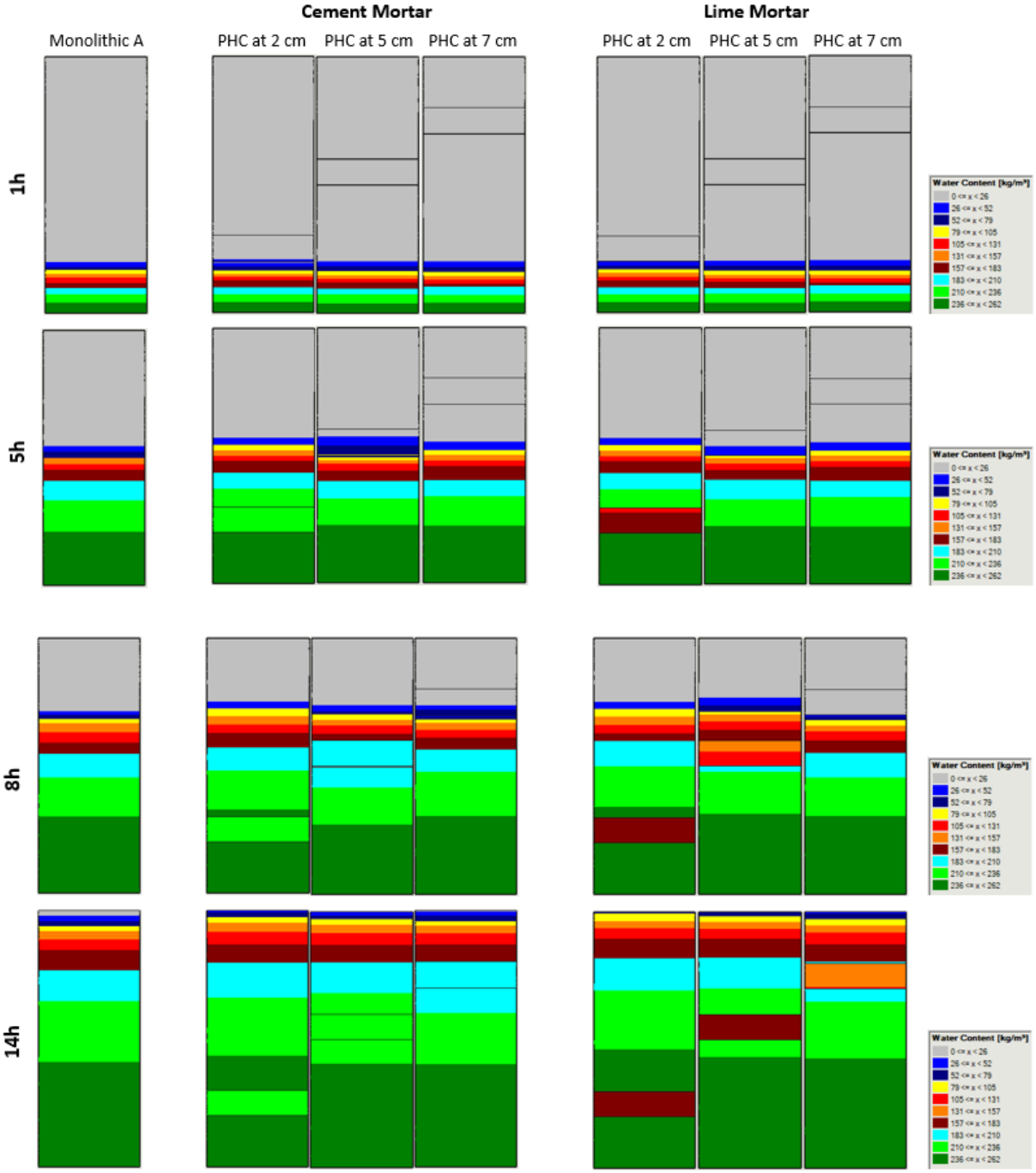

Source: Author.

Figure 35 - Effect of perfect hydraulic contact on moisture surface progression (high water content) after cement mortar and lime mortar interface at different simulation times for ceramic block A.

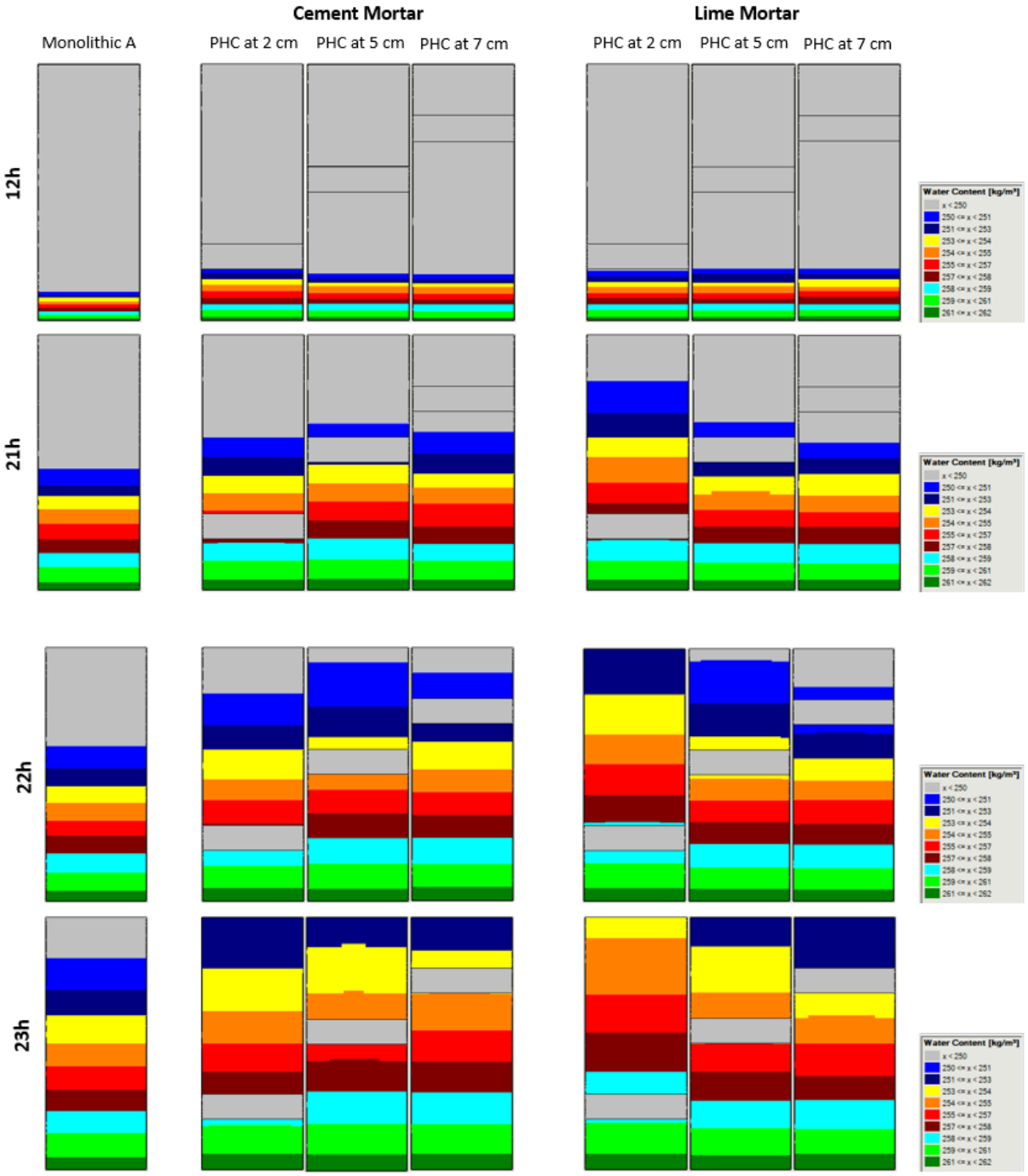

Source: Author.

Figure 36 - Water content along the sample with brick A after 72h of simulated transport for perfect hydraulic contact.

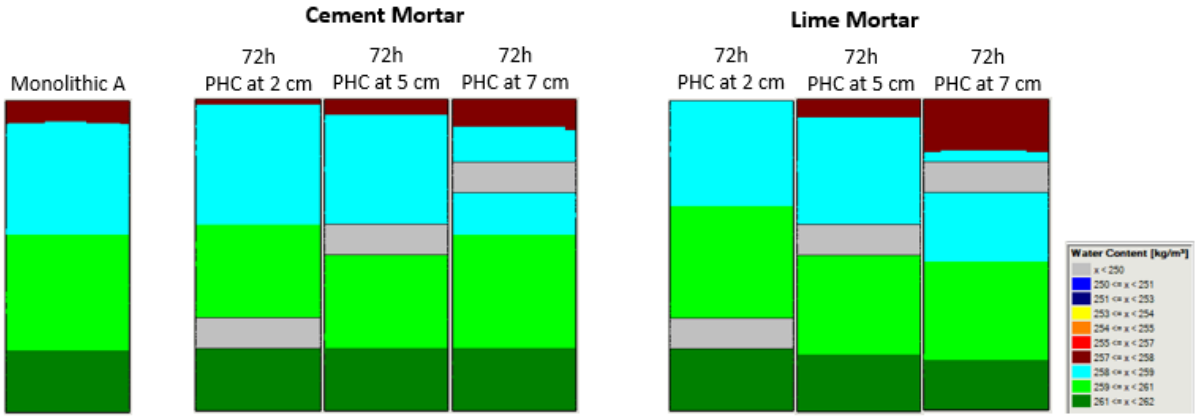

Source: Author.

Figure 36 shows the water content on the surface of the samples with perfect hydraulic contact after 72h of water transport simulation, compared to the monolithic sample A. For the samples with interface positioned at 2cm with greater access to the saturated wet front, there is an increase in surface moisture content on the surface compared to the monolithic sample A. For the samples with interfaces far from the wet front, there is a visible reduction in the surface moisture content compared to the monolithic sample.

For an open scale (Figure 37), it can be seen that the transport of the water content on the surface of the samples with brick B is similar for all samples when a low water content is transported on the wet front. Compared to the monolithic sample, there is also a small delay in moisture transport when transported across the interface due to the porosity of the interface material being smaller than the porosity of brick B. For this condition the material interface's influence on water vapor transport is verified. This condition is also verified when analyzing the transport of high water contents (Figure 38). For brick B, this retardance is explained by the resistance to water transport through the interface of cement and lime mortar that are more impermeable than brick B.

Figure 37 - Effect of perfect hydraulic contact on moisture surface progression after cement mortar and lime mortar interface at different simulation times for ceramic block B.

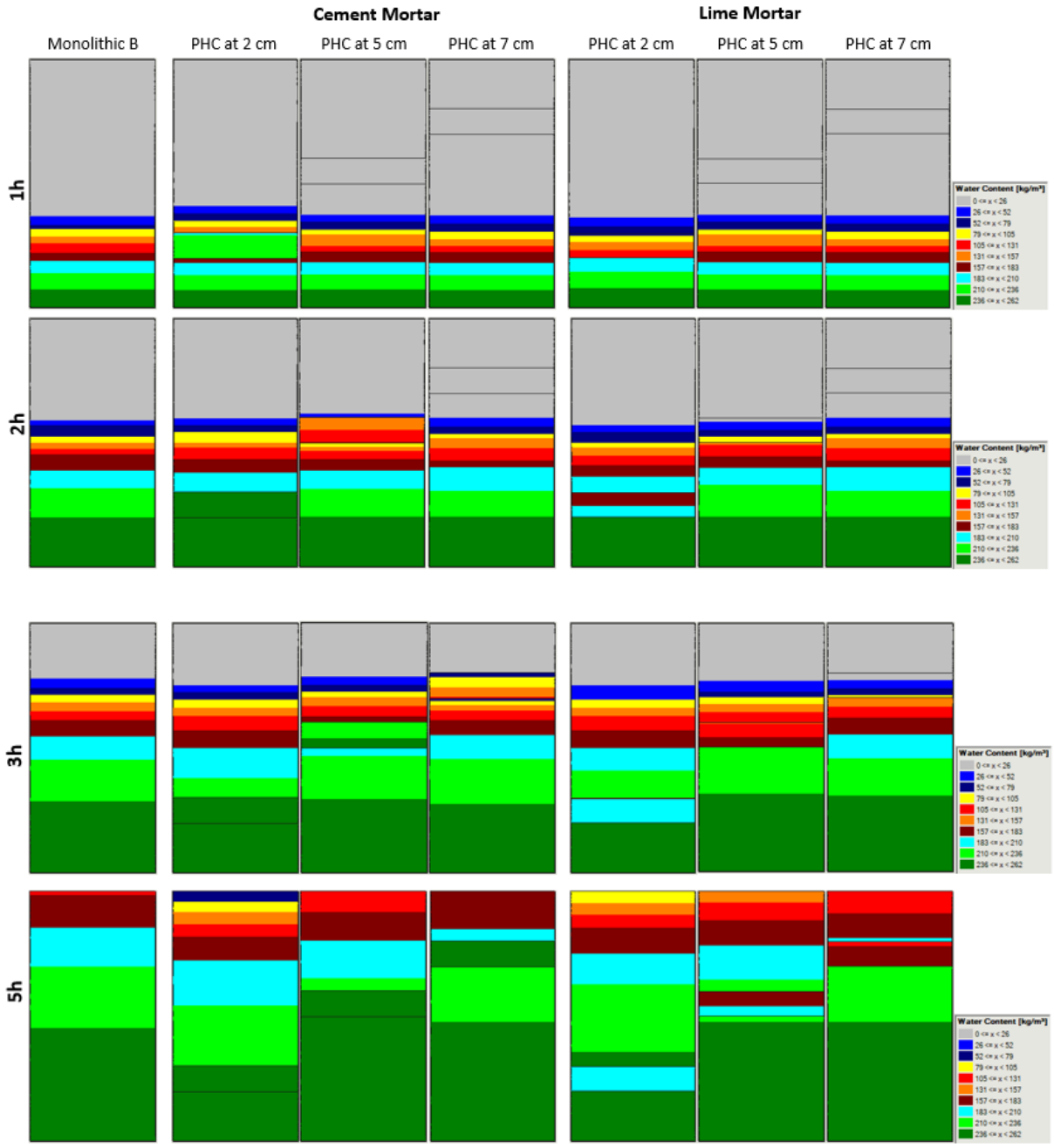

Source: Author.

Figure 38 - Effect of perfect hydraulic contact on moisture surface progression (high water content) after cement mortar and lime mortar interface at different simulation times for ceramic block B.

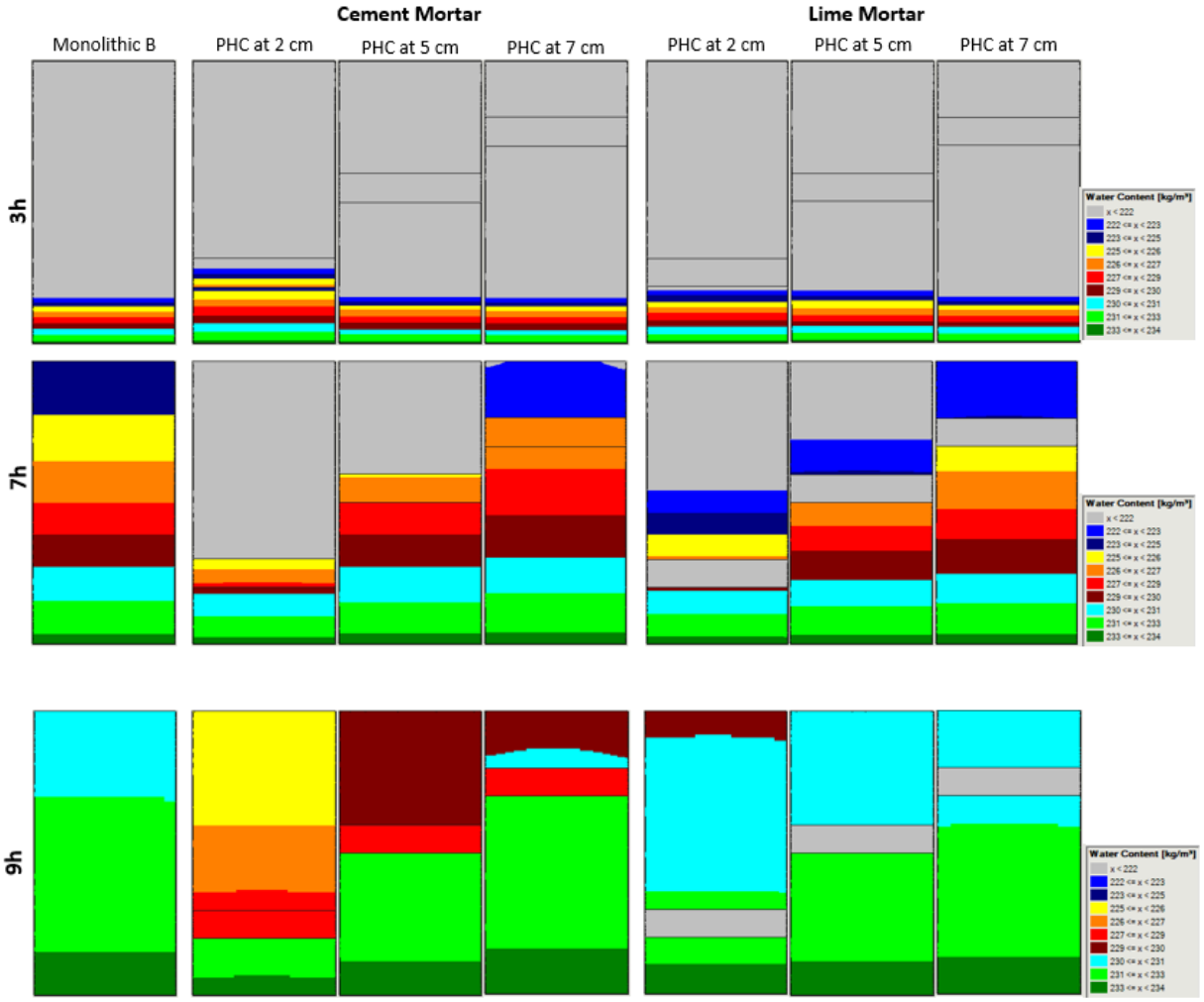

Source: Author.

Figure 39 - Water content along the sample with brick B after 72h of simulated transport for perfect hydraulic contact.

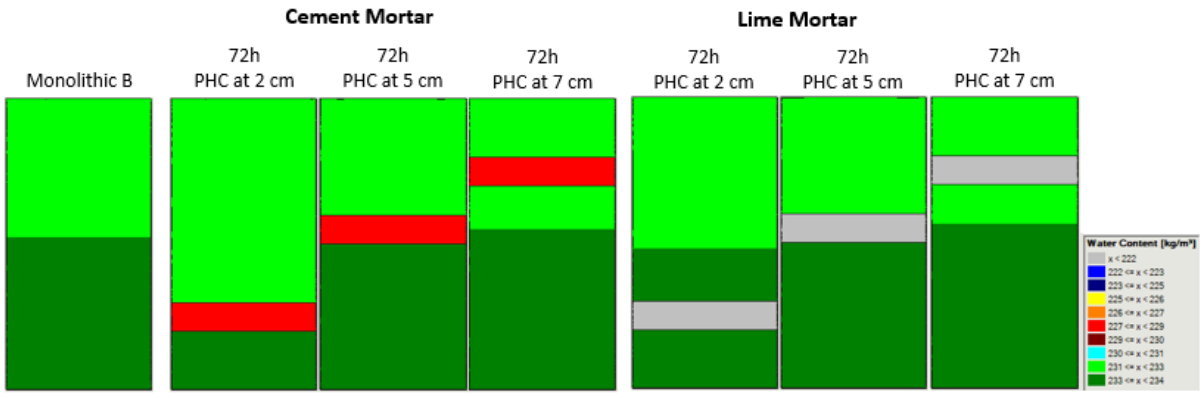

Source: Author.

Therefore, the samples with interfaces located at 2cm (Figure 38) have higher resistance to water transport and the samples with interfaces located at 7cm have lower resistance to water transport. Compared to the monolithic sample it is possible to observe the influence of the material interface on water transport. Comparing the samples with cement mortar and lime mortar, the samples with lime mortar cause a lower moisture transport resistance after the interface, may due to the quick lime layer saturation which then facilitates the transport to the brick B layer. It can be concluded that the water transport resistance is higher for interfaces located at lower heights of the sample base, due to the higher impermeability of the mortars compared to brick B.

Figure 39 shows the water content on the surface of the samples with perfect hydraulic contact after 72h of water transport simulation, compared to the monolithic sample B. For the samples with interface positioned at 2cm with greater access to the saturated wet front, there is a reduction in wet front across the lime interface compared to the monolithic sample. For the cement interface, the wet front does not go beyond the cement layer. For the samples with interfaces far from the saturated wet front (interface at 7 cm), there is an increase in the height reached by the wet front compared to the monolithic sample.

Azevedo (2019) compared the progression of the wet front on surface of different hydraulic interfaces (cement lime and mortar lime) by calculating the velocity at which the wet front overcomes the interface and reaches the top face of the sample.

Similarly, Tables 7 and 8 presents the velocities obtained from the simulation times for the moisture surface progression of the samples after the transition from the interface to the top face. As the results presented by WUFI-2D are only in hour interval, the image analysis of the moisture surface progression is necessary to better understand the transport.

For the samples with brick A, the transport of the low water content was faster in the samples positioned at 2 cm. The transport through the lime was faster compared to the cement. For the samples with interfaces at 5cm and 7cm the velocity values were the same, but for the same time, through the surface of the samples with lime, higher water contents were transported. A higher transport velocity can then be considered for the samples with perfect hydraulic contact with the lime mortar.

For the samples with brick A, the transport of high water content was slow for the samples positioned at 2cm and greater for the interfaces positioned at greater heights (5cm and 7cm).

The velocity values found for the samples with brick A were consistent with the values presented in the experimental test for the samples with cement mortar, but diverged in the values found for the lime mortars.

Table 7 - Comparison of the velocity of moisture surface progression of different hydraulic interfaces (cement mortar and lime mortar), for brick A.

Contact Type PHC - BRICK A	**Cement mortar**			**Lime mortar**		
Interface level	**2 cm**	**5 cm**	**7 cm**	**2 cm**	**5 cm**	**7 cm**
Measured distance after the interface transition (cm)	8 cm	5 cm	3 cm	8 cm	5 cm	3 cm
Measured time (h)	13h	9h	6h	13h	9h	6h
Velocity (cm/h) of progression after the interface transition (cm/h) - water content.	0.62	0.56	0.50	0.73	0.56	0.50
Measured time (h)	11h	2h	1h	9h	2h	1h
Velocity (cm/h) of progression after the interface transition (cm/h) - High water content.	0.73	2.50	3.00	0.89	2.50	3.00
Velocity of progression after the interface transition (m/s)(AZEVEDO, 2019)	$2.3x10^{-7}$	2.9 - $1.9x10^{-7}$	$3.2x10^{-7}$	$4.8x10^{-7}$	$6.3x10^{-7}$	$3.8x10^{-7}$

Source: Author.

For samples with brick B, the velocity results of the surface moisture progression in the samples showed similar behavior to those obtained from samples with brick A. Although, in comparison with the values obtained in the experimental test, greater divergences were presented.

However, it can be concluded that this methodology for analyzing the velocity of moisture progression at the interface is not clear, considering that the interval between the analyses is 1h and the water content carried on the surfaces are different in the

Table 8 - Comparison of the velocity of moisture surface progression of different hydraulic interfaces (cement mortar and lime mortar), for brick B.

Contact Type PHC - BRICK B	**Cement mortar**			**Lime mortar**		
Interface level	**2 cm**	**5 cm**	**7 cm**	**2 cm**	**5 cm**	**7 cm**
Measured distance after the interface transition (cm)	8 cm	5 cm	3 cm	8 cm	5 cm	3 cm
Measured time (h)	4h	3h	2h	4h	3h	2h
Velocity (cm/h) of progression after the interface transition (cm/h) - water content.	2.00	1.67	1.50	2.00	1.67	1.50
Measured time (h)	6h	2h	2h	4h	2h	2h
Velocity (cm/h) of progression after the interface transition (cm/h) - High water content.	1.33	2.50	3.00	2.00	2.50	3.00
Velocity of progression after the interface transition (m/s)(AZEVEDO, 2019)	3.5 - $2.3x10^{-7}$	5.6 - $2.9x10^{-7}$	$1.8x10^{-7}$	$3.5x10^{-7}$	$6.3x10^{-7}$	$3.8x10^{-7}$

Source: Author.

samples. The best way to analyze the surface moisture progression is by analyzing the transported water content through the simulation images that also allow access to the value of the water content at any point on the surface. Analyzing the images presented above (Figure 34 to Figure 39), it can be concluded that the water progression on the surface of the samples is faster in the samples with lime mortar compared to the samples with cement mortar. This result is consistent with the result presented in the experimental study.

Also, it can be concluded that the transport of low water content in the samples is slower than the transport of high water content. The progression of water on the surface of the samples is faster in the samples with brick B compared to the samples with brick A.

4.1.1.1 Section results overview

- There is a reduction in the absorbed water content in the samples with cement mortar and lime mortar perfect hydraulic contact, compared to the absorbed water content by the monolithic sample; This result was consistent with the Azevedo (2019) experimental result.
- No significant change was observed in the curves for samples with perfect hydraulic contact in comparison with the curve for monolithic samples. Therefore, not characterizing a discontinuity caused by the interface of the materials in the mortar samples, but considering the layer material properties as influencing the water transport resistance. This result diverges from the experimental result of Azevedo (2019).
- The samples with perfect hydraulic contact interface with cement mortar show higher absorption rates than the samples with lime mortar; This result diverged with the Azevedo (2019) experimental result. As well as for the previous divergence, the explanation for this result may be related to the type of perfect contact that the program calculates. In the experimental test the type of contact is imperfect, with a discontinuity ("layer") at the interface, of unknown property, caused by the brick layer absorbing particles from the fresh cement mortar layer, characterizing an imperfect hydraulic contact and attributing a higher resistance to water transport.
- Brick A proved to be more impermeable than cement and lime mortars, considering that brick A has a lower water absorption coefficient. This impermeability interfered in the water transport through the top layer of the samples, causing a slower absorption.
- The cement and lime mortars proved to be more impermeable than brick B, considering that brick B has a higher water absorption coefficient. This impermeability interfered in water transport through the interface of perfect hydraulic contact, causing a water barrier and slowing the water transport through the mortar layer.
- The moisture progression on the brick B samples surface were faster than the moisture progression on the brick A samples surface. This result proved to be consistent with the experimental result; The velocity influence may be related to the higher permeability and surface area for brick B.

- The moisture progression on the surface of monolithic brick A sample is slower compared to the samples with perfect hydraulic contact interface due to higher mortar permeability compared to brick A permeability.
- The material layer less permeable than the brick in the joint will reduce the water absorption in the sample when positioned at a shorter distance from the saturated wet front.

4.1.2 Moisture transport across air space interface – Absorption process

In order to study the influence of an air space between material layers, moisture transport simulations were performed on samples with two configurations of air layers placed between the brick layers at different heights (as presented previously in table 3): 2mm air space positioned at 2cm, 5cm and 7cm from the base of the sample and 5mm air space positioned at 2cm, 5cm and 7cm.

Figure 40 and Figure 41 shows the plot of the simulations after 72h for the moisture transport (kg/m³) per hour along the samples with an air space interface between brick A and brick B layers, comparing with the moisture transport behavior in the monolithic brick sample.

Figure 40 - Water content graph along brick A after 72h of simulated transport for air space interface between brick A layers.

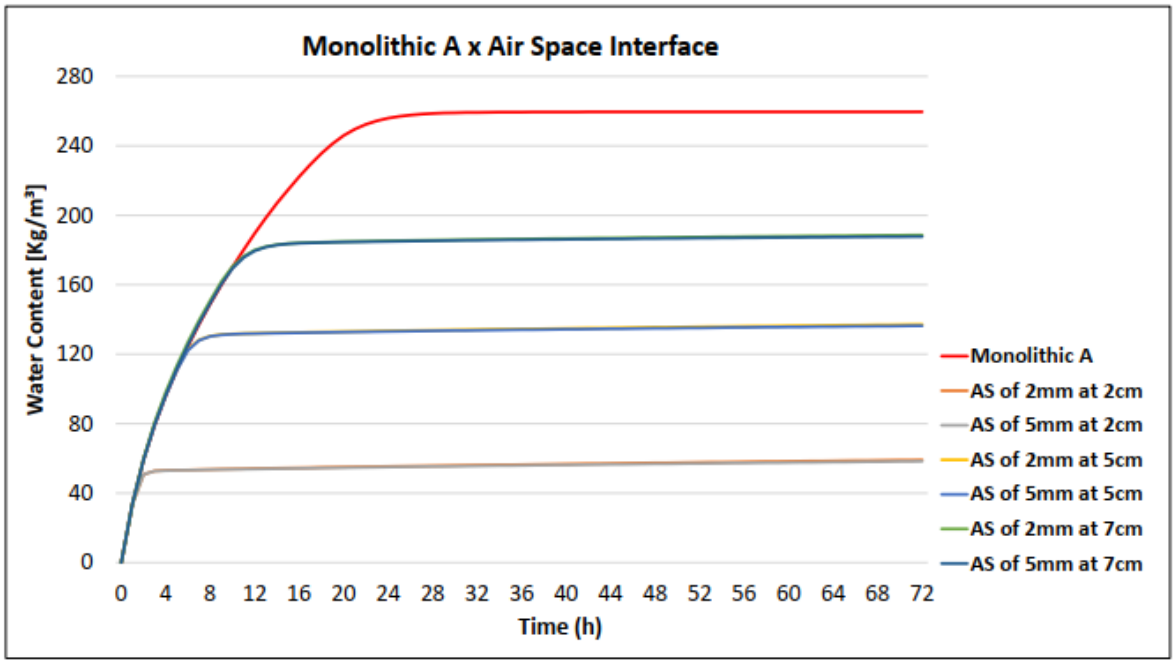

Source: Author.

Figure 41 - Water content graph along brick A after 72h of simulated transport for air space interface between brick B layers.

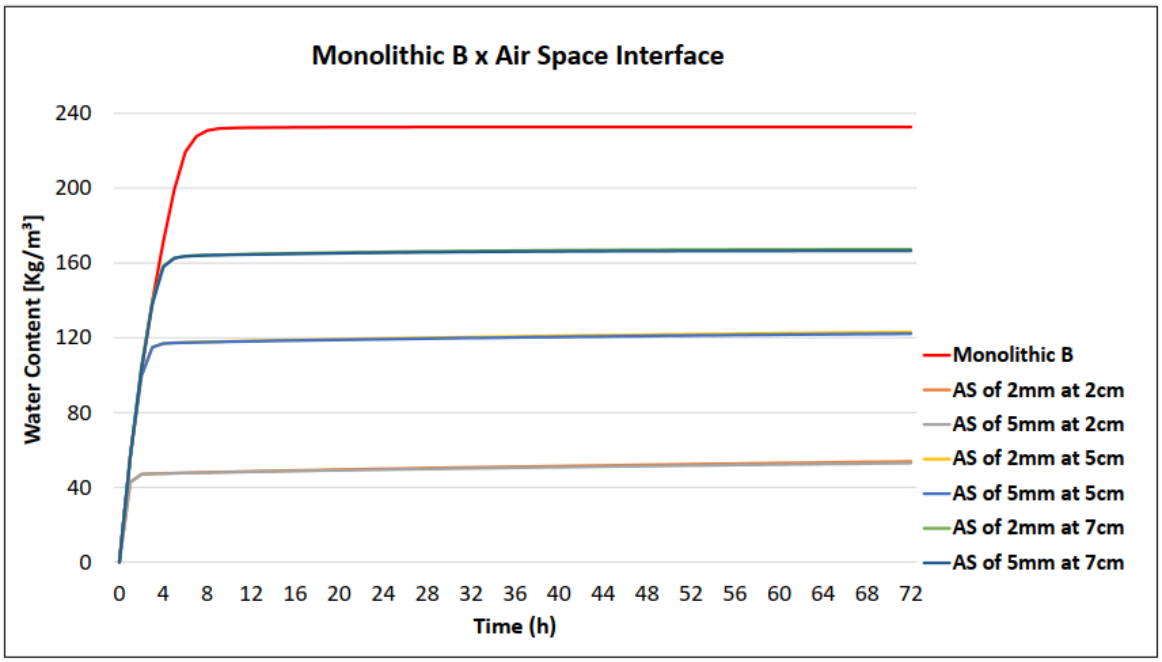

Source: Author.

Figure 40 and Figure 41 reveals a water resistance when the water content reaches the interface (at 2cm, 5cm and 7cm height), reducing and almost stopping the water content transport across the interface. The results are similar for the samples with 2mm air space and 5mm air space, but by analyzing the simulation results, a higher water content transported through the samples with 2mm air space was observed.

Table 9 shows the values obtained for the hydric resistance of the simulated samples, using the same methodology as Azevedo (2019).

Table 9 - Values of hydric resistance for air space interface between brick layers.

Material	Sample / (interface type)	Hydric Resistance (AZEVEDO,2019) Kg/m²s	Hydric Resistance kg/m³h
Red brick Type "A"	Air space 2mm at 2cm	0.8x10-5	0.3570
	Air space 5mm at 2cm	0.4x10-5	0.3469
	Air space 2mm at 5cm	0.9x10-5	0.2154
	Air space 5mm at 5cm	0.8x10-5	0.3800
	Air space 2mm at 7cm	0.9x10-5	0.1989
	Air space 5mm at 7cm	0.4x10-5	0.2944
Red brick Type "B"	Air space 2mm at 2cm	0.7x10-5	0.1569
	Air space 5mm at 2cm	0.8x10-5	0.1450
	Air space 2mm at 5cm	1.0x10-5	0.3325
	Air space 5mm at 5cm	0.7x10-5	0.9219
	Air space 2mm at 7cm	0.7x10-5	0.1313
	Air space 5mm at 7cm	0.9x10-5	0.4144

Source: Author.

The presented results for hydric resistances at the air space interface were similar in samples with brick A and samples with brick B. For the samples with interface positioned at 2cm, the samples with 2mm air space interface showed higher resistances compared to the samples with 5mm air space interface. For the samples with interface positioned at 5cm and 7cm, higher resistances were presented for the 5mm air space interface. It is concluded that for 2mm air layers the influence on water transport resistance is greater when the interface is close to the saturated wet front. For 5mm air layers the influence is greater at interfaces positioned at 5cm compared to samples with an interface positioned at 7cm. According to the properties of the air layers, the 5mm air layer has a higher water vapor resistance compared with the 2mm air layer.

In the WUFI physics background, in vapor-tight assemblies, the high moisture capacity of these air layers may distort the moisture distribution, since the air absorbs too large a fraction of the moisture present in the assembly. In vapor-permeable assemblies this is less of an issue because the high moisture content accumulating in the air layer is not at the expense of the moisture in the other materials.

The hydric resistances for the simulated samples show a mostly different behavior than the resistance values found for the experimental samples.

Figure 42 - Effect of air space interface on moisture surface progression at different simulation times for ceramic block A.

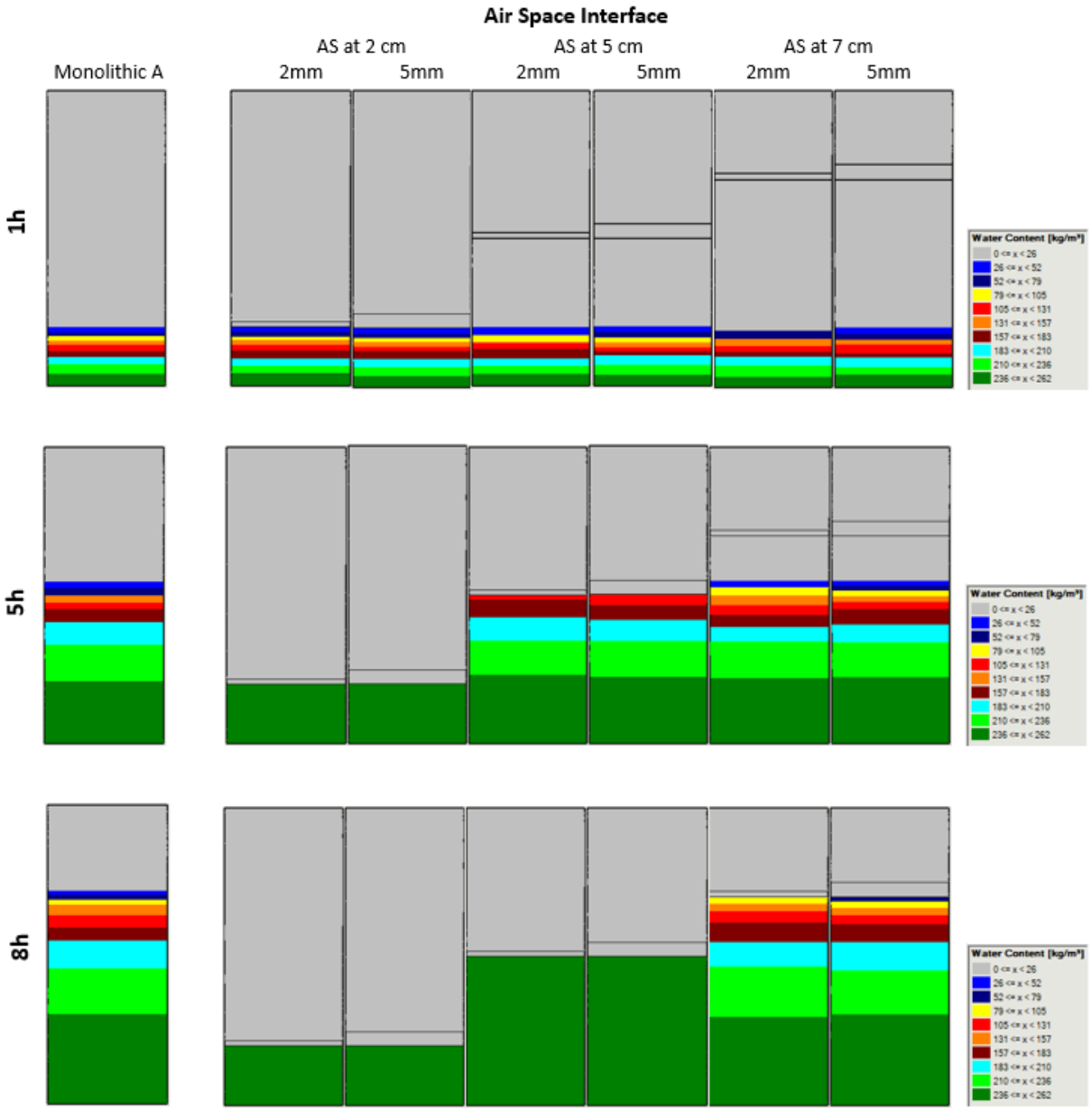

Source: Author.

In Figure 42 brick A samples with interface positioned at 2cm shows slower moisture transport through the 2mm air space layer compared to the 5mm air space layer. For the interfaces positioned at 5m and 7cm, the moisture transport is slower through the 5mm air layer compared to the 2mm air layer. In Figure 43 brick B samples show the same moisture transport behavior as brick A samples. The results prove the consistency of the values found for the resistances presented in table 9.

Figure 43 - Effect of air space interface on moisture surface progression at different simulation times for ceramic block B.

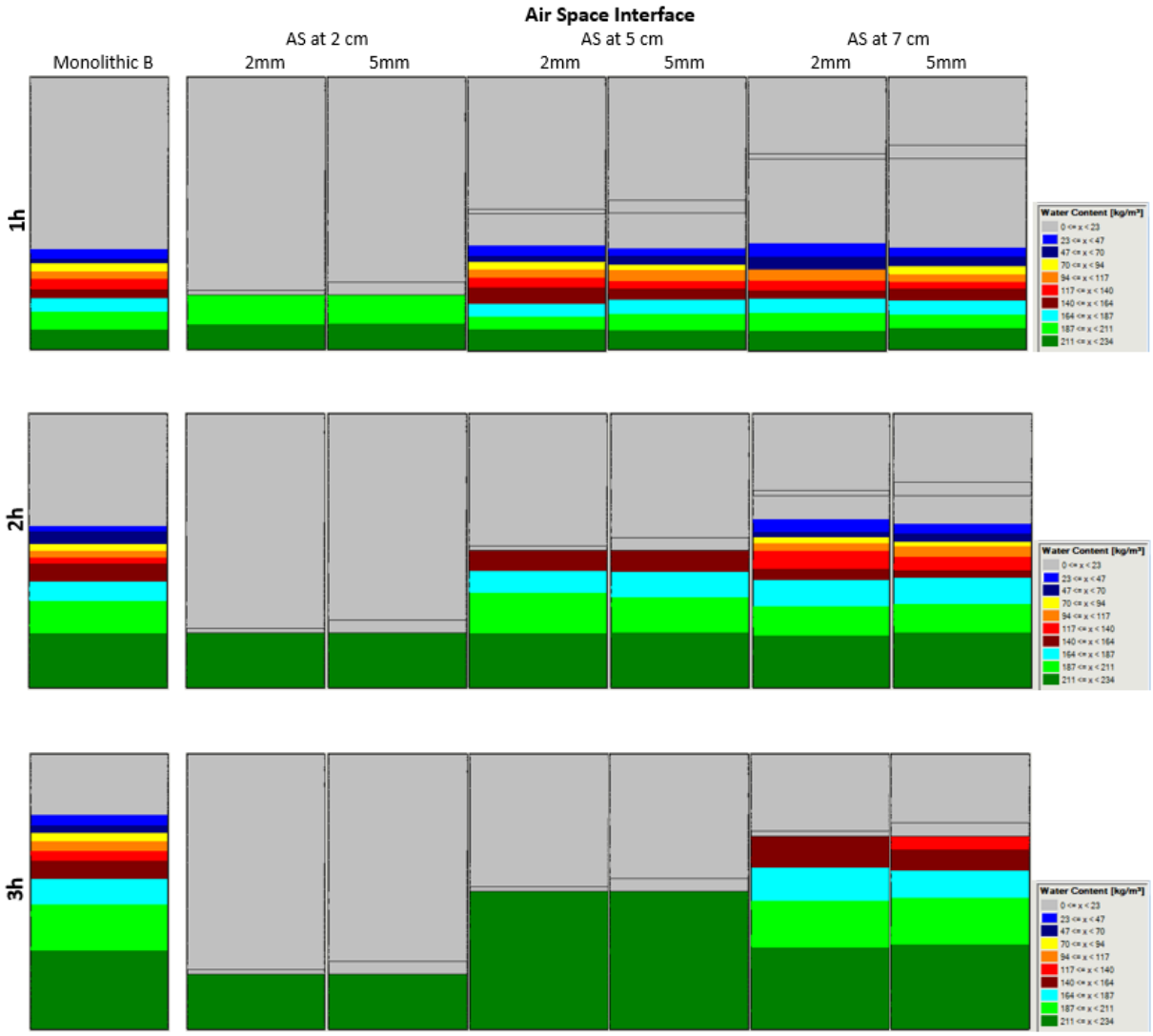

Source: Author.

Figure 44 and Figure 45 shows the water content in the samples with air space interface at the end of the 72h water absorption test simulation. In order to check the water content progression height on the surface after crossing the airspace interface, the water content values at different points on the surface of the samples at the end of the simulation were measured (Table 10).

Figure 44 - Water content along the sample with brick A after 72h of simulated transport for air space interface between brick A layers – a) open scale, b) reduced scale.

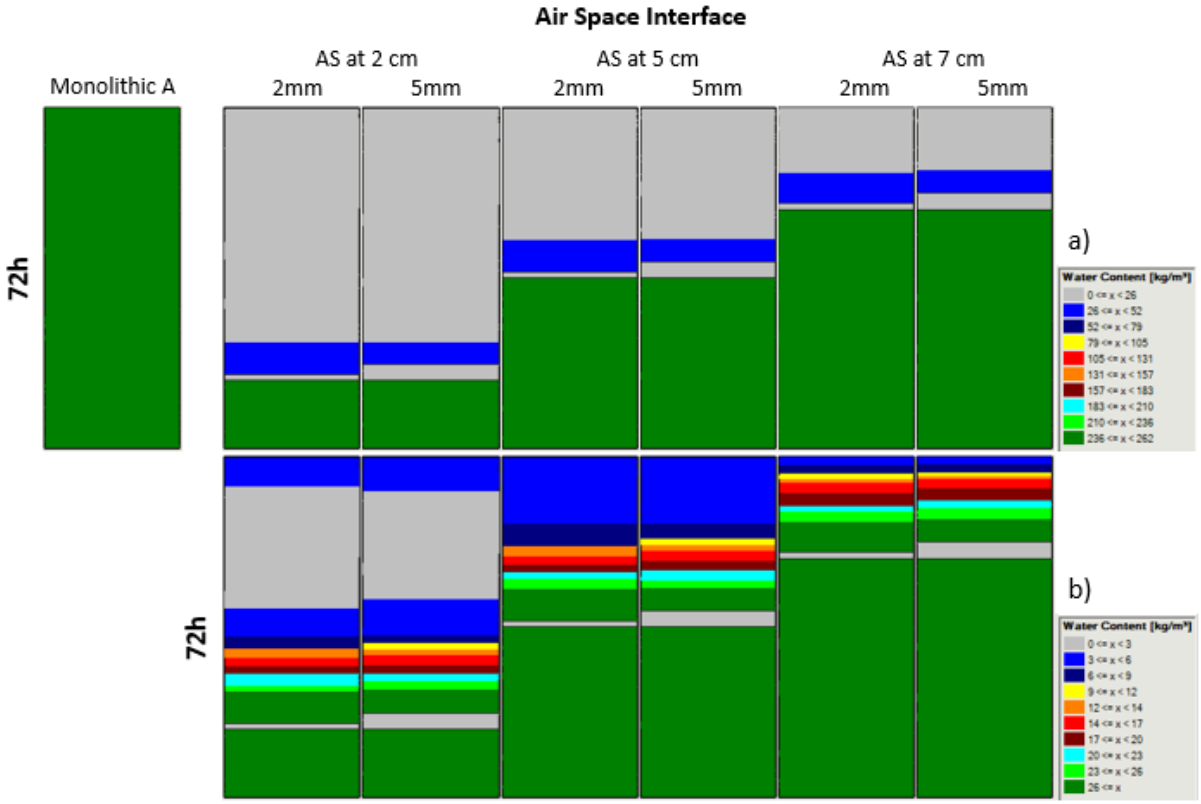

Source: Author.

Figure 45 - Water content along the sample with brick A after 72h of simulated transport for air space interface between brick B layers – a) open scale, b) reduced scale.

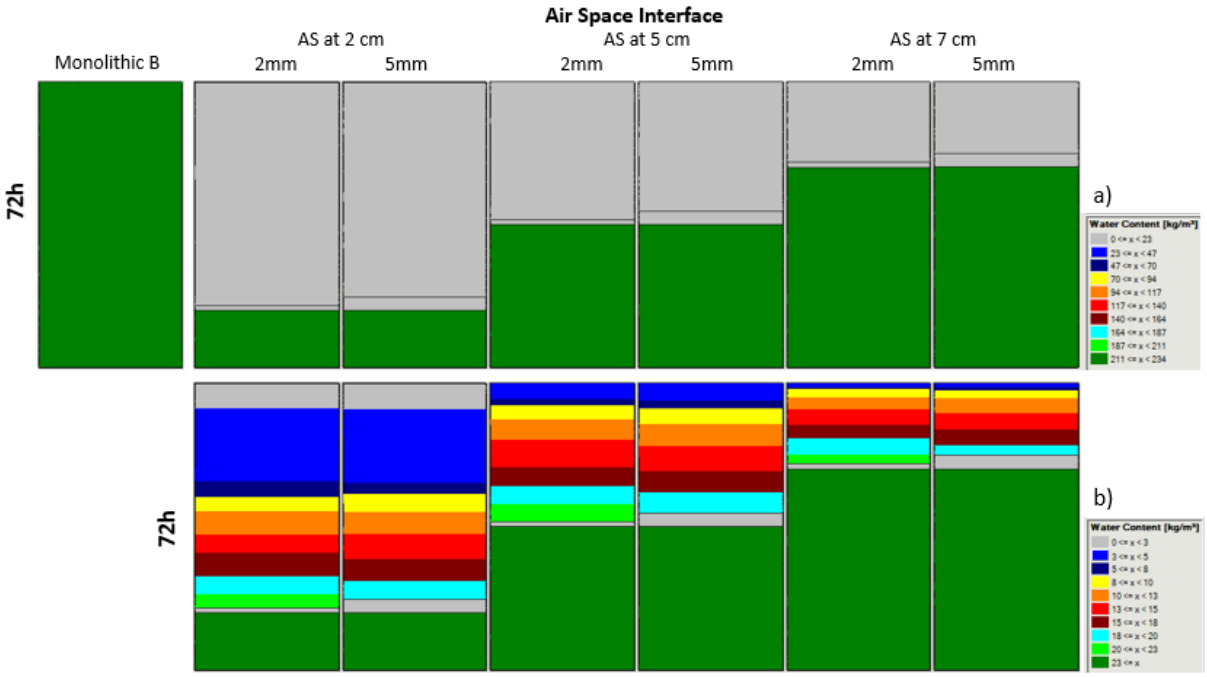

Source: Author.

Table 10 - water content values at different points on the surface of the samples at the end of the simulation.

	Interface	Air Space	Water content at the surface points (kg/m³)			
			3cm	6cm	9cm	10cm
Brick A	2cm	2mm	27.75	2.672	-	-
		5mm	27.99	2.672	-	-
	5cm	2mm	-	27.95	4.071	-
		5mm	-	28.36	4.203	-
	7cm	2mm	-	-	16.52	4.276
		5mm	-	-	17.47	4.316
Brick B	2cm	2mm	18.91	9.474	2.558	-
		5mm	18.46	8.611	2.556	-
	5cm	2mm	-	19.35	9.357	2.774
		5mm	-	18.92	8.772	2.687
	7cm	2mm	-	-	13.12	3.111
		5mm	-	-	12.68	3.052

Source: Author.

In Figure 44 it can be seen that a low moisture content passes the air space interface in the samples with brick A. An image with reduced water content scale was selected to evaluate the water content in the second brick A layer. Samples with 5mm airspace interface showed a wet front with higher water content compared to samples with 2mm air space interface.

In Figure 45 it can be seen that significant water contents do not pass the air space interface in the samples with brick B. An image with reduced water content scale was selected to evaluate the water content in the second brick B layer. Samples with 2mm air space interface showed a wet front with higher water content compared to samples with 5mm air space interface.

4.1.2.1 Section results overview

- The two tested ceramic materials with air space interface show a constant initial absorption rate and, when moisture reaches the interface, a very slow absorption; This result was shown to be consistent with Azevedo's (2019) experimental results.
- The 2mm air space interfaces positioned at a shorter distance from the saturated moisture front generates a higher water transport resistance

compared to the 5mm air space interfaces. Conversely, the 5mm air space interfaces positioned at a greater distance from the wet front generate greater moisture transport resistance in the samples compared to the 2mm air space interfaces.

4.1.3 Comparison of the experimental results with the results obtained by the WUFI-2D 4.3 program – Absorption process

In this section an attempt was made to validate the water absorption results over time in the samples obtained with the WUFI 2D 4.3 program, comparing them with the experimental results obtained by Azevedo (2019). Also, it was chosen to perform new simulations in order to compare the results obtained for the moisture content profiles in the experimental test and with the use of the program, in order to highlight some potentialities of the numerical model that uses the relative humidity gradient as the driver in moisture transfer.

The experimental results obtained by Azevedo (2019) relied on measuring moisture contents by gamma radiation attenuation for the experimental determination of moisture content profiles and were approximated by a polynomial function.

The results in Figures 46 to 49 of water absorption over time in the samples showed a good relationship between the results obtained with the program and the experimental results. The differences obtained in the results are characteristic of the different contact type, emphasizing that the experimental tests on the samples with mortar ensure an imperfect hydraulic contact and the samples in the program are simulated with the perfect contact interpretation. In relation to the samples with air space, the only difference in the parameters corresponds to a small presence of moisture in the air layer created in the program.

Figure 46 - Comparison of water absorption for the brick A samples with perfect hydraulic contact, obtained experimentally and by the simulation program WUFI-2D 4.3.

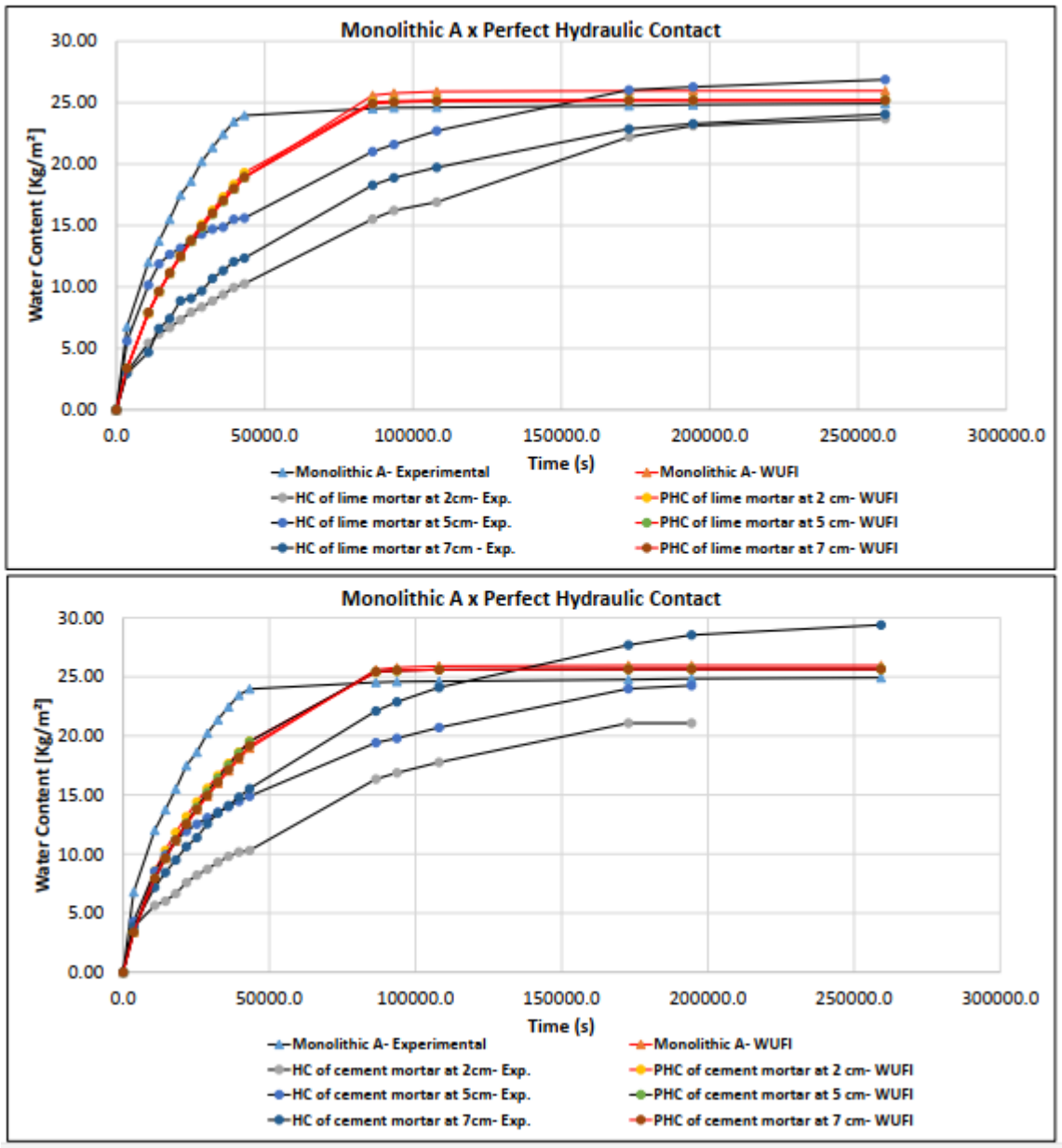

Source: Author.

Figure 47 - Comparison of water absorption for the brick B samples with perfect hydraulic contact, obtained experimentally and by the simulation program WUFI-2D 4.3.

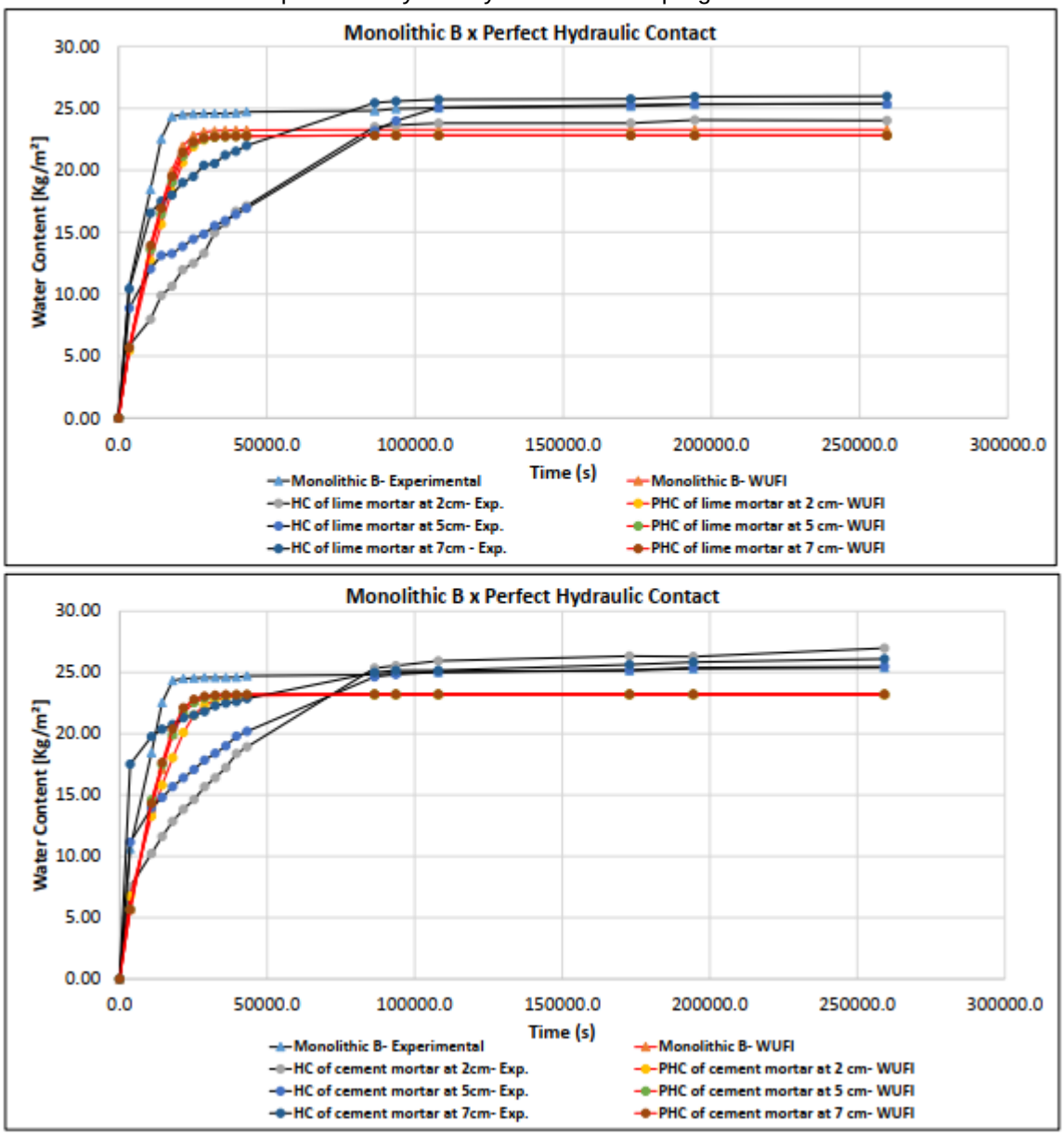

Source: Author.

Figure 48 - Comparison of water absorption for the brick A samples with air space interface, obtained experimentally and by the simulation program WUFI-2D 4.3.

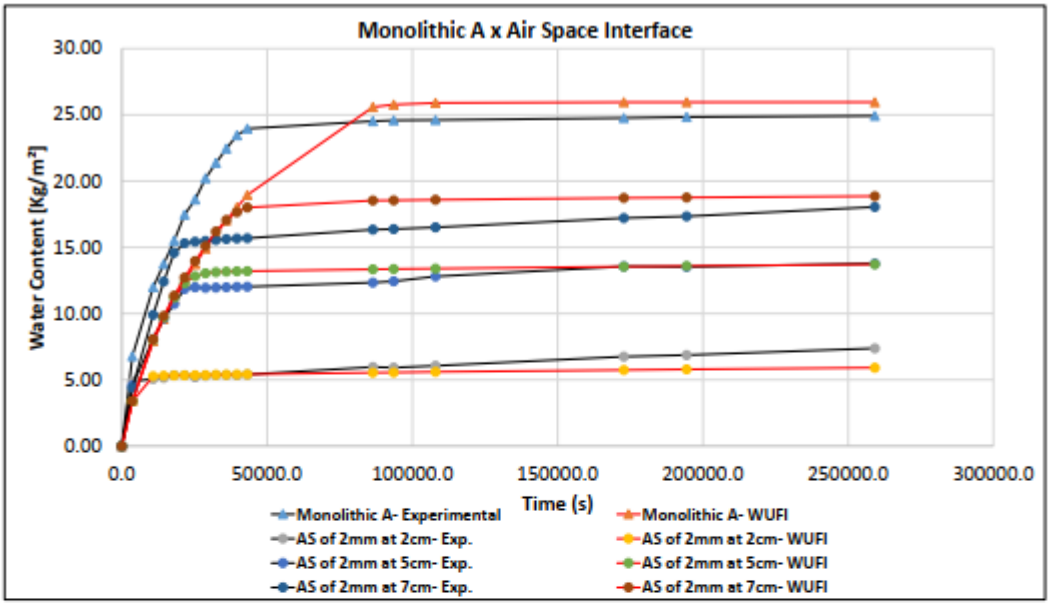

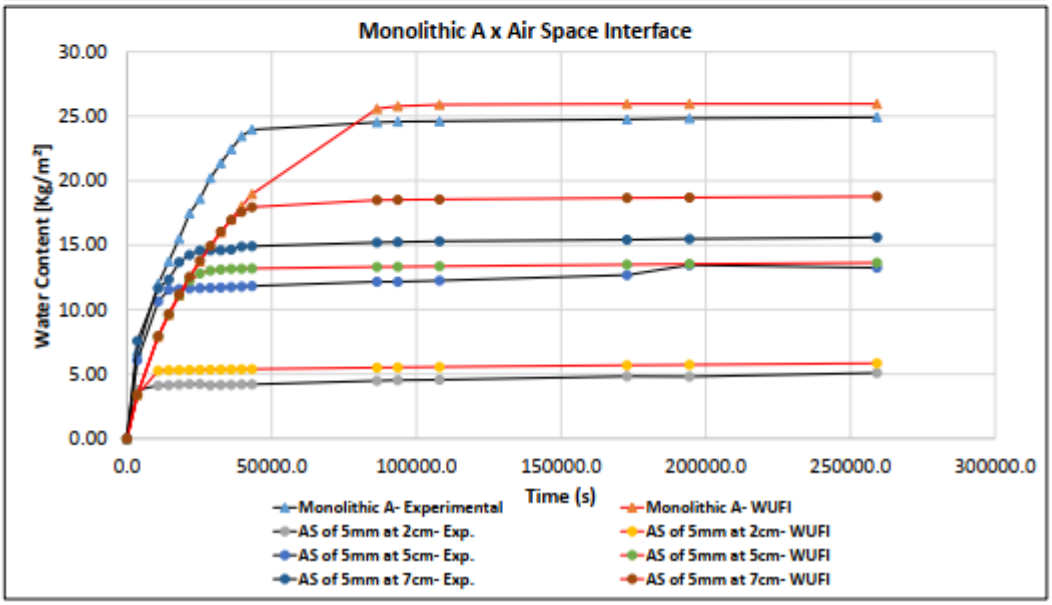

Source: Author.

Figure 49 - Comparison of water absorption for the brick B samples with air space interface, obtained experimentally and by the simulation program WUFI-2D 4.3.

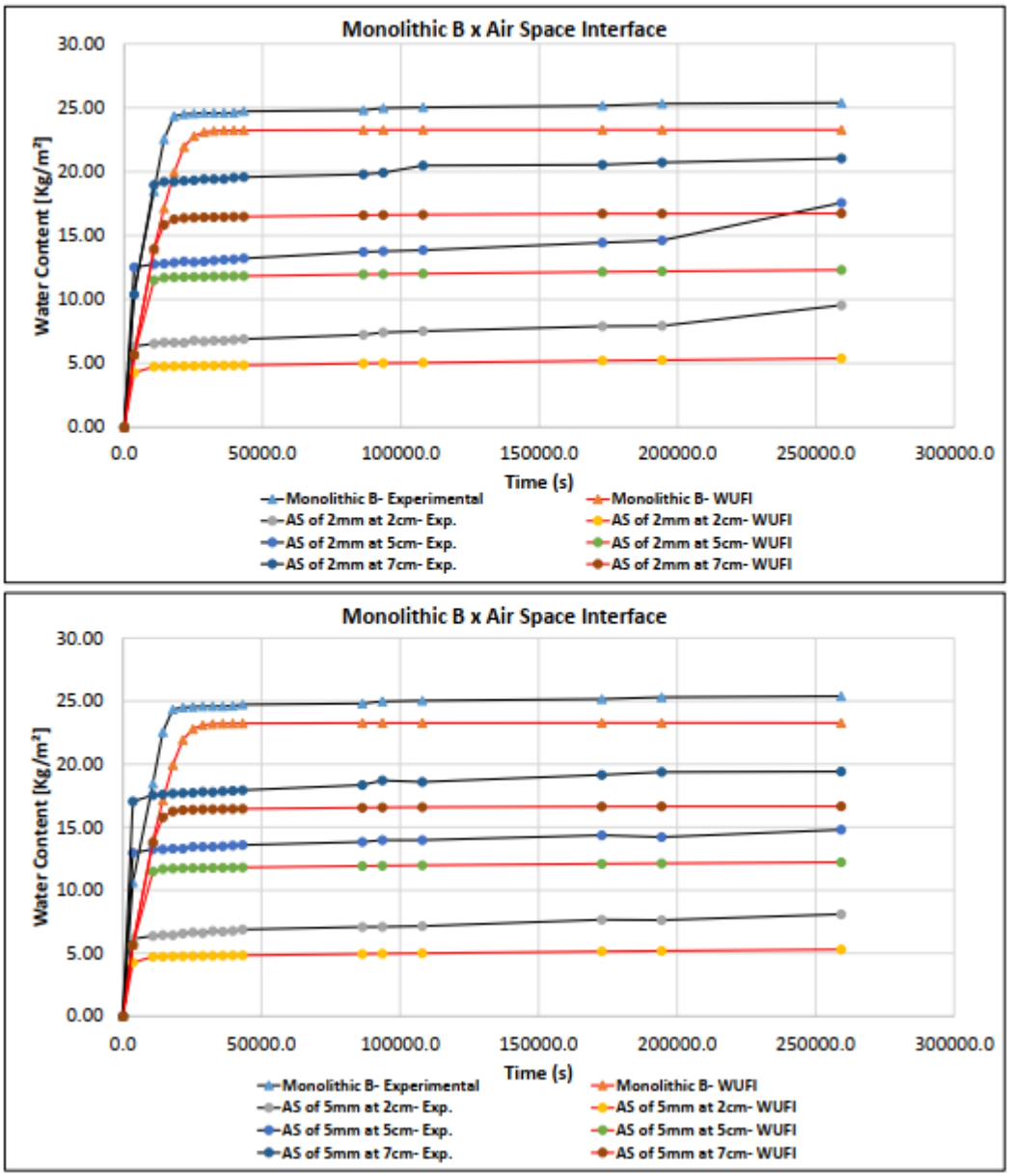

Source: Author.

Figure 50 and Table 11 present example of hydraulic contact equations for imbibition curve and tested models for modelling imbibition hydraulic contact, ceramic block A and B obtained experimentally and by WUFI-2D program.

Figure 50 - Comparison of hydraulic contact example equations for imbibition curve, Ceramic block A and B, obtained experimentally and by the simulation program WUFI-2D 4.3.

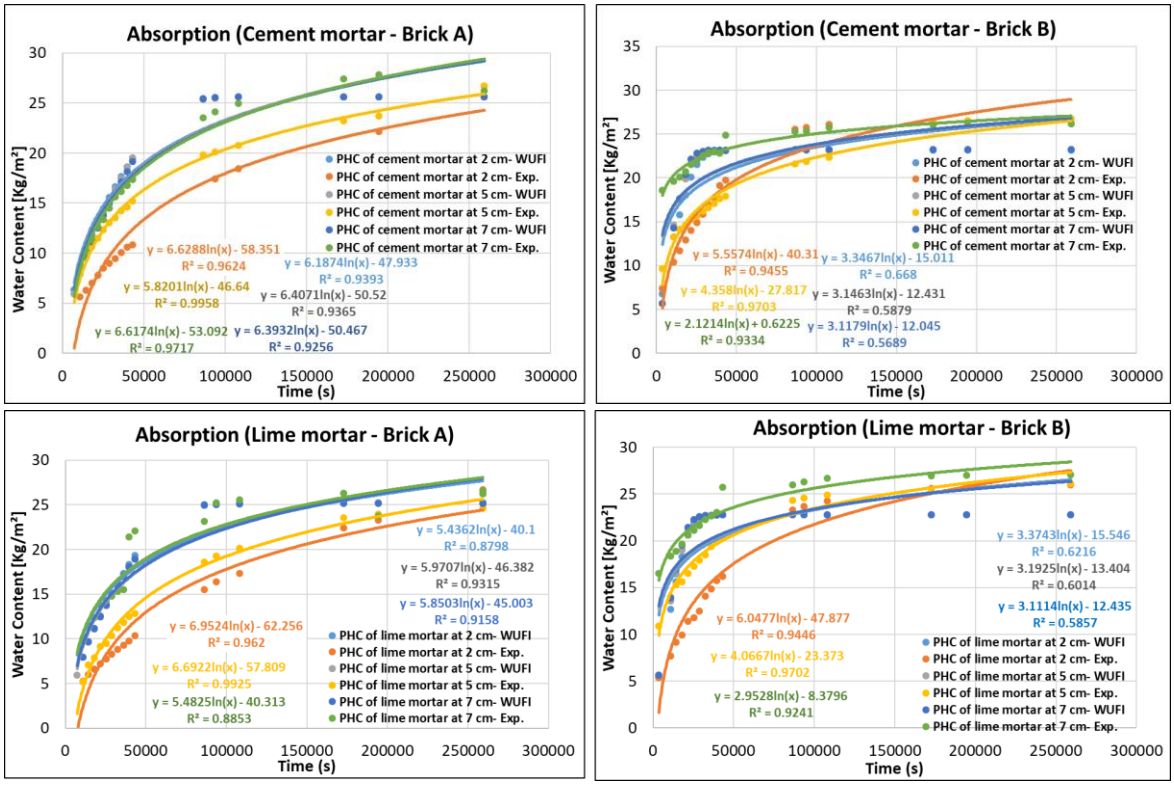

Source: Author.

Table 11 - Tested models for modelling imbibition hydraulic contact, Ceramic Block A and B.

Model name	Model equation at 2cm	Model equation at 5cm	Model equation at 7cm
Cement mortar - Ceramic A Exp.	$g(t) = \frac{d(6.63\ln(t) - 58.3)}{dt}$ $g(t) = \frac{6.63}{t}$ $t_k = 86.400\ s$ $\boldsymbol{RH = 7.7\ x\ 10^{-5}}$	$g(t) = \frac{d(5.82\ln(t) - 46.6)}{dt}$ $g(t) = \frac{5.82}{t}$ $t_k = 86.400\ s$ $\boldsymbol{RH = 6.7\ x\ 10^{-5}}$	$g(t) = \frac{d(6.62\ln(t) - 53.0)}{dt}$ $g(t) = \frac{6.62}{t}$ $t_k = 86.400\ s$ $\boldsymbol{RH = 7.7\ x\ 10^{-5}}$
Cement mortar - Ceramic A (WUFI)	$g(t) = \frac{d(6.19\ln(t) - 47.9)}{dt}$ $g(t) = \frac{6.19}{t}$ $t_k = 86.400\ s$ $\boldsymbol{RH = 7.2\ x\ 10^{-5}}$	$g(t) = \frac{d(6.41\ln(t) - 50.5)}{dt}$ $g(t) = \frac{6.41}{t}$ $t_k = 86.400\ s$ $\boldsymbol{RH = 7.4\ x\ 10^{-5}}$	$g(t) = \frac{d(6.39\ln(t) - 50.4)}{dt}$ $g(t) = \frac{6.39}{t}$ $t_k = 86.400\ s$ $\boldsymbol{RH = 7.4\ x\ 10^{-5}}$
Cement mortar - Ceramic B Exp.	$g(t) = \frac{d(5.56\ln(t) - 40.3)}{dt}$ $g(t) = \frac{5.56}{t}$ $t_k = 86.400\ s$ $\boldsymbol{RH = 6.4\ x\ 10^{-5}}$	$g(t) = \frac{d(4.36\ln(t) - 27.8)}{dt}$ $g(t) = \frac{4.36}{t}$ $t_k = 86.400\ s$ $\boldsymbol{RH = 5.0\ x\ 10^{-5}}$	$g(t) = \frac{d(2.12\ln(t) + 0.6)}{dt}$ $g(t) = \frac{2.12}{t}$ $t_k = 86.400\ s$ $\boldsymbol{RH = 2.4\ x\ 10^{-5}}$

Cement mortar - Ceramic B (WUFI)	$g(t) = \frac{d(3.35\ln(t) - 15.0)}{dt}$ $g(t) = \frac{3.35}{t}$ $t_k = 86.400\ s$ $\boldsymbol{RH = 3.9\ x\ 10^{-5}}$	$g(t) = \frac{d(3.15\ln(t) - 12.4)}{dt}$ $g(t) = \frac{3.15}{t}$ $t_k = 86.400\ s$ $\boldsymbol{RH = 3.6\ x\ 10^{-5}}$	$g(t) = \frac{d(3.12\ln(t) + 12.0)}{dt}$ $g(t) = \frac{3.12}{t}$ $t_k = 86.400\ s$ $\boldsymbol{RH = 3.6\ x\ 10^{-5}}$
Lime mortar - Ceramic A Exp.	$g(t) = \frac{d(6.95\ln(t) - 62.2)}{dt}$ $g(t) = \frac{6.95}{t}$ $t_k = 86.400\ s$ $\boldsymbol{RH = 8.4\ x\ 10^{-5}}$	$g(t) = \frac{d(6.69\ln(t) - 57.8)}{dt}$ $g(t) = \frac{6.69}{t}$ $t_k = 86.400\ s$ $\boldsymbol{RH = 7.7\ x\ 10^{-5}}$	$g(t) = \frac{d(5.48\ln(t) - 40.3)}{dt}$ $g(t) = \frac{5.48}{t}$ $t_k = 86.400\ s$ $\boldsymbol{RH = 6.3\ x\ 10^{-5}}$
Lime mortar - Ceramic A (WUFI)	$g(t) = \frac{d(5.44\ln(t) - 40.1)}{dt}$ $g(t) = \frac{5.44}{t}$ $t_k = 86.400\ s$ $\boldsymbol{RH = 6.\ 3\ x\ 10^{-5}}$	$g(t) = \frac{d(5.97\ln(t) - 46.4)}{dt}$ $g(t) = \frac{5.97}{t}$ $t_k = 86.400\ s$ $\boldsymbol{RH = 6.9\ x\ 10^{-5}}$	$g(t) = \frac{d(5.85\ln(t) - 45.0)}{dt}$ $g(t) = \frac{5.85}{t}$ $t_k = 86.400\ s$ $\boldsymbol{RH = 6.8\ x\ 10^{-5}}$
Lime mortar - Ceramic B Exp.	$g(t) = \frac{d(6.05\ln(t) - 47.9)}{dt}$ $g(t) = \frac{6.05}{t}$ $t_k = 86.400\ s$ $\boldsymbol{RH = 7.0\ x\ 10^{-5}}$	$g(t) = \frac{d(4.07\ln(t) - 23.4)}{dt}$ $g(t) = \frac{4.07}{t}$ $t_k = 86.400\ s$ $\boldsymbol{RH = 4.7\ x\ 10^{-5}}$	$g(t) = \frac{d(2.95\ln(t) - 8.38)}{dt}$ $g(t) = \frac{2.95}{t}$ $t_k = 86.400\ s$ $\boldsymbol{RH = 3.4\ x\ 10^{-5}}$
Lime mortar - Ceramic B (WUFI)	$g(t) = \frac{d(3.37\ln(t) - 15.5)}{dt}$ $g(t) = \frac{3.37}{t}$ $t_k = 86.400\ s$ $\boldsymbol{RH = 3.\ 9\ x\ 10^{-5}}$	$g(t) = \frac{d(3.19\ln(t) - 13.4)}{dt}$ $g(t) = \frac{3.19}{t}$ $t_k = 86.400\ s$ $\boldsymbol{RH = 3.7\ x\ 10^{-5}}$	$g(t) = \frac{d(3.11\ln(t) - 12.4)}{dt}$ $g(t) = \frac{3.11}{t}$ $t_k = 86.400\ s$ $\boldsymbol{RH = 3.6\ x\ 10^{-5}}$

Source: Author.

With the RH values presented, the resistance will be a function of time. For both brick types, the RH results found were similar with the results found in section 4.1.1 due to the non-influence of the interface, considering only the resistance caused due to the differences in material properties. However, the methodology proved to be more effective, since the values found for the hydric resistances were very close, in agreement with the results presented in the figures 46 and 47 graphs. For the samples with brick B, the values of hydric resistance for the two types of mortar gave similar comparisons in the same position, in both numerical and experimental results.

Figure 51 show the best linear functions that describe the mass variation per area in function of time, after the “knee point”, for samples with air space interface. For the calculation of the hydric resistance, the derivative of the best fit function is proposed.

Figure 51 - Comparison of Air space equation of imbibition curve, Ceramic block A and B, obtained experimentally and by the simulation program WUFI-2D 4.3.

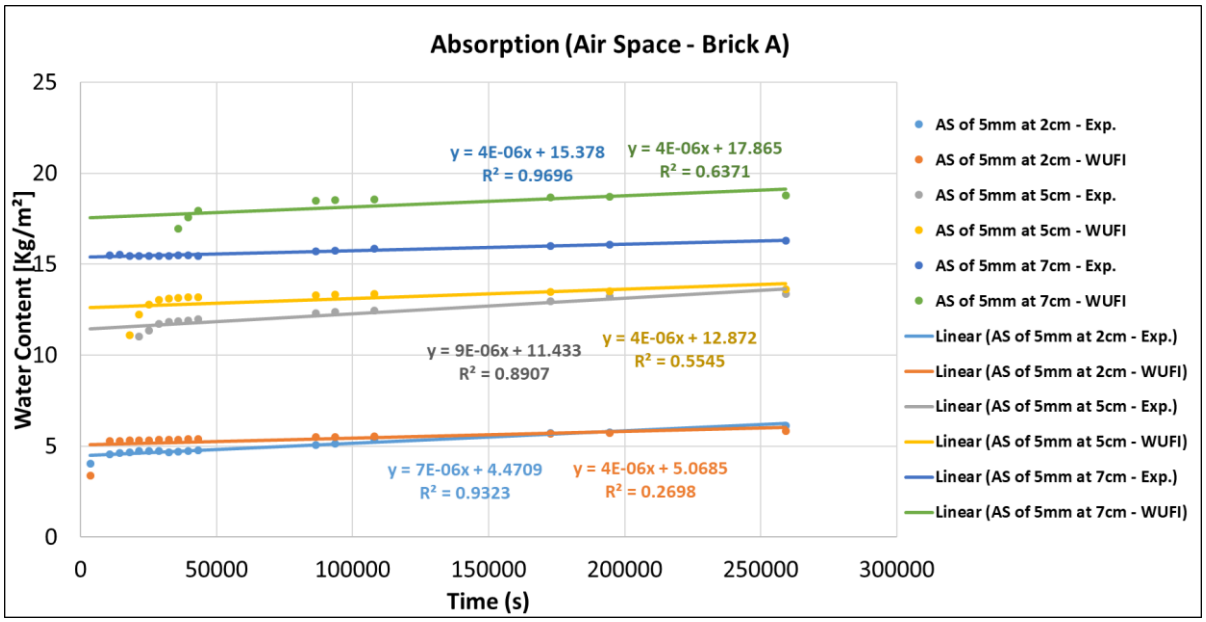

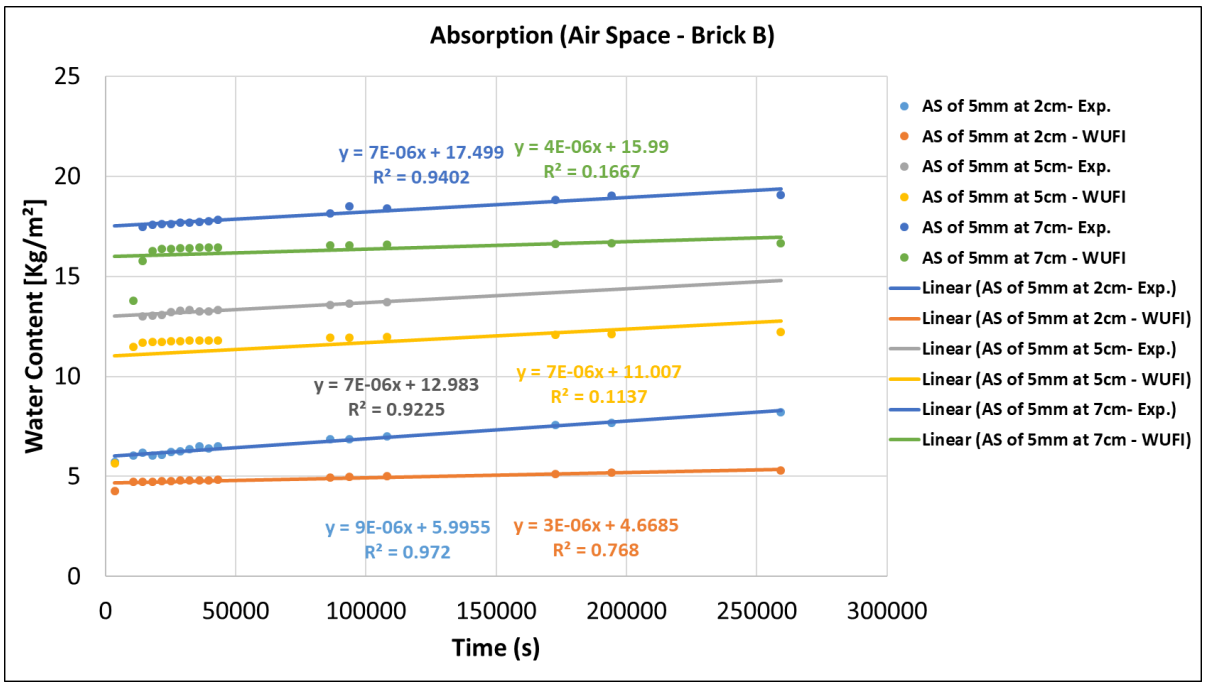

Source: Author.

Table 12 - Tested models for modelling of air space.

Interface Type	Model equation (Brick A)	Model equation (Brick B)
Air Space at 2cm - Exp.	$g(t) =$ 7E-06t + 4.479 $\boldsymbol{RH = 7E\ -06}$	$g(t) =$ 9E-06t + 5.9955 $\boldsymbol{RH = 9E\ -06}$
Air Space at 2cm - (WUFI)	$g(t) =$ 4E-06t + 5.0685 $\boldsymbol{RH = 4E\ -06}$	$g(t) =$ 3E-06t + 4.6685 $\boldsymbol{RH = 3E\ -06}$
Air Space at 5cm - Exp.	$g(t) =$ 9E-06t + 11.433 $\boldsymbol{RH = 9E\ -06}$	$g(t) =$ 7E-06t + 12.983 $\boldsymbol{RH = 7E\ -06}$
Air Space at 5cm - (WUFI)	$g(t) =$ 4E-06t + 12.872 $\boldsymbol{RH = 4E\ -06}$	$g(t) =$ 7E-06t + 11.007 $\boldsymbol{RH = 7E\ -06}$
Air Space at 7cm - Exp.	$g(t) =$ 4E-06t + 15.378 $\boldsymbol{RH = 4E\ -06}$	$g(t) =$ 7E-06t + 17.499 $\boldsymbol{RH = 7E - 06}$
Air Space at 7cm - (WUFI)	$g(t) =$ 4E-06t + 17.865 $\boldsymbol{RH = 4E\ -06}$	$g(t) =$ 4E-06t + 15.99 $\boldsymbol{RH = 4E\ -06}$

Source: Author.

Analyzing the results in Table 12 it is possible to arrive in the same conclusion that it was reported by Azevedo (2019), where it wasn't identified relation between the transfer of humidity in the interface with air space and the position of the interface, which may, however, be related to moisture transfer in the vapor phase. It was considering one hypothesis, which is to report that the hydric resistance to airspace interface is in the order of 10-6 (kg/m²s). The models for the WUFI results haven't achieved good prediction performance (R ≤ 90 %). The explanation can be related to the knees points choose considering a drop in relation to the monolithic samples, but this drop is not abrupt, taking a few more hours to start linear water absorption.

4.1.3.1 Comparison of moisture profiles obtained during the wetting process

The results obtained in the experimental test using HUMIGAMA to obtain moisture profiles along the thickness of the sample, allowed to know the distribution of the moisture content. The results of monolithic samples were used to compare with samples having air space interface and perfect hydraulic contact (cement and lime

mortar) (with different interface locations). With the software WUFI-2D it was possible to use the mass water content made available by the program, requiring simulations for each hour of analysis.

Figure 52 presents the moisture content profiles along the specimen thickness for the monolithic samples tested with gamma ray attenuation (Experimental) and by numerical modeling (WUFI-2D 4.3) in absorption process.

Figure 52 - Moisture content along the monolithic samples thickness of ceramic block A and B.

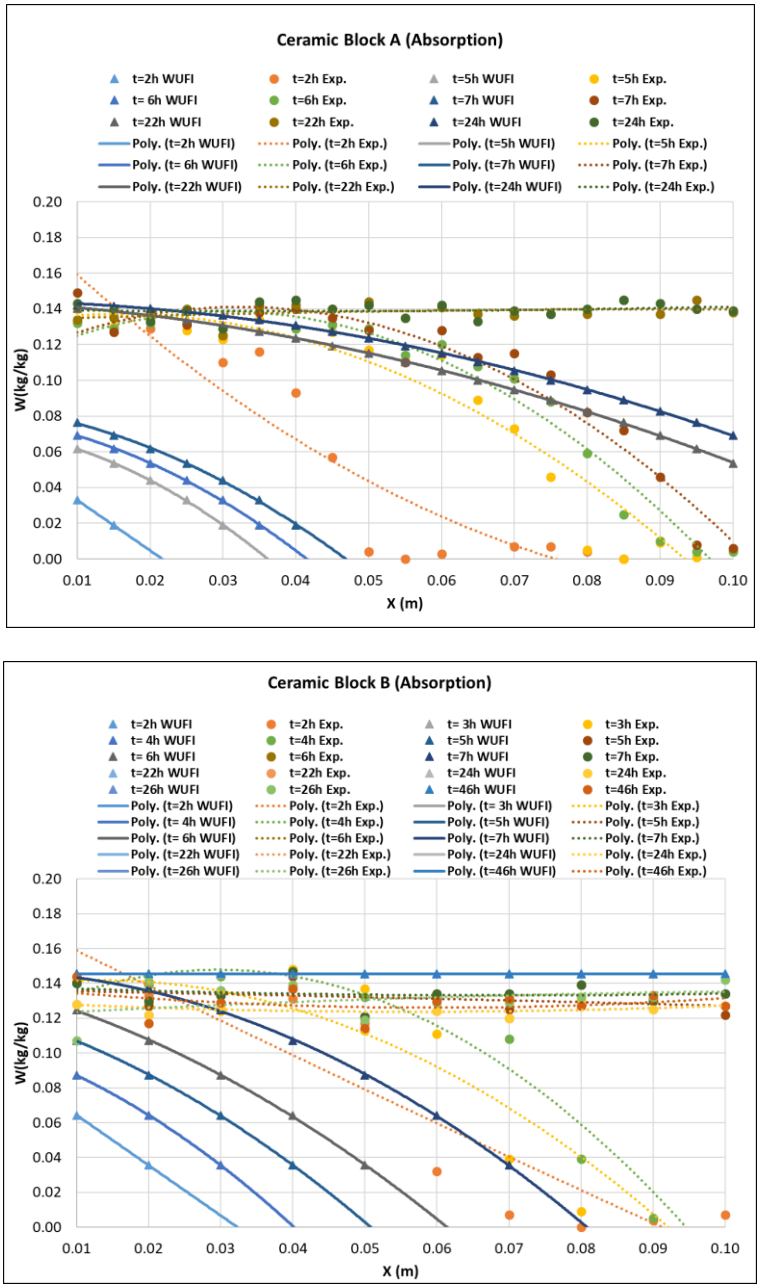

Source: Author.

Figure 53 shows the moisture profiles in the monolithic samples obtained in the experimental test and in the numerical simulations. It is possible to verify a good relationship between the results obtained.

Figure 53 - Moisture content along the thickness of ceramic block A and B samples with cement hydraulic contact, at 2, 5 and 7 cm.

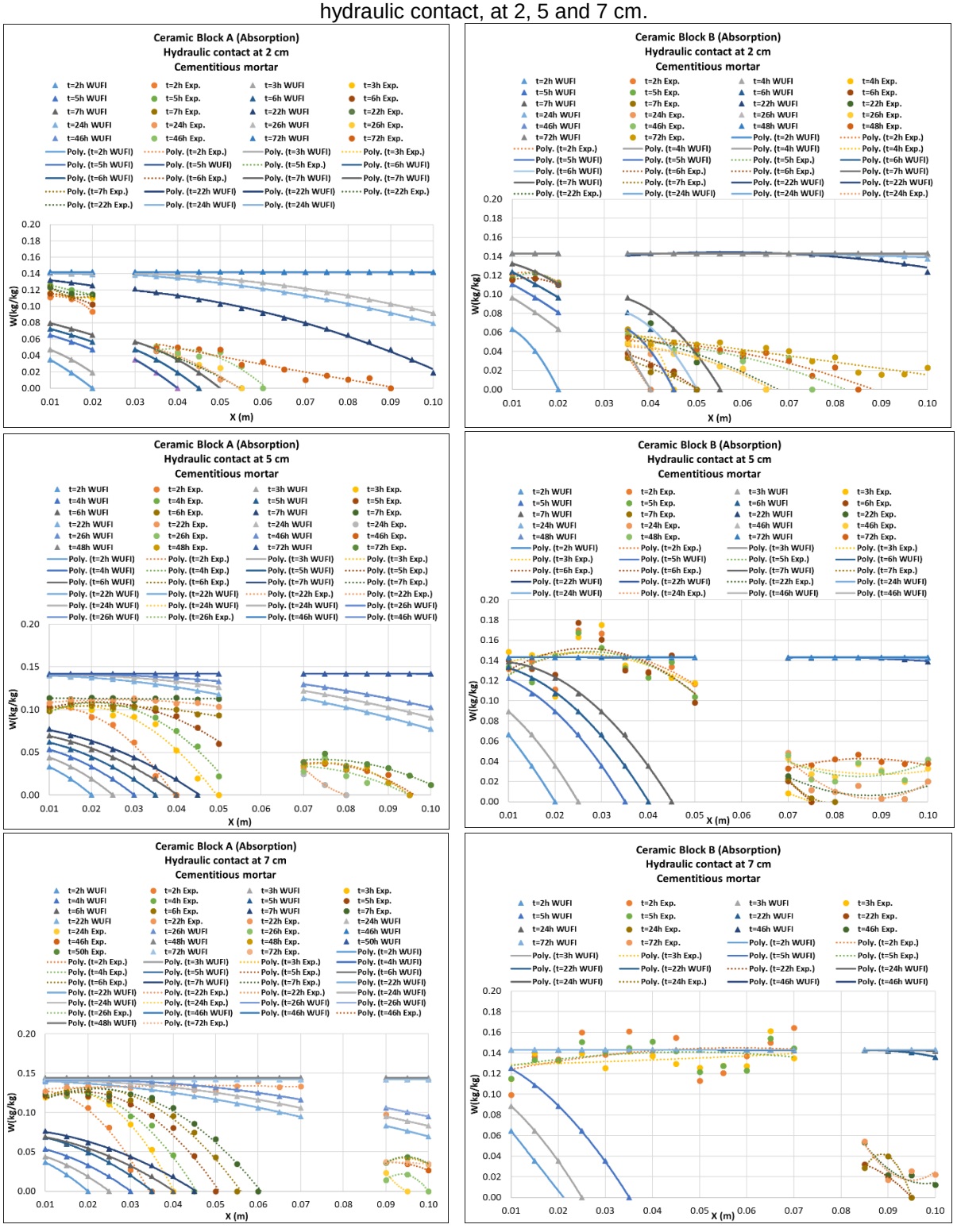

Source: Author.

In Figure 53, the moisture content is distributed uniformly throughout the thickness of the specimen and decreases homogeneously, like monolithic specimens. The influence of the interface in the imperfect hydraulic contact represented by the experimental results is verified, compared to the profiles obtained through the numerical simulation of the perfect hydraulic contact. In the imperfect hydraulic contact (HC) a large reduction of water absorption occurs after the mortar interface. When comparing the two profile types in hydraulic contact (cement mortar) it can be observed:

- Ceramic blocks A:

- In the brick A simulated sample with cement mortar, the wet front in all samples reached the 10cm level by 22h. The transported water content increased in proportion as the height of the interface location increased.
- In the brick A experimental sample with cement mortar, in the sample with interface at 2cm, after 72 hours, it did not reach the 10cm level. The wet front in the other samples reached the 10 cm level at the times of 72h (5cm) and 26h (7cm).

- Ceramics blocks B:

- In the brick B simulated sample with cement mortar, the wet front in all samples reached the 10cm level by 22h. The transported water content increased in proportion as the height of the interface location increased.
- In the brick B experimental sample with cement mortar, the wet front on the samples reached the 10 cm level at the times of 72h (2cm), 48h (5cm), 46h (7cm).

In Figure 54, the moisture content is distributed uniformly throughout the thickness of the specimen and decreases homogeneously, like monolithic specimens. The influence of the interface in the imperfect hydraulic contact represented by the experimental results is verified, compared to the profiles obtained through the numerical simulation of the perfect hydraulic contact. In the imperfect hydraulic contact (HC) a large reduction of water absorption occurs after the mortar interface.

Figure 54 - Moisture content along the thickness of red brick type A and B samples with lime hydraulic contact, at 2, 5 and 7 cm.

Source: Author.

When comparing the two profile types in hydraulic contact (lime mortar) it can be observed (Figure 54):

- Ceramics blocks A:

- In the brick A simulated sample with lime mortar, the wet front in all samples reached the 10cm level by 22h. The transported water content decreased in proportion as the height of the interface location increased.
- In the brick A experimental sample with lime mortar, the wet front on the samples reached the 10 cm level at the times of 46h (2cm), 22h (5cm), 24h (7cm).

- Ceramics blocks B:

- In the brick B simulated sample with lime mortar, the wet front in all samples reached the 10cm level by 22h. The transported water content increased in proportion as the height of the interface location increased.
- In the brick B experimental sample with lime mortar, in the sample with interface at 2cm, after 48-72 hours, reached the 8cm level. The wet front in the other samples reached the 10 cm level at the times of 46h (5cm) and 24h (7cm).

In Figure 55, the moisture content is distributed uniformly throughout the thickness of the specimen, but differs from the monolithic specimens, where there is a homogeneously decreases for the simulated samples. The influence of the air space interface is verified in both experimental and simulated test.

However, the water mass results obtained for the simulated samples are evenly distributed for the two brick layers, and this result is not realistic with the results presented in section 4.1.2 and the experimental results, which shows a greater amount of water mass in the layer in contact with the moisture source.

Figure 55 - Moisture content along the thickness of red brick type A and B samples with air space interface, at 2, 5 and 7 cm.

Source: Author.

When comparing the two profile types in hydraulic contact (lime mortar) it can be observed (Figure 55):

- Ceramics blocks A:

- In the brick A simulated sample with air space interface, the wet front in all samples reached the 10cm level by 22h. The transported water content increased in proportion as the height of the interface location increased.
- In the brick A experimental sample with air space interface, the wet front on the samples reached the 5 cm level at the time of 72h (2cm), 8 cm level at the time 72h (5cm), 10 cm level at the time 72h (7cm).

- Ceramics blocks B:

- In the brick B simulated sample with air space interface, the wet front in the samples reached the 10cm level by 22h (2cm), 24h (5cm) and 22h (7cm). The transported water content increased in proportion as the height of the interface location increased.
- In the brick B experimental sample with air space interface, the wet front on the samples reached the 5,5 cm level at the time of 72h (2cm), 7 cm level at the time 72h (5cm), 10 cm level at the time 50h (7cm).

4.1.3.2 Section results overview

- The water absorption over time in the samples showed a good relationship between the results obtained with the program and the experimental results.
- The interface influence was verified in the samples with imperfect hydraulic contact represented by the experimental results compared to results obtained through the numerical simulation of the samples with perfect hydraulic contact.
- The samples with hydraulic contact interface with cement mortar present lower absorption rates than the samples with lime mortar;
- The two materials tested with air space interface show an initial constant absorption rate and, when the humidity reaches the interface, a very slow absorption;
- The new methodology to calculate hydric resistance in hydraulic contact proved to be consistent effective, since the values found for the hydric resistances were consistent with the analysis.

- It wasn't identified relation between the transfer of humidity in the interface with air space and the position of the interface with the simulated results, just as it was also not found in Azevedo's (2019) work.
- The damp front obtained with ceramic brick B reached the top face of the specimens faster and with higher mass water content compared to ceramic brick A in the simulated results. This results may be related to the water absorption coefficient (Aw) value of brick B.
- The air space interfaces increase the mass water content in damp front as the distances of the air layer from the contact with water increase.

4.1.4 Moisture transport across perfect hydraulic contact – Drying process

In order to study the influence on the drying process of brick samples with perfect hydraulic contact (cement and lime mortar) at different heights, simulations were performed to compare the water transport behavior in the drying process for the monolithic samples and samples with perfect hydraulic contact aiming to find the influence of each contact configuration.

The samples used in the drying process were the same ones used in the absorption test. The samples had saturated initial condition for the materials and for the samples' base surface adiabatic system conditions were applied. The samples were exposed to two types of environments (Environment 1: T=20ºC and 50% RH; Environment 2: T= 70ºC and 3% RH).

For the results analysis, the 1-D isothermal drying process is highlighted as explained in section 2.1.4.3. The drying process can occur in three phases: Phase I- When the material is saturated, with high moisture concentration on the material surface and the water transport occurs by capillarity. In this phase the drying rate is controlled by the environmental conditions, becoming constant due to the constant environmental conditions of the test. In Phase II there is no longer an equilibrium between the liquid transported to the surface and the liquid that is being evaporated, causing a regression of the wet front to the interior of the material and a reduction in the drying rate. In this phase the drying process becomes dependent on the moisture transport properties of the material. Phase III is characterized by a slow, residual drying rate, close to the steady state condition and the main moisture transport mechanism is vapor diffusion.

Figure 56 - Water content graph along brick A of simulated transport on the drying process for perfect hydraulic contact (cement x lime).

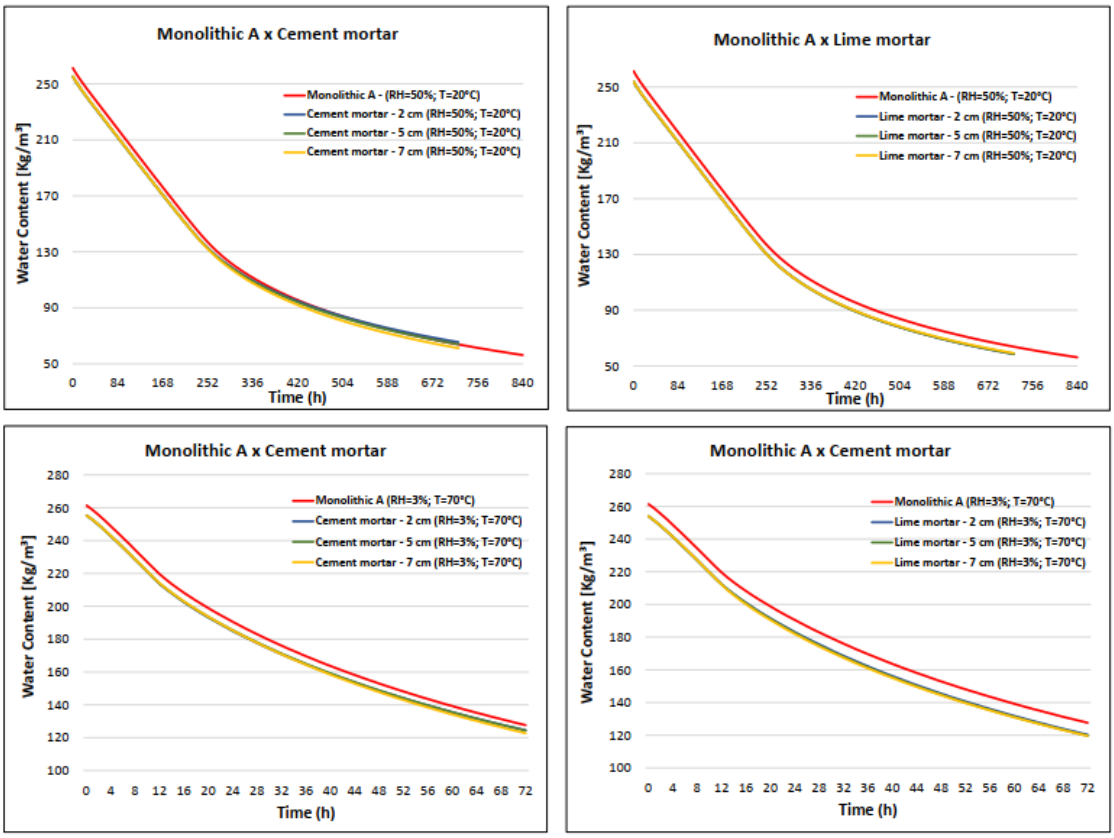

Source: Author.

Figure 57 - Water content on the surface of samples with brick A at the end of simulated transport on the drying process for perfect hydraulic contact (cement x lime).

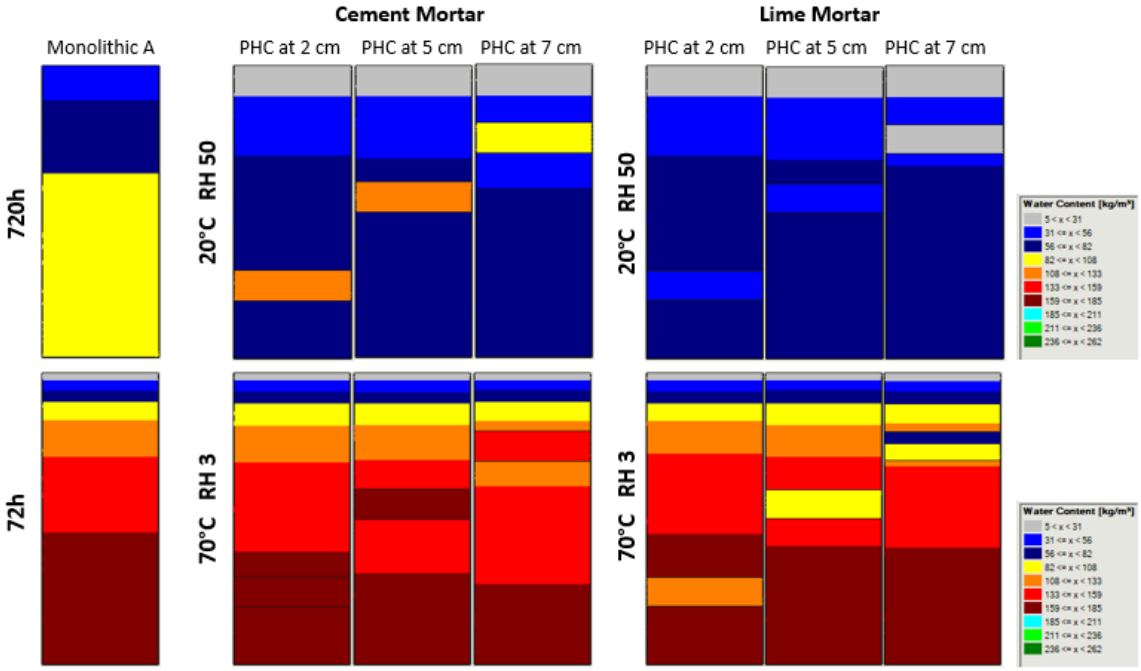

Source: Author.

The curves in Figure 56 showed different drying trends for the brick A samples with cement mortar and the samples with lime mortar. In drying with RH 50% and T=20ºC environment, both samples experienced an initial long linear water loss characterized by Phase I of the drying process. However, the samples with cement mortar initiated a faster Phase II compared to the samples with lime mortar, presenting a slow progressive drying rate. This result is consistent with the result found for the water absorption simulation in the lime samples which is faster compared to the monolithic brick A sample. Therefore, in the drying process, the transport phase by capillarity and vapor diffusion shows to be more favorable in the samples with perfect hydraulic contact with lime mortar, in comparison with the monolithic brick A sample, which has a lower liquid transport coefficient and a lower water vapor permeability.

However, for none of the perfect hydraulic contact configurations was observed a significant change in the curves compared to the curve of the monolithic sample, not characterizing a discontinuity caused by the materials interface in the samples with mortar. This result diverges from Azevedo's (2019) experimental result that found a moisture content discontinuity across the interface, indicating a capillary pressure difference across the interface. With this, it can be concluded that the assumption of perfect contact for samples with hydraulic contact is negligent in the numerical calculation.

Figure 57 shows the water content on the brick A samples' surface at the end of the drying process simulation. The samples with hydraulic contact have lower water content on the surface, and it can be concluded that they have a higher drying rate compared to the monolithic sample which is more impermeable and retains more water due to capillary pressure in the small pores.

Figure 57 also verifies that the interfaces in the samples with brick A located at a greater distance from the base, present a faster moisture content progression to the surface, requiring less time in the drying process for these samples. In all samples, the second layer of brick A exposed to the ambient conditions present lower water contents, which characterizes a greater drying in the region. These results were proven for the Azevedo’s (2019) experimental study.

Figure 58 - Water content graph along brick B of simulated transport on the drying process for perfect hydraulic contact (cement x lime).

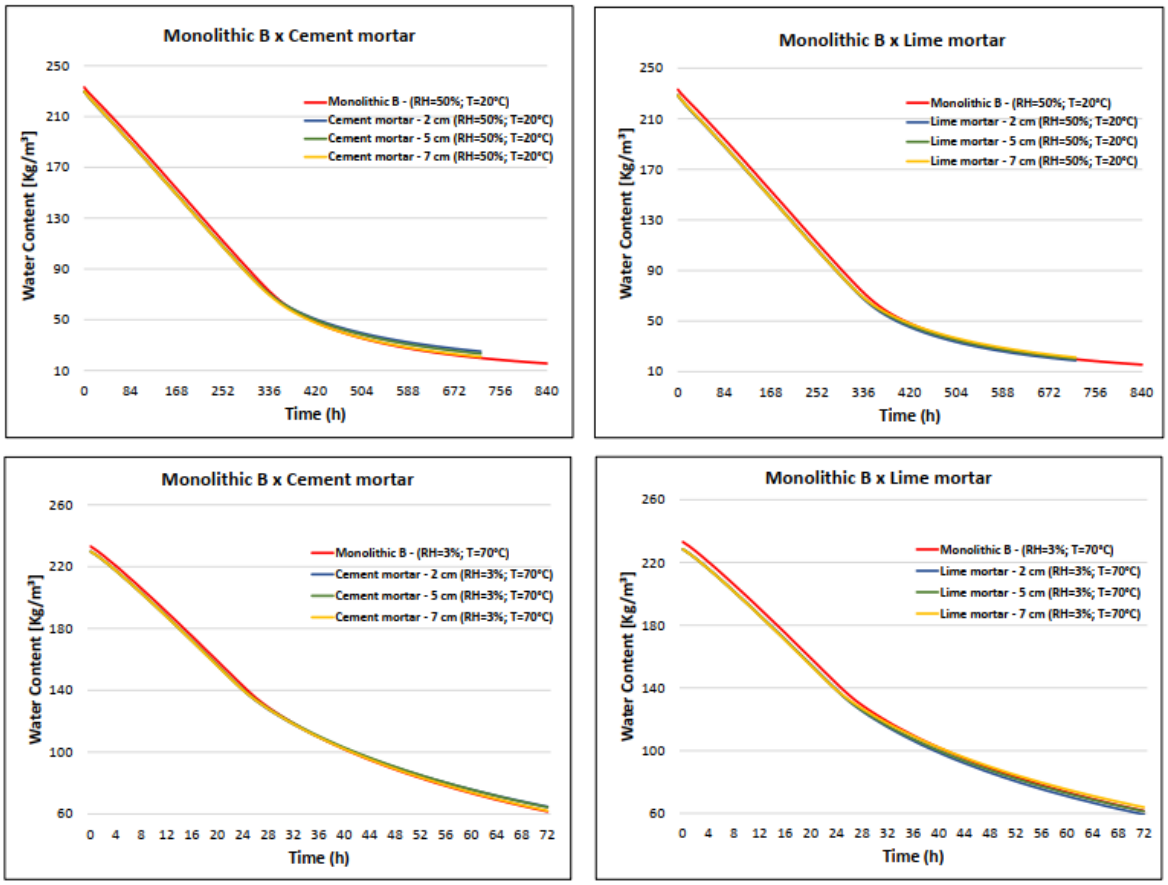

Source: Author.

Figure 59 - Water content on the surface of samples with brick B at the end of simulated transport on the drying process for perfect hydraulic contact (cement x lime)

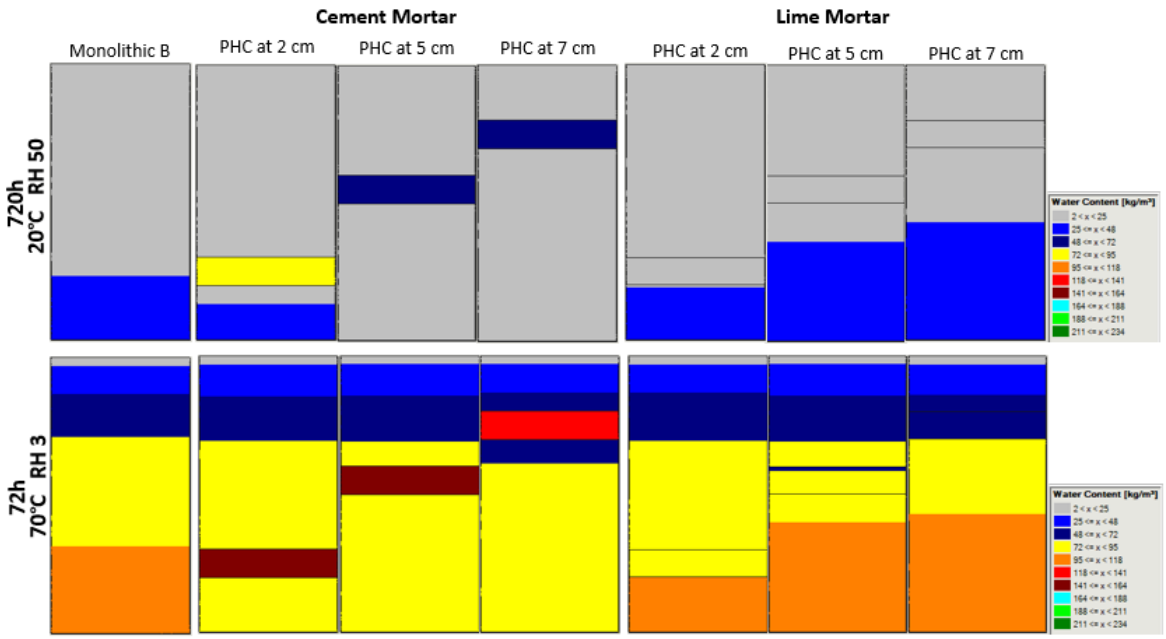

Source: Author.

The curves in Figure 58 displayed similar drying tendency for the brick B samples with cement mortar and the samples with lime mortar. In both drying environments, both samples experienced a long initial linear water loss characterized by Phase I capillary transport of the drying process. The samples with cement mortar showed faster drying in Phase I and slower drying in Phase II compared to the samples with lime mortar and the monolithic sample. This result is coherent with the water absorption process simulation result, where the samples with cement mortar showed a faster water transport by capillary absorption, which makes the second drying phase slower by the water shortage and a water vapor diffusion process is initiated earlier compared to the monolithic sample and lime mortar sample.

The graph (Figure 58) shows that the sample with cement mortar perfect hydraulic contact with interface positioned at 2cm had a lower drying rate and the sample with interface positioned at 7cm had a higher drying rate. The opposite was observed for samples with lime mortar perfect hydraulic contact. Figure 59 shows the water content on the brick B samples' surface at the end of the drying process simulation. The samples with lime mortar hydraulic contact have more water content on the surface.

4.1.4.1 Section results overview

- In all samples, the second layer of brick A and brick B exposed to ambient conditions have lower water contents, which characterizes greater drying in the region. These results were proven for the experimental study by Azevedo (2019).
- The brick A samples with perfect hydraulic contact indicate that the greater the interface placement distance from the base, the shorter the time required for the drying process in the samples.
- The brick B samples with perfect hydraulic contact with cement mortar indicate that the further away from the saturated wet front the material interface is positioned, the more capable it will be to effectively transport the liquid water to the surface where evaporation occurs. This result is due to the greater water vapor diffusion resistance in concrete in Phase II of drying, acting as a water

barrier in the sample with interface positioned at a smaller distance from the saturated wet front.

- The further distant from the saturated wet front the interface is positioned, the longer the drying time in the samples with perfect hydraulic contact with lime mortar.
- The water absorption coefficient and water vapor diffusion resistance of the mortar as well as the permeability of the brick are the main influential properties in an effective drying process.

4.1.5 Moisture transport across air space interface – Drying process

Figure 60 shows the water transport during the drying process simulation for the brick A samples with air space interface. The water content in the samples is transported uniformly through a linear curve for all samples. The decline in water flow in the samples from a point considered as the interface evidences that an air space interface reduces the transport capacity of water content in the sample, characterizing it as a hydric resistance.

Analyzing the graph (Figure 60) observed a long transport during the capillary transport phase for the monolithic sample A. The samples with air space interface located at 7cm from the base had a faster drying rate reduction than the other samples. It can be seen that the further the distance of the interface from the sealed base (without contact with external environmental conditions and with higher moisture concentration in relation to the top surface), the greater the resistance caused by the interface and the lower the drying rate in the samples.

Figure 60 - Water content graph along brick A of simulated transport on the drying process for air space interface.

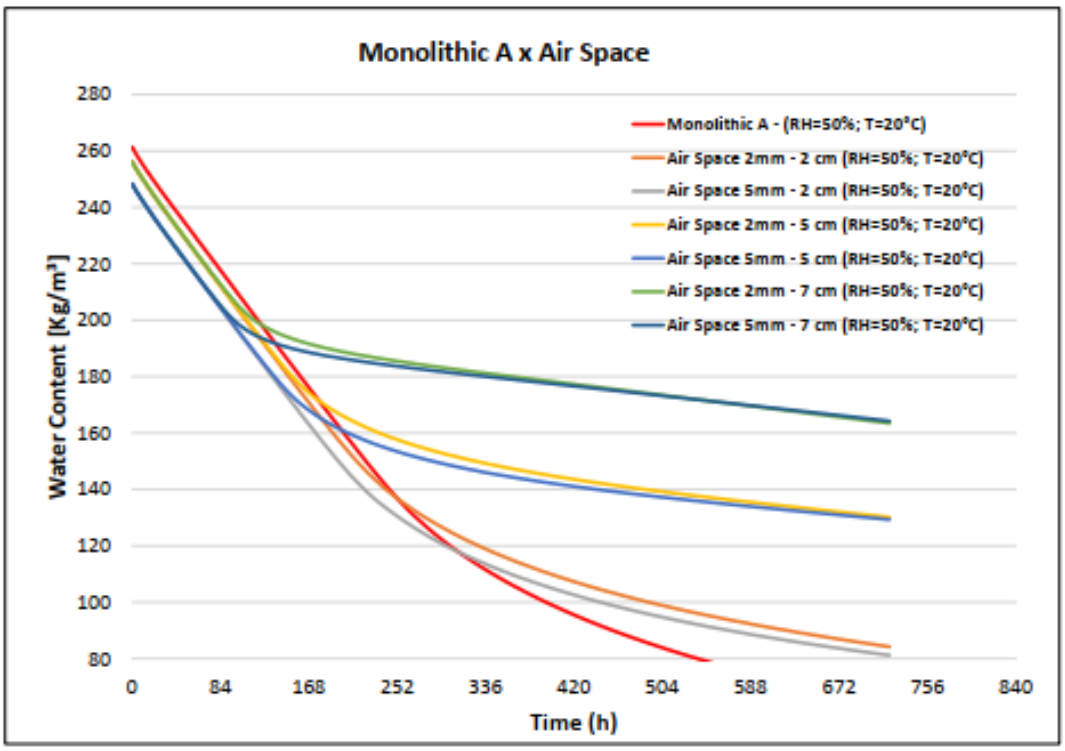

Source: Author.

Figure 61 - Water content on the surface of samples with brick A at the end of simulated transport on the drying process for air space interface.

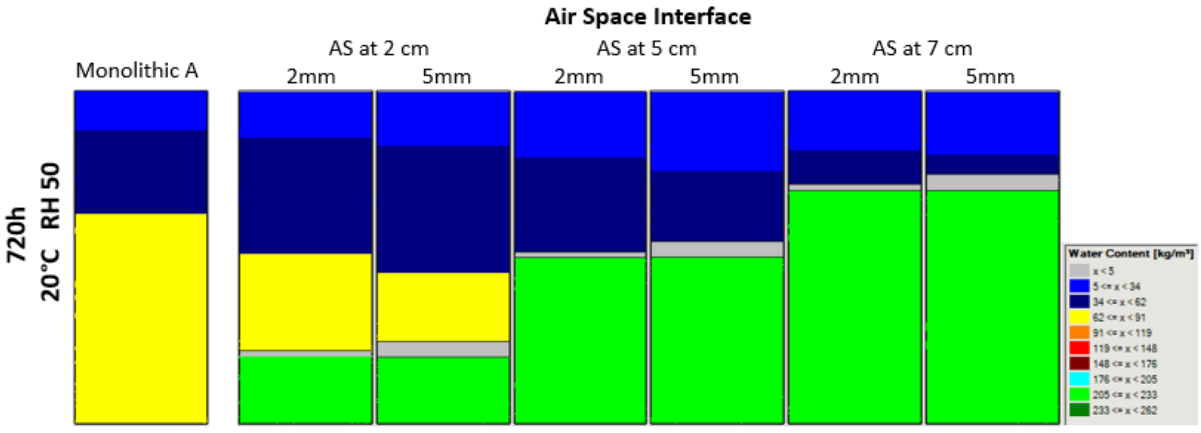

Source: Author.

The reduction in drying rate is greater for samples with a 2mm air space interface compared to samples with a 5mm air space interface. However, there is an approximation in the drying rate for the two air interface configurations after a few hours of the drying process.

Figure 61 shows the water content on the surface of brick A samples with 2mm and 5mm air space interface at different heights at the end of 720h simulated drying process. The samples with 5mm air space interface showed lower water content on the surface.

Figure 62 shows the water transport during the drying process simulation for brick B samples with air space interface. The water content in the samples is transported uniformly through a linear curve for all samples. The decline in the water flow in the samples from a point considered as the interface evidences that presence of an air space interface reduces the water content transport capacity in the sample, characterizing it as a hydric resistance.

Analyzing the graph (Figure 62) observed a long transport during the capillary transport phase for the monolithic sample B. The samples with air interface located at a height of 7cm from the base had a faster drying rate reduction than the other samples. It can be seen that the further the distance of the interface from the sealed base (without contact with the external environmental conditions and with higher moisture concentration in relation to the top surface), the greater the resistance caused by the interface and the lower the drying rate in the samples.

The reduction in drying rate is greater for samples with a 2mm air space interface compared to samples with a 5mm air space interface. However, there is an approximation in the drying rate for the two air interface configurations after a few hours of the drying process. Yet, by the end of the simulation, the samples with 2mm air space interface will show an increase in drying rate compared to the 5mm air interface sample. This explains a higher water vapor permeability caused by the sample assembly, since the 2mm air layer has a higher water vapor diffusion resistance compared to the 5mm air layer, but the more permeable brick B layer is thick in the 2mm air space sample.

Figure 62 - Water content graph along brick B of simulated transport on the drying process for air space interface.

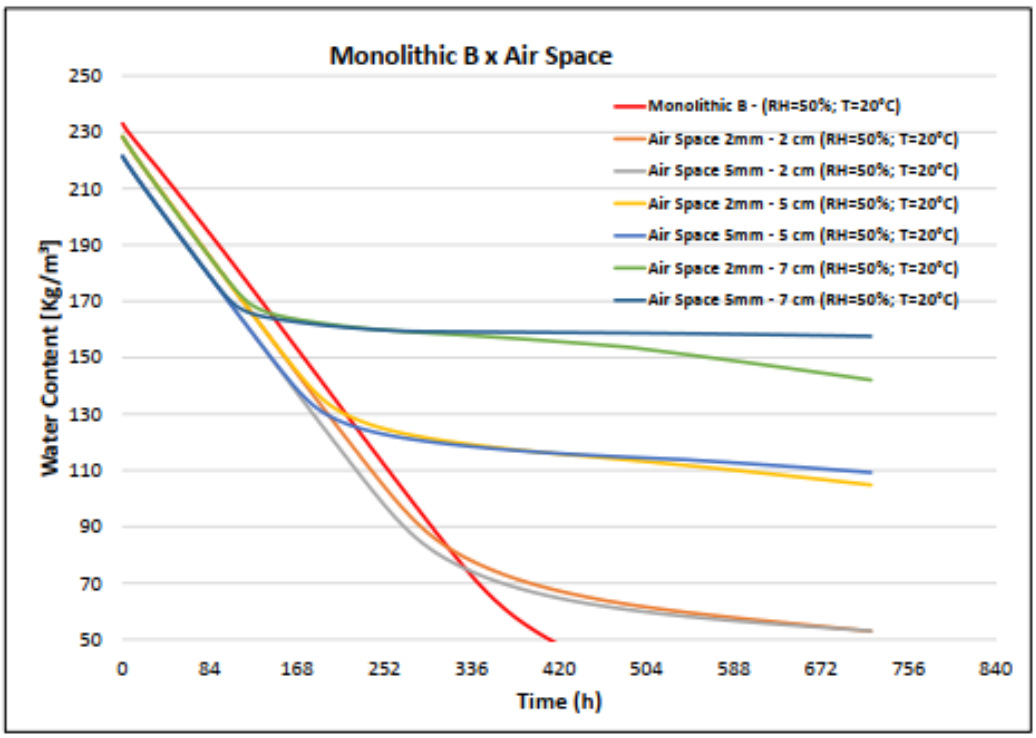

Source: Author.

Figure 63 - Water content on the surface of samples with brick B at the end of simulated transport on the drying process for air space interface.

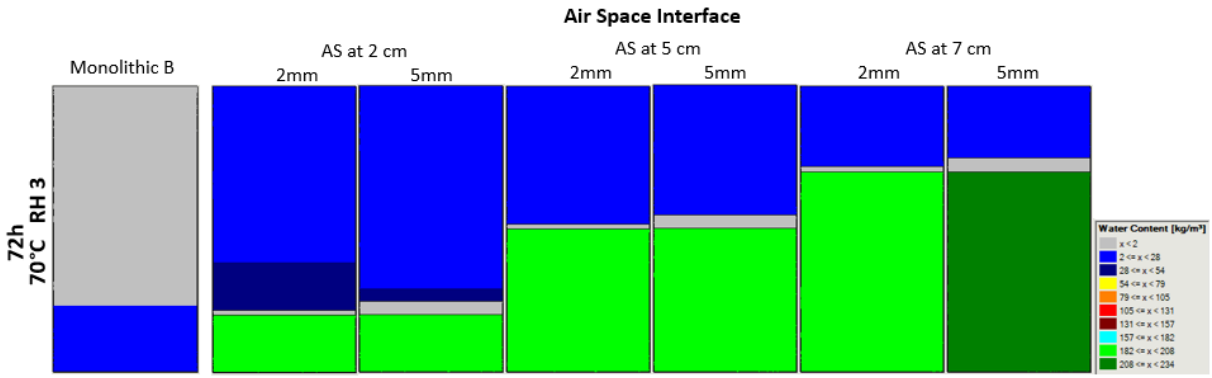

Source: Author.

Figure 63 shows the water content on the surfaces of brick B samples with 2mm and 5mm air space interface at different heights by the end of 720h drying process simulation. The sample with 5mm air space interface positioned at 2cm showed lower water contents on the surface.

4.1.5.1 Section results overview

- Significant change was observed in the curves for samples with air space interface in comparison with the curve for monolithic samples in the drying process. This result was verified in the experimental result of Azevedo (2019).
- The brick B samples with air space interface, as well as the monolithic sample B, showed a faster drying rate in Phase I. The higher permeability of brick B compared to brick A and mortars explains this fact.
- The water transport behavior in the drying process with air space interface in brick A samples were similar to the water transport behavior in the drying process for samples with brick B.
- The 2mm air layers caused a higher water resistance in water transport through the air space interface.
- The brick permeability will influence the resistance caused by the air space interface in water transport in the drying process. The more permeable the second brick layer is, the smaller the effect caused by the water vapor diffusion resistance of the air layer.
- It can be seen that the further the distance of the interface from the sealed base, the greater the resistance caused by the interface and the lower the drying rate in the samples. This result this result was verified in the experimental result of Azevedo (2019).

4.2 LIMITATIONS OF THE STUDY

In this study, the unidirectional moisture transport through the interface between brick and mortar and brick-brick in multilayer prismatic specimens was analyzed. Therefore, it was considered that the interface does not interfere with moisture transport for the configurations with brick and mortar, performing idealistic simulations for this type of contact between materials. Thus, to analyze the influence of the interface, the numerical simulation results were compared with the experimental results to obtain information about the behavior of moisture through the interface of hydraulic contact between the materials.

The use of WUFI-2D v.4.3 software in Brazil is not well known and makes the understanding and skills limited in the application of the tool in numerical studies. Although the software is a commercial program, a student license is available for the time needed to complete the academic study, through a student request. The program presents an interface considered user-friendly because it is easy to understand the steps and the input information request. However, the lack of knowledge of the data required by the program and the results interpretation makes the use of the tool challenging for predicting the tests of interest. However, the program has a large amount of information about the physics considered in the program, as well as a question and answer forum between users and experts that makes it easy to access information and clarify doubts while using the program, making the tool attractive to inexperienced users.

Modeling the complex heat and moisture transfer processes coupled in building components always involves simplifying reality. Most databases assume isotropic properties and very few references point to anisotropic behavior, which, however, has been demonstrated for both molded and extruded bricks (RAMIREZ et al., 2021). Also, to enter the properties of an anisotropic material, the program enables the properties to be entered in two directions. In this study where the properties were used from experimental tests, the materials were considered to be isotropic. The errors caused by these general inaccuracies can be negligible or serious, so comparing the numerical results with the experimental results and understanding the physics between the material properties is essential to determine the reliability of the calculations.

The material properties in this study were determined experimentally under boundary conditions similar to those in practical use, except for the specific heat thermal property which were taken from the WUFI 2D v4.3 materials database.

The boundary conditions applied in the hygrothermal simulations were determined based on the experimental test characteristics. For the simulation, applying the adiabatic system to the surfaces of the samples that had waterproofed surfaces in the experimental tests can idealize the behavior of minimal energy loss between the environments in the laboratory tests.

As discussed in this session, there were inaccuracies in the calculations caused by the limitations of the hygrothermal model, the determination of boundary conditions, and the lack of documented material properties. While these inaccuracies must be acknowledged when interpreting the moisture transport calculation, they are considered of minor importance to the main results and conclusions in this work.

CHAPTER 5. CONCLUSIONS

5.1 SYNTHESIS OF THE CONCLUSIONS OBTAINED

The development of this study made it possible to verify with the numerical calculation program WUFI-2D, the moisture transport behavior through samples with perfect hydraulic contact and through samples with air space interface.

In this work, an attempt was made to numerically simulate the samples studied in Azevedo's (2019) experimental research with the aim of validating the results found in the laboratory and resorting to further analysis with the results obtained in the simulation through the resources made available by the software application.

The results obtained allowed to develop a thorough analysis of water transport through material layers with different hygroscopic properties and to analyze the influence of the material layer interface on water transport during water absorption process and during drying process in multilayer components.

With the results obtained from the numerical simulations performed, and resorting to the results obtained in the laboratory studies performed in the scope of the Master's Thesis with the theme "Interface influence on moisture transport in building components" by Antônio Augusto Costa de Azevêdo, it was then possible to analyze the interface effect on moisture transport in multilayer components. The investigations showed that the water absorption tests for the moisture transport study in multilayer components simulated with the two-dimensional moisture transport program WUFI-2D neglects on a large scale the effects caused by the interface on the hydraulic contact during moisture transport when water is absorbed. For the calculations, some idealizing assumptions were made that are favorable for water transport, but according to the experimental result, due to the differences in the suction pressures of the materials in contact and the transfer resistances, there was a barrier that delays the water transport across the interface.

The most significant results from the simulations and which contributed to the experimental study validation are the following:

- No significant change was observed in the water content transport curves for samples with perfect hydraulic contact in comparison with the curve for monolithic samples. Therefore, not characterizing a discontinuity caused by the interface of the materials in the mortar samples, but considering the layer material properties as influencing the water transport resistance. This result diverges from the experimental result of Azevedo (2019).
- The samples with perfect hydraulic contact interface with cement mortar show higher absorption rates than the samples with lime mortar; This result diverged with the Azevedo (2019) experimental result. As well as for the previous divergence, the explanation for this result may be related to the type of perfect contact that the program calculates. In the experimental test the type of contact is imperfect, with a discontinuity ("layer") at the interface of unknown property caused by the brick layer absorbing particles from the fresh cement mortar layer, characterizing an imperfect hydraulic contact and attributing a higher resistance to water transport.
- With the results obtained in the water absorption test simulation using samples with perfect hydraulic contact, it could be concluded that in a brick and mortar masonry composed with a brick more impermeable than the mortar, the mortar layers with access to a significant moisture content will raise the moisture front on the surface of the component. In the case where the mortar of the composite is more impermeable than the brick, the mortar layer will act as a moisture barrier in the moisture transport.
- The material layer less permeable than the brick in the joint will reduce the water absorption in the sample when positioned at a shorter distance from the saturated wet front.
- The surface exposed to environmental conditions for the water transport direction in the drying process will show lower water content.
- The further distant from the saturated wet front the interface is positioned, the longer the drying time in the samples with perfect hydraulic contact with lime mortar. This result was verified in the experimental test.
- The water absorption coefficient and water vapor diffusion resistance of the mortar as well as the permeability of the brick are the main influential properties in an effective drying process.

- Significant change was observed in the curves for samples with air space interface in comparison with the curve for monolithic samples in the drying process. This result was verified in the experimental test.
- The thinner air layer causes a higher water resistance in water transport through the air space interface.
- The brick permeability will influence the resistance caused by the air space interface in water transport in the drying process. The more permeable the second brick layer is, the smaller the effect caused by the water vapor diffusion resistance of the air layer.
- Although the software physics neglects the discontinuity effect caused by the interface between the material layers, the program proved to be helpful for studies of effective assemblies and solutions for moisture transport.
- The water absorption over time in the samples showed a good relationship between the results obtained with the program and the experimental results.
- The interface influence was verified in the samples with imperfect hydraulic contact represented by the experimental results compared to results obtained through the numerical simulation of the samples with perfect hydraulic contact.
- The new methodology to calculate hydric resistance in hydraulic contact proved to be consistent effective, since the values found for the hydric resistances were consistent with the analysis.
- It wasn't identified relation between the transfer of humidity in the interface with air space and the position of the interface with the simulated results, just as it was also not found in Azevedo's (2019) work.
- The damp front obtained with ceramic brick B reached the top face of the specimens faster and with higher mass water content compared to ceramic brick A in the simulated results. This results may be related to the water absorption coefficient (Aw) value of brick B.

5.2 FUTURE WORKS

This work has made progress in the field of moisture transport through multilayer components, however, further studies in this domain could solve the interface problem, such as:

- Experimental characterization of different interface types in the perfect hydraulic contact with different materials and the design a mathematical model that simulates the discontinuity between the material layers during the numerical calculation.
- To perform an experimental study on a masonry with materials of known properties and monitor points on the surface exposed to real weather conditions. Perform the simulation with the monitoring at the selected points and obtain the full scale influence of neglecting the hydric resistance in the numerical calculations of moisture transport in multilayer components.

CHAPTER 6. REFERENCES

KUMARAN, M. K., Heat, Air and Moisture Transfer in Insulated Envelope Parts. Final Report, Vol. 3, Task 3: Material Properties, International Energy Agency Annex 24, Laboratorium Bouwfysica, K. U.-Leuven, Belgium, 1996, p. 135.

Schirmer, R., ZVDI, Beiheft Verfahrenstechnik, Nr. 6, S. 170, 1938.

Kuenzel, M. H., "Simultaneous Heat and Moisture Transport in Building Components, One- and Two-DimensionalCalculation Using Simple Parameters," Ph.D. thesis, Fraunhofer Institute in Bauphysics, IRB Verlag, 1995.

Krus, M., "Moisture Transport and Storage Coefficients of Porous Mineral Building Materials--Theoretical Principles and New Test Methods," Ph.D. thesis, Fraunhofer IRB Verlag,1996.

Kohonen, R., "Transient Analysis of Thermal and Moisture Physical Behavior of Building Constructions, Building and Environment, Vol. 19, No. 1, 1984, pp. 1-11.

Janssens, E, "Reliable Control of Interstitial Condensation in Lightweight Roof Systems," Ph.D. thesis, Catholic Universityof Leuven, Belgium, 1998.

Luikov, A. V., Heat and Mass Transfer in Capillary-Porous Bodies, Pergamon Press, 1966.

Pel, L., "Moisture Transport in Porous Building Materials," Ph.D. thesis, Einhoven University of Technology, the Netherlands, 1995.

TRECHSEL, Hr (Org.). Moisture Analysis and Condensation Control in Building Envelopes. 100 Barr Harbor Drive, PO Box C700, West Conshohocken, PA 19428-2959: ASTM International, 2001.

Keresteciogiu, A., Swami, M., and Gu, L., "Combined Heat and Moisture Transfer in Building Structures," ASME Winter Annual Meeting, San Francisco, CA, 10-15 Dec. 1989.

Kaviany, M., Principles of Heat Transfer in Porous Media, Springer-Verlag, 1993.

BELARBI, Rafik; QIN, Menghao; AÏT-MOKHTAR, Abdelkarim. Modeling of Moisture Transport in Porous Building Materials by Gravimetric Sorption-desportion Tests. p. 15, 2006.

Darcy, H., Les Fountaines Publiques de ville de Dijon, Dalmont Paris, 1856.

J. Bear and Y. Bachmat, Introduction to modeling of transport phenomena in porous media, vol. 4. Springer Science & Business Media, 2012

Yuliang ZOU, “Modelling of the dynamic effects in capillary pressure in coupling with deformation on the desiccation of porous materials”, Ph.D. thesis.L’école Centrale de Nantes, 2020.

Airaksinen, S. Role of Excipients in Moisture Sorption and Physical Stability of Solid Pharmaceutical Formulations. PhD thesis, Dissertationes bioscientiarum molecularium Universitatis Helsingiensis in Viikki 20/2005, Helsinki, Finland, 2005; p. 57.

Rode, C., "Combined Heat and Moisture Transfer in Building Constructions," Ph.D. thesis, Thermal Insulation Laboratory, Technical University of Denmark, 1990.

H. R. Trechsel, Ed., Manual on Moisture Control in Buildings, ASTM M N L 18 American Society for Testing and Materials, West Conshohocken, PA, 1994.

F. Benboudjema, Modélisation des déformations différées du béton sous solicitations biaxiales. Application aux enceintes de confinement de bâtiments réacteurs des centrales nucléaires. Thesis, Universite de Marne la Vallée, 2002.

M. Iwamatsu and K. Horii, “Capillary condensation and adhesion of two wetter surfaces,” Journal of colloida interface science, vol. 182, no. 2, pp. 400–406, 1996.

M. Tuller and D. Or, “Hydraulic conductivity of variably saturated porous media: Film and corner flow in angular pore space,” Water Resources Research, vol. 37, no. 5, pp. 1257–1276, 2001.

E. A. Mason, M. EA, and M. AP, “Gas transportin porous media: The dusty-gas model,” 1983.

K. Higashi, H. Ito, and J. Oishi, “Surface diffusion phenomena in gaseous diffusion. i. surface diffusion of pure gas,” Nippon Genshiryoku Gakkaishi, vol. 5, 1963

Y. Xi, Z. P. Bazant, L. Molina, and H. M. Jennings, “Moisture diffusion in cementitious materials moisture capacity and diffusivity,” Advanced Cement Based Materials, vol. 1, no. 6, pp. 258–266, 1994.

Qiu, X. Moisture transport across interfaces between building materials. Dissertação de
Doutoramento, Universidade Concordia, Montreal, 2003.

Gonçalves, T. Salt crystallization in plastered or rendered walls. Dissertação de Doutoramento, Instituto Superior Técnico e Laboratório Nacional de Engenharia Civil. 2007.

AZEVEDO, J. Absorção por capilaridade de soluções Salinas em materiais porosos. Dissertação de Mestrado. Porto: Faculdade de Engenharia da Universidade do Porto, 2013.

AZEVEDO, AC. Interface influence on moisture transport in building components. Dissertação de Doutoramento. Porto: Faculdade de Engenharia da Universidade do Porto, 2019.

FREITAS, V., CRAUSSE, P. e ABRANTES, V. – Moisture diffusion in thermal insulating materials, Seconde Symposium on Insulation Materials: Testing and Applications, Vol. 2. ASTM STP 1116,pp 389 a 400, Philadelphia. 1991.

Freitas, V. Transferência de humidade em paredes de edifícios – Análise do fenómeno de interface. Dissertação de Doutoramento, Faculdade de Engenharia da Universidade do Porto, Porto, 1992.

H. Derluyn, H. Janssen, J. Carmeliet, Influence of the nature of interfaces on the capillary transport in layered materials, Construct. Build. Mater. 25 (2011).

kunze

C. Groot, J. Gunneweg, The influence of materials characteristics and workmanship on rain penetration in historic fired clay brick masonry, Heron 55 (2010) 141–154.

H.J.P. Brocken, Moisture Transport in Brick Masonry: the Grey Area between Bricks, Ph.D. dissertation, Dept. Built Environment, Technische Universiteit Eindhoven, 1998.

Freitas VP, Abrantes V, Crausse P. Moisture migration in building walls – analysis of the interface phenomena. Build Environ 1996;31:99–108.

KAROGLOU, M. et al. A powerful simulator for moisture transfer in buildings. Building and Environment, v. 42, n. 2, p. 902–912, fev. 2007.

C. Hall, W.D. Hoff, Water Transport in Brick, Stone and Concrete, second ed., CRC Press, London, 2009

J. Selih, A. Sousa, T. Bremner, Moisture transport in initially fully saturated concrete during drying, Transport Porous Media 24 (1996) 81–106.

M. Azenha, Numerical Simulation of the Structural Behavior of Concrete since its Early Ages, Ph.D. dissertation, Dept. Civil Engineering, University of Porto, 2009.

M. Mainguy, O. Coussy, and V. Baroghel-Bouny, “Role of air pressure in drying of weakly permeable materials,” Journal of Engineering Mechanics, vol. 127, no. 6, pp. 582–592, 2001.

L. Derdour, H. Desmorieux, J. Andrieu, A contribution to the characteristic drying curve concept: Application to the drying of plaster, Drying Technology, 18(1-2), 237- 260, 2000

Rêgo, T. S. M. R. 2014. "Efeito de soluções aquosas salinas nos processos de embebição de paredes com múltiplas camadas". Dissertação de Mestrado, Faculdade de Engenharia da Universidade do Porto.

Guimaraes, ˜ A.S., Delgado, J.M.P.Q., Azevedo, A.C., de Freitas, V.P., 2018. Interface influence on moisture transport in buildings. Construct. Build. Mater. 162, 480–488. https://doi.org/10.1016/j.conbuildmat.2017.12.040.

W.K. Lewis, The rate of drying of solid materials. The journal of industrial and engineering chemistry, Symp. Drying (1921) 427–432.

L.A. Richards, Capillary conduction of liquids through porous mediums, Physics 1 (1931) 318–333.

J.R. Philip, D.A. De Vries, Moisture movement in porous media under temperature gradients, Trans. Am. Geophys. Union 38 (1957) 222–232.

Whitaker S. Simultaneous heat, mass, and momentum transfer in porous media: a theory of drying. Advances in heat transfer. Elsevier; 1977. p. 119–203.

C.R. Pedersen, Prediction of moisture transfer in building constructions, Building Environ. 27 (3) (1992) 387–397.

Mendes N, Ridley I, Lamberts R, Philippi PC, Budag K. UMIDUS: a PC program for the prediction of heat and moisture transfer in porous building elements. Building Simulation Conference-IBPSA. 1999,277–83

N. Mendes, P.C. Philippi, R. Lamberts, A new mathematical method to solve highly coupled equations of heat and mass transfer in porous media, Int. J. Heat Mass Transfer 45 (2002) 509–518.

J. Langmans, A. Nicolai, R. Klein, S. Roels, A quasi-steady state implementation of air convection in a transient heat and moisture building component model, Build. Environ. 58 (2012) 208–218, https://doi.org/10.1016/j.buildenv.2012.07.011.

U. Ruisinger, P. Kautsch, Comparison of hygrothermal 2D- and 3D-simulation results with measurements from a test house, E3S Web Conf. 172 (2020), 08004, https://doi.org/10.1051/e3sconf/202017208004

NAKASONE, Y.; YOSHIMOTO, S.; STOLARSKI, T. A. Engineering analysis with ANSYS software. Amsterdam ; Boston: Butterworth-Heinemann, 2006.

CHANG, Seong Jin et al. Numerical analysis on the hygrothermal behavior of building envelope according to CLT wall assembly considering the hygrothermal-environmental zone in Korea. Environmental Research, v. 191, p. 110198, dez. 2020.

H. Hens, Heat, Air and Moisture Transfer in Highly Insulated Building Envelopes (HAMTIE), FaberMaunsell Ltd, 2002. https://www.ieaebc.org/Data/publications/EBC_Annex_24_tsr.pdf.

H. Hens, Modeling the heat, air, and moisture response of building envelopes: what material properties are needed, how trustful are the predictions? JAI 4 (2007) 1–11, https://doi.org/10.1520/JAI100460.

VERMA, Shubham Kumar et al. Hygrothermal dynamics for developing energy-efficient buildings: Building materials and ventilation system considerations. Energy and Buildings, v. 260, p. 111932, abr. 2022.

M.H. Benzaama, L.H. Rajaoarisoa, B. Ajib, S. Lecoeuche, A data-driven methodology to predict thermal behavior of residential buildings using piecewise linear models, J. Build. Eng. 32 (2020) 101523, https://doi.org/10.1016/j.jobe.2020.101523

H. Künzel, K. Kiesel, Calculation of heat and moisture transfer in exposed building components, Int. J. Heat Mass Transf. 40 (1) (1997) 159–167.

CRAWLEY, Drury B. et al. EnergyPlus: creating a new-generation building energy simulation program. Energy and Buildings, v. 33, n. 4, p. 319–331, abr. 2001.

KLEIN, S.A., et al., 2007. TRNSYS 16 – A Transient System Simulation Program. University of WisconsinMadison Solar Energy Laboratory, Madison, WI, USA.

R. Djedjig, E. Bozonnet, R. Belarbi, Analysis of thermal effects of vegetated envelopes: Integration of a validated model in a building energy simulation program, Energy Build. 86 (Jan. 2015) 93–103, https://doi.org/10.1016/j. enbuild.2014.09.057.

J. Preuss. Moisture Balance. in TRaNsient SYstem Simulation program 18: Multizone Building modeling with Type56 and TRNBuild, TRNSYS, pp. 191– 195.

M. Steeman, A. Janssens, H.J. Steeman, M.V. Belleghem, M.D. Paepe, On coupling 1D non isothermal heat and mass transfer in porous materials with a multizone building energy simulation model, Build. Environ. (2010)

Qiao sun˙ Zhou meng-yu˙ Bai lang. Exploration electromagnetic field theory [M]. Xuzhou˖ China Mining University Press˙ 1991.

WANG, Xiaolong et al. The Application of COMSOL Multiphysics in Direct Current Method Forward Modeling. Procedia Earth and Planetary Science, v. 3, p. 266–272, 2011.

NICOLAI, A.; GRUNEWALD, J; ZHANG J.S. Calculation of Heat and Moisture Transfer in Exposed Building Components. Salztransport und Phasenumwandlung - Modellierung und numerische Lösung im Simulationsprogramm Delphin 5, 2007, pgs. 231-239, Bauphysik

Karagiozis, A. Advanced hygrothermal modeling of building materials using MOISTUREEXPERT 1.0. in 35th International Particleboard Composite Materials Symposium, Pullman, Washington, April. 2001.

Finite element analysis—theory and application with ANSYS. *Minerals Engineering*, v. 12, n. 8, p. 992–993, ago. 1999.

MURRAY, Malcolm C et al. LIVE ENERGY TRNSYS: TRNSYS SIMULATION WITHIN GOOGLE SKETCHUP. p. 8, 2009.

Freitas, V. P., Guimarães. A. S., Torres, M. I. Humidade Ascensional. FEUP edições, Porto, 2008.

Ramirez, R. et al. Experimental characterization of moisture transport in brick masonry with natural hydraulic lime mortar. Building and Environment, v. 205, p. 108256, nov. 2021.